

DIRECT SYNTHESIS OF LPG FROM CO₂ BY USING CZZA AND HY ZEOLITE HYBRID
CATALYST



A Dissertation Submitted in Partial Fulfillment of the Requirements
for the Degree of Doctor of Philosophy in Chemical Technology

Department of Chemical Technology

FACULTY OF SCIENCE

Chulalongkorn University

Academic Year 2020

Copyright of Chulalongkorn University

การสังเคราะห์แอลพีจีโดยตรงจากคาร์บอนไดออกไซด์โดยใช้ตัวเร่งปฏิกิริยาไฮบริด CZZA และ HY
ซีโอไลต์



วิทยานิพนธ์นี้เป็นส่วนหนึ่งของการศึกษาตามหลักสูตรปริญญาวิทยาศาสตรดุษฎีบัณฑิต
สาขาวิชาเคมีเทคนิค ภาควิชาเคมีเทคนิค
คณะวิทยาศาสตร์ จุฬาลงกรณ์มหาวิทยาลัย
ปีการศึกษา 2563
ลิขสิทธิ์ของจุฬาลงกรณ์มหาวิทยาลัย

Thesis Title	DIRECT SYNTHESIS OF LPG FROM CO ₂ BY USING CZZA AND HY ZEOLITE HYBRID CATALYST
By	Mr. Jaru Natakaranakul
Field of Study	Chemical Technology
Thesis Advisor	Professor THARAPONG VITIDSANT, Ph.D.
Thesis Co Advisor	Professor Noritatsu Tsubaki, Ph.D.

Accepted by the FACULTY OF SCIENCE, Chulalongkorn University in Partial Fulfillment of the Requirement for the Doctor of Philosophy

..... Dean of the FACULTY OF SCIENCE
(Professor POLKIT SANGVANICH, Ph.D.)

DISSERTATION COMMITTEE

..... Chairman
(Associate Professor PRASERT REUBROYCHAROEN, Ph.D.)

..... Thesis Advisor
(Professor THARAPONG VITIDSANT, Ph.D.)

..... Thesis Co-Advisor
(Professor Noritatsu Tsubaki, Ph.D.)

..... Examiner
(Professor Chawalit Ngamcharussrivichai, Ph.D.)

..... Examiner
(Professor NAPIDA HINCHIRANAN, Ph.D.)

..... External Examiner
(Rungravee Phienluphon, Ph.D.)

จารุ นาถกรณกุล : การสังเคราะห์แอลพีจีโดยตรงจากคาร์บอนไดออกไซด์โดยใช้ตัวเร่งปฏิกิริยาไฮบริด CZZA และ HYซีโอไลต์. (DIRECT SYNTHESIS OF LPG FROM CO₂ BY USING CZZA AND HY ZEOLITE HYBRID CATALYST) อ.ที่ปรึกษาหลัก : ศ. ดร. ธารพงษ์ วิทิตสานต์, อ.ที่ปรึกษาร่วม : ศ. ดร. โนริทัตชี ชิบาเกิ

การเปลี่ยนคาร์บอนไดออกไซด์เป็นสารประกอบไฮโดรคาร์บอนสายโซ่สั้นเป็นกระบวนการที่มีศักยภาพสูงในการลดปัญหาการปล่อยแก๊สเรือนกระจกในระยะยาว อีกทั้ง แก๊สหุงต้ม หรือ แอลพีจี ซึ่งประกอบด้วย โพรเพน และ บิวเทน ถูกใช้อย่างแพร่หลายทั้งในภาคครัวเรือนและการขนส่ง นอกจากนี้ ชีวมวลได้รับความสนใจมากขึ้นในการนำไปใช้เป็นพลังงานทดแทนเพื่อลดปริมาณการปล่อยแก๊สคาร์บอนไดออกไซด์ โดยสังเคราะห์เป็นเชื้อเพลิงเหลวใช้ในยานพาหนะ ดังนั้น ในงานวิจัยนี้จึงศึกษาการสังเคราะห์แอลพีจีโดยตรงจากกระบวนการไฮโดรจีเนชันของคาร์บอนไดออกไซด์โดยใช้ตัวเร่งปฏิกิริยาไฮบริด คอปเปอร์/ซิงก์ออกไซด์/เซอร์โคเนียม/อะลูมินา (CZZA) และHY ซีโอไลต์ ในเครื่องปฏิกรณ์แบบเบดนิ่ง โดยใช้แก๊สไฮโดรเจน คาร์บอนไดออกไซด์ คาร์บอนมอนอกไซด์เป็นสารตั้งต้น ทำการศึกษาหาภาวะที่เหมาะสม พบว่า วิธีการผสมตัวเร่งปฏิกิริยาทั้งสองชนิดมีอิทธิพลอย่างมีนัยสำคัญต่อร้อยละการเลือกเกิดของสารประกอบไฮโดรคาร์บอน และ ที่ภาวะที่เหมาะสมในการสังเคราะห์แอลพีจีได้ร้อยละการเปลี่ยนของคาร์บอนไดออกไซด์ ร้อยละ 27.39 ร้อยละการเลือกเกิดสารประกอบไฮโดรคาร์บอน ร้อยละ 98.70 และ ร้อยละการเลือกเกิดแอลพีจี ร้อยละ 66.56 วัตถุประสงค์ที่สองในงานวิจัยนี้ ศึกษาต้นแบบกระบวนการสังเคราะห์เชื้อเพลิงเหลวจากชีวมวล โดยศึกษากระบวนการแก๊สซิฟิเคชันของชีวมวล ในเครื่องปฏิกรณ์แนวนอน ที่อุณหภูมิ 900 องศาเซลเซียส พบว่า การคงที่ของอุณหภูมิในเครื่องปฏิกรณ์ส่งผลให้อัตราส่วนโดยโมลระหว่างไฮโดรเจนกับคาร์บอนมอนอกไซด์ในแก๊สสังเคราะห์คงที่อยู่ในช่วง 1.75 - 2.25 จากนั้นนำแก๊สสังเคราะห์ที่ได้ผ่านกระบวนการฟิชเชอร์-ทรอปส์เพื่อสังเคราะห์เป็นเชื้อเพลิงเหลว ที่อุณหภูมิ 280 องศาเซลเซียส ความดัน 2 เมกาปาสกาล ได้ร้อยละการเปลี่ยนของแก๊สสังเคราะห์ ร้อยละ 28.56

สาขาวิชา เคมีเทคนิค

ปีการศึกษา 2563

ลายมือชื่อนิสิต

ลายมือชื่อ อ.ที่ปรึกษาหลัก

ลายมือชื่อ อ.ที่ปรึกษาร่วม

6072841023 : MAJOR CHEMICAL TECHNOLOGY

KEYWORD: LPG synthesis, Hybrid catalyst, CZZA, Y zeolite, CO₂ hydrogenation

Jaru Natakaranakul : DIRECT SYNTHESIS OF LPG FROM CO₂ BY USING CZZA AND HY ZEOLITE HYBRID CATALYST. Advisor: Prof. THARAPONG VITIDSANT, Ph.D. Co-advisor: Prof. Noritatsu Tsubaki, Ph.D.

CO₂ conversion to lower hydrocarbons (HCs) is a high-potential method that can significantly reduce and manage this greenhouse gas in the long term. Liquefied petroleum gas (LPG) is widely utilized in transportation. Furthermore, biomass appears to be more attractive for decreasing CO₂ emissions through conversion to liquid transportation fuels, as it is a renewable and sustainable energy source. The objectives of this work were to examine the direct synthesis of LPG from CO₂ hydrogenation using a mixed metal catalyst composed of copper, zinc oxide, zirconium, and alumina (CZZA), and an HY zeolite as a hybrid catalyst. The study tested four production conditions in a fixed bed reactor with hydrogen/CO₂/carbon monoxide as the reactant gas. The mixing between the CZZA and HY zeolite catalysts had a major impact on the HCs selectivity, significantly suppressing the reverse water gas shift reaction. A CO₂ conversion rate of 27.39 % was obtained at optimal conditions, along with high selectivity for HC (98.70 %) and LPG (66.56 %). The second part involved a pilot horizontal gasifier to evaluate the Biomass to Liquids Process (BTL). Due to the gasifier's temperature stability at 900 °C, the H₂/CO molar ratio remained constant between 1.75 and 2.25. Syngas was converted to liquid fuels at a conversion of 28.56 % in FT synthesis which was carried out at 280 °C and 2 MPa.

Field of Study: Chemical Technology

Student's Signature

Academic Year: 2020

Advisor's Signature

Co-advisor's Signature

ACKNOWLEDGEMENTS

The author wishes to express his profound gratitude and sincere appreciation to his advisor, Professor Dr. Tharapong Vitidsant, and co-advisor, Professor Dr. Noritatsu Tsubaki, for their invaluable helpful discussion, encouraging direction, and kind supervision during this work. Furthermore, the author wishes to express gratitude to Assoc. Prof. Dr. Prasert Reubroycharoen, Prof. Dr. Chawalit Ngamcharussrivichai, Prof. Dr. Napida Hinchiranan, and Dr. Rungravee Phienluphon for serving as dissertation chairman and member of the dissertation committee, respectively, and for their valuable advice and discussion.

The author appreciatively acknowledge the financial supports from the Research Program on Materials for Future Energy, Center of Excellent on Petrochemical and Materials Technology, Chulalongkorn University (PETROMAT), Japan International Cooperation Agency (JICA) and Japan Science and Technology Agency (JST) in the project of "Comprehensive Conversion of Biomass and Waste to Super Clean Fuels by New Solid Catalysts", Department of Applied Chemistry, School of Engineering, University of Toyama.

The author would also like to express his gratitude to the Department of Chemical Technology at Chulalongkorn University's Faculty of Science, the Department of Applied Chemistry at the University of Toyama's School of Engineering, and the Center of Fuels and Energy from Biomass at Chulalongkorn University for providing research facilities throughout this research.

Most importantly, the author wishes to express his appreciation to his family for their love, support, and encouragement throughout his graduate studies. In Addition, the author wishes to express his gratitude to his friends, who have consistently provided encouragement and support throughout this study.

Jaru Natakaranakul

TABLE OF CONTENTS

	Page
.....	iii
ABSTRACT (THAI).....	iii
.....	iv
ABSTRACT (ENGLISH).....	iv
ACKNOWLEDGEMENTS.....	v
TABLE OF CONTENTS.....	vi
LIST OF TABLES.....	xi
LIST OF FIGURES.....	xii
Chapter 1 Introduction.....	16
1.1. Introduction.....	16
1.2. Objectives.....	22
1.3. Research methodology and Experimental procedures.....	22
Chapter 2 Theory and Literature Reviews.....	23
2.1. Hydrocarbon synthesis from CO ₂ Hydrogenation.....	23
2.1.1. CO ₂ hydrogenation to methanol.....	24
2.1.1.1. Cu-based catalysts.....	25
2.1.1.2. Noble metal catalysts.....	28
2.1.1.3. Other catalytic systems.....	28
2.1.2. Methanol to hydrocarbons.....	29
2.1.2.1. Catalyst.....	29
2.1.2.2. Synthesis of olefins.....	30

2.1.2.3. Synthesis of LPG	30
2.1.2.4. Synthesis of gasoline	31
2.2. Biomass to Liquid Process (BTL)	33
2.2.1. Biomass Gasification to Produce Syngas	34
2.2.1.1. Fixed Bed Gasifiers.....	39
2.2.1.2. Downdraft Gasifier section.....	39
2.2.1.3. Fluidized Bed Gasifiers.....	40
2.2.1.4. Syngas Cleaning	43
2.2.2. Fischer-Tropsch Synthesis	45
2.2.2.1. FT mechanism.....	45
Alkyl mechanism.....	45
Alkenyl mechanism.....	46
Enol mechanism.....	46
CO-insertion mechanism.....	49
2.2.2.2. The Profile of FT Products.....	49
2.2.2.3. FT Catalyst	51
2.3. Litterature Review.....	53
Chapter 3 Experimental	57
3.1. Material and Reagents	57
3.1.1. Preparation of CZZA catalyst	57
3.1.2. Preparation of synthesis Na-Y zeolite.....	57
3.1.3. Biomass feedstock for gasification.....	58
3.2. Catalyst Preparation	58
3.2.1. Preparation of CZZA catalyst	58

3.2.2. Na-Y zeolite Synthesis Observation	59
3.3. Characterization	62
3.3.1. Catalyst characterization	62
3.3.1.1. X-ray Diffraction (XRD)	62
3.3.1.2. The Brunauer-Emmett-Teller (BET).....	63
3.3.1.3. Ammonia Temperature-Programmed Reduction (NH ₃ -TPD) and N ₂ O-titration measurements	64
3.3.1.4. Energy dispersive X-ray spectrometry (EDX)	65
3.3.2. Biomass characterization	65
3.4. CO ₂ hydrogenation investigation	67
3.5. BTL Process	70
3.5.1. Gasification Process and System Configuration	70
3.5.1.1. Laboratory scale gasification	71
3.5.1.2. Pilot scale gasification	71
3.5.1.2.1. Feeding system.....	74
3.5.1.2.2. Gasifier Reactor.....	74
3.5.1.2.3. Steam generator.....	75
3.5.1.2.4. Tar reformer	75
3.5.1.2.5. Gas cleaning unit.....	77
3.5.1.2.6. Gas compression unit.....	80
3.5.1.2.7. Gas storage tank.....	82
3.5.2. Experimental Setup	82
3.5.2.1. The Lab-scale Gasification	82
3.5.2.2. The pilot horizontal gasification	83

3.5.3. Fischer-Tropsch Synthesis and Process configuration	85
Chapter 4 Results and Discussion	88
4.1. Catalyst characterization	88
4.1.1. CZZA catalyst	88
4.1.2. NaY and HY Zeolite Characterization	90
4.1.3. Reaction conditions Investigation	92
4.1.3.1. Effect of the Mixing method	92
4.1.3.2. Effect of the reaction temperature.....	95
4.1.3.3. Effect of the CZZA: HY zeolite mass ratio.....	97
4.1.3.4. Effect of the W/F ratio.....	100
4.1.4. RWGS reaction Suppression.....	101
4.2. BTL Process.....	106
4.2.1. Biomass Gasification	106
4.2.1.1. Feedstock characterization.....	106
4.2.1.2. Influence of temperature on tar yield in lab-scale reactor.....	107
4.2.1.3. Investigation of Steam to Biomass ratio	109
4.2.1.4. Investigation of long-term operation gasification.....	110
Average syngas composition.....	111
Temperature profile	114
Material balance of syngas production	118
4.2.2. FT synthesis.....	121
Chapter 5 Conclusions and Recommendations	123
5.1. Conclusions.....	123

5.1.1. The effects of reaction parameters of direct synthesis of LPG from CO ₂ by using CZZA and HY zeolite as hybrid catalyst.....	123
5.1.2. The long-term operation of biomass to liquid process which combined with biomass gasification unit and Fischer-Tropsch synthesis	124
5.2. Recommendations.....	125
5.2.1. The effects of reaction parameters of direct synthesis of LPG from CO ₂ by using CZZA and HY zeolite as hybrid catalyst.....	125
5.2.2. The long-term operation of biomass to liquid process which combined with biomass gasification unit and Fischer-Tropsch synthesis	125
APPENDICES.....	126
REFERENCES	146
VITA.....	158

LIST OF TABLES

	Page
Table 1 Main Chemical Reactions Involved in Biomass Gasification Process	38
Table 2 Examples of Syngas Specifications Required for Specific Applications.....	44
Table 3 The EDX results of the CZZA mixed metal catalyst.....	89
Table 4 The BET surface area and pore characteristics of the catalysts.....	90
Table 5 Metallic properties of the reduced CZZA.....	90
Table 6 Reaction results with difference inlet gas composition	105
Table 7 Characteristics of Biomass	107
Table 8 Product yield and gas composition of variation temperature.....	109
Table 9 Gasification results for two differences of Steam/Biomass	111
Table 10 Summary of gasification conditions and results for two types of biomass.....	119
Table 11 Characteristics of Bio char	120
Table 12 Composition of liquid products from FT synthesis.....	121

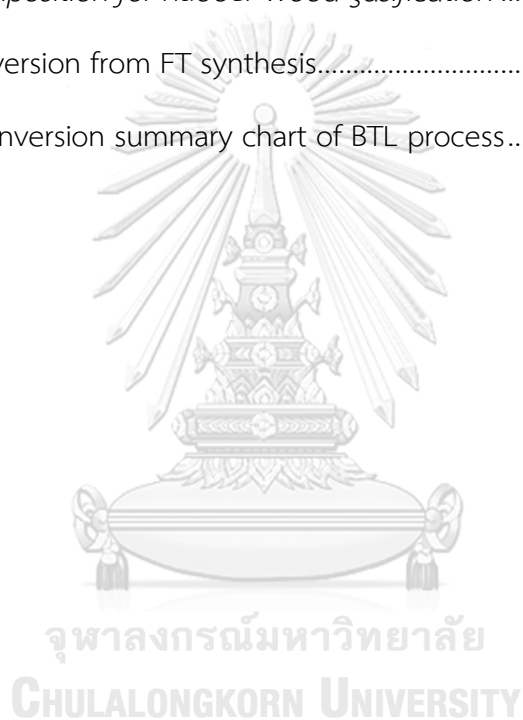
LIST OF FIGURES

	Page
Figure 1 Primary energy consumption by source	17
Figure 2 World energy consumption by energy source (1990-2040).....	19
Figure 3 Carbon emissions by sector	19
Figure 4 Production of Hydrocarbons via a variety of CO ₂ hydrogenation techniques (olefins, LPG, gasoline, aromatics, etc).....	24
Figure 5 Proposed chemical method for producing methanol from CO ₂ utilizing a Cu/ZrO ₂ catalyst.....	27
Figure 6 Pathways for producing methanol from CO ₂ /H ₂ using a palladium/gallia catalyst.....	27
Figure 7 On the D ₄ faulty In ₂ O ₃ (110) surface, there are potential energy surfaces for CO ₂ hydrogenation to methanol.....	29
Figure 8 CO ₂ hydrogenation into hydrocarbons at the molecular level using an In ₂ O ₃ /HZSM-5 bifunctional catalyst.	32
Figure 9 The effect of the active components' integration method	33
Figure 10 Overall process block diagram for the Fischer-Tropsch synthesis.....	35
Figure 11 Schematic of the multistage production process of syngas or H ₂ from biomass gasification. [41].....	36
Figure 12 Schematic representation of the main processes involved in a biomass gasifier.	36
Figure 13 Schematic of a downdraft gasifier.....	40
Figure 14 Schematic of the dual fluidized bed gasification process.	42
Figure 15 Alkyl mechanism	47
Figure 16 Alkenyl mechanism.....	47

Figure 17 Enol mechanism	48
Figure 18 CO-insertion mechanism.....	48
Figure 19 (a) Anderson-Schulz-Flory (ASF) plot and (b) FT product distribution	52
Figure 20 Schematic flow chart of CZZA catalyst preparation by co-precipitation method.....	60
Figure 21 Schematic flow chart of NaY zeolite.....	61
Figure 22 X-ray Diffraction (XRD), Rigaku RINT2000	62
Figure 23 N ₂ adsorption-desorption, Quantachrome Nova 2200e	63
Figure 24 Ammonia Temperature-Programmed Reduction (NH ₃ -TPD).....	64
Figure 25 Energy dispersive X-ray spectrometry (EDX).....	65
Figure 26 Heating value analysis, Leco - AC500.....	66
Figure 27 Ultimate analysis, element analyzer (Leco - CHNS 628).....	66
Figure 28 Gas chromatograph equipped with TCD.....	68
Figure 29 Gas chromatograph equipped with FID	68
Figure 30 Physical mixing methods for CZZA catalyst.....	69
Figure 31 Schematic flow chart of LPG synthesis fixed bed reactor	70
Figure 32 Schematic flow chart of laboratory-scale batch fixed bed gasifier.....	72
Figure 33 The schematic view of pilot horizontal gasification unit	73
Figure 34 Feeding system	74
Figure 35 Horizontal gasifier	75
Figure 36 Steam generator.....	76
Figure 37 Tar reformer	76
Figure 38 Water scrubber.....	78
Figure 39 Gas cooler	79

Figure 40 Set of Gas cleaning Unit	79
Figure 41 H ₂ O remover	80
Figure 42 The first gas compression unit	81
Figure 43 The second gas compression unit.....	81
Figure 44 Gas storage tanks (Buffer Tank).....	82
Figure 45 FT flow chart	87
Figure 46 XRD pattern of calcined CZZA.....	89
Figure 47 Representative XRD patterns of the (a) com-HY, (b) syn-NaY zeolites	91
Figure 48 Representative N ₂ adsorption (●) – desorption (x) isotherm of com- HY ..	91
Figure 49 Representative NH ₃ -TPD profiles of the (a) syn-NaY and (b) com-HY zeolites	92
Figure 50 The influence of various catalyst mixing techniques on reaction results ...	94
Figure 51 Carbon distribution in produced HC products using various catalyst mixing techniques.....	95
Figure 52 The influence of various Temperature on reaction results.....	96
Figure 53 Carbon distribution in produced HC products using various different reaction temperatures.....	97
Figure 54 The influence of various CZZA: HY zeolite mass ratios on reaction results	99
Figure 55 Carbon distribution in produced HC products using various different CZZA: HY zeolite mass ratios	99
Figure 56 The influence of various W/F ratios on reaction results.....	100
Figure 57 Carbon distribution in produced HC products using various different W/F ratios.....	101
Figure 58 Chromatogram of products from LPG synthesis	104
Figure 59 Overall gas composition of Eucalyptus gasification for 7 days operation .	112

Figure 60 Overall gas composition of Rubber Wood gasification for 7 days operation	113
Figure 61 Temperature profile at gasifier zone for Eucalyptus gasification.....	115
Figure 62 Temperature profile at tar reformer zone for Eucalyptus gasification.....	116
Figure 63 Pressure accumulation in Buffer Tank for Eucalyptus gasification	116
Figure 64 Gas composition for Eucalyptus gasification.....	117
<i>Figure 65 Gas composition for Rubber Wood gasification</i>	<i>117</i>
Figure 66 CO conversion from FT synthesis.....	122
Figure 67 Mass conversion summary chart of BTL process.....	122



Chapter 1

Introduction

1.1. Introduction

According to BP's report on the global energy situation, there are three main scenarios (shown in Figure 1): The Rapid Transition Scenario (Rapid) proposes a series of policy measures, led by a significant increase in carbon prices and complemented by more targeted sector-specific measures, that result in carbon emissions from energy use falling by around 70% by 2050. The Net Zero Scenario (Net Zero) proposes a series of policy measures, led by a significant increase in carbon prices and complemented by The Business-as-Usual Scenario (BAU) is based on the assumption that government regulations, technology, and societal preferences continue to change at the same rate and magnitude as in the recent past. Energy usage was discovered to be increasing constantly in all three scenarios for the next 30 years. Primarily, energy derived from fossil fuels (oil, natural gas, and coal) will remain high in 2050, at 480 EJ under the BAU scenario. Additionally, burning fossil fuels contributes directly to global climate change by releasing greenhouse gases (carbon dioxide, CO₂) into the atmosphere and forming a greenhouse dome, reflecting heat radiation back to the earth, resulting in an increase in the average world temperature [1].

Additionally, the Thai energy situation was presented in the 2020 annual report by the General of Energy Policy and Planning Office of the Thai Ministry of Energy, which was titled Trend of primary energy consumption in Thailand. The statistics indicated that the demand for energy consumption tends to increase year after year as the economic size and population expand [2].

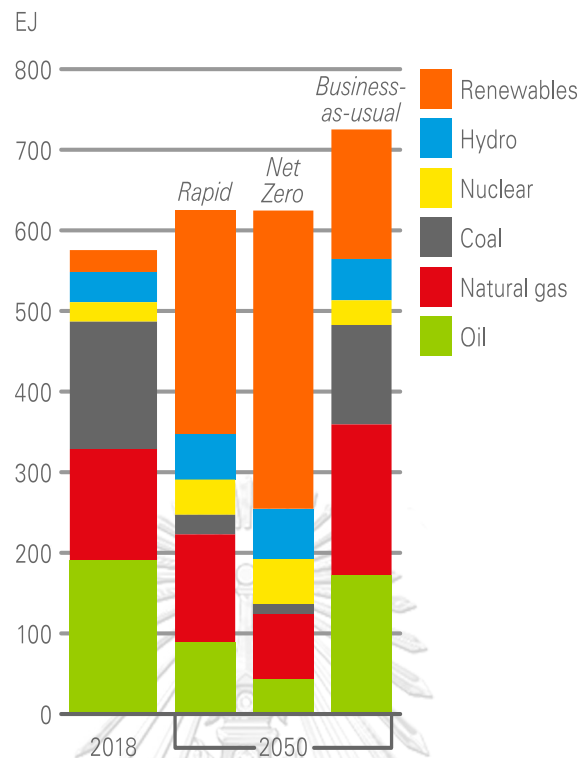


Figure 1 Primary energy consumption by source [1]

Due to the severity of climate change caused by the use of non-renewable energy, alternative energy has been investigated for many years in order to identify a high-potential source of substitute energy. Biomass is a well-known resource for generating fresh energy. According to the EIA's World Energy Consumption by Energy Source (1990-2040), renewable energy sources appear to be more appealing owing to the rising consumption level seen in Figure 2. Furthermore, according to BP's assessment on primary energy consumption by source, renewable sources appear to account for a sizable portion of energy consumption in Rapid and Net Zero scenarios. Biomass should be considered an alternate energy source due to its rapidly renewable nature. Numerous biomass species have a rapid growth rate and a short harvest cycle, for example, Eucalyptus and Leucaena, which can crop in as little as 2-3 years. Additionally, biomass includes agricultural wastes such as cassava root and corn crop,

which are capable of being converted into alternative energy sources. However, utilizing biomass still emits CO₂, but another biomass may absorb it and use it to grow.

The many biomass conversion processes result in the production of energy or fuels, including fast pyrolysis, direct liquid fractionation, transesterification of vegetable oils, bioethanol from agricultural crops, biooil from algae, and the Fischer Tropsch (FT) process for converting biomass from syngas to higher hydrocarbons. The most interesting method, however, is the conversion of biomass to liquid fuels via the FT process using biomass syngas or BTL. BTL is a process that transforms biomass to synthesis gas (syngas), which is a mixture of hydrogen (H₂) and carbon monoxide (CO), by gasification, which is a technique for converting solid fuels (coal, biomass, plastic, or trash) into a gaseous fuel. It is accomplished by heating the material to a high temperature (>950 K) in the presence of a gasification agent in a regulated amount [13]. Following that, syngas was compressed in the Fischer-Tropsch synthesis process to generate hydrocarbon products such as gasoline, diesel, and jet fuel. However, during the biomass gasification process, elevated CO₂ levels in syngas were discovered due to the high oxygen content of the biomass feedstock. Additionally, a high %age of CO₂ in syngas is likely to dilute the syngas concentration in the product stream. Additionally, CO₂ is a relatively inert gas that is stable in the majority of reaction types. Thus, a large CO₂ output from biomass gasification is a concern for biomass conversion. In addition, CO₂ is raised in the atmosphere shown in Figure 3 due to increasing fossil fuel according to the BP report. CO₂ was reported, which tends to increase in the future. However, CO₂ is a vast carbon resource. Thus, there is a lot of research interesting in converting CO₂ to liquid fuels.

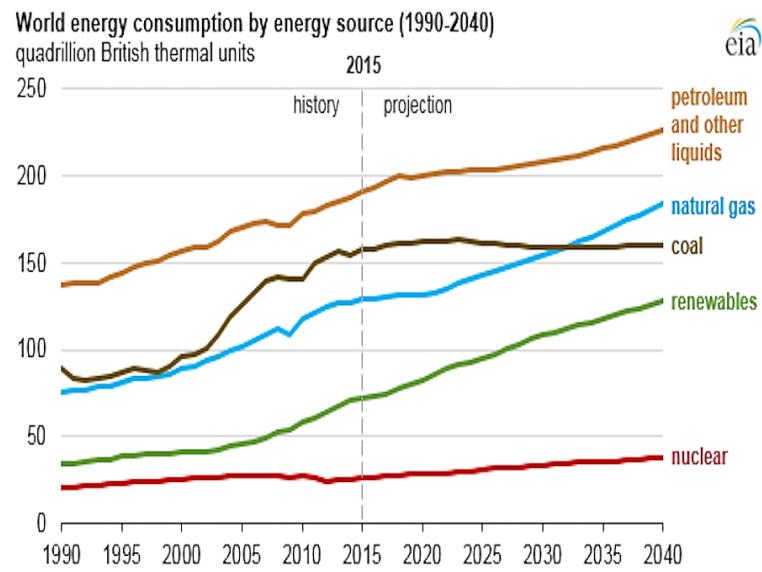


Figure 2 World energy consumption by energy source (1990-2040) [3]

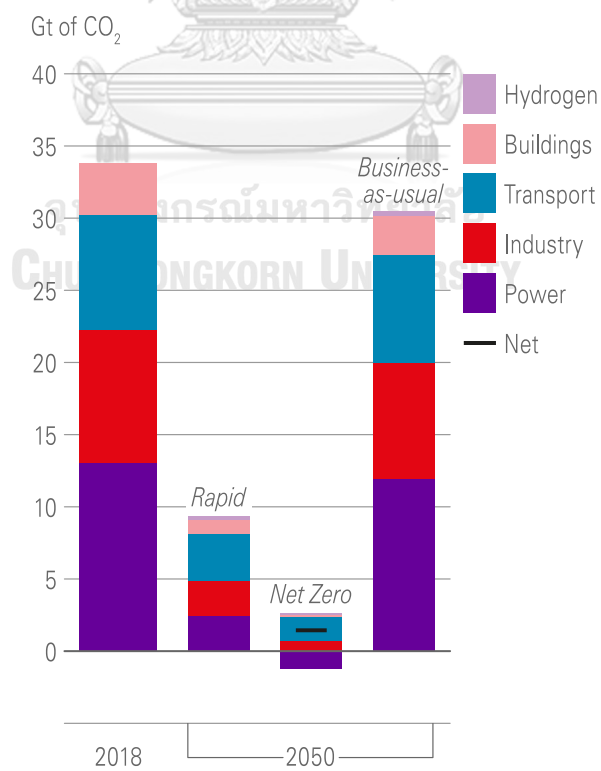


Figure 3 Carbon emissions by sector [1]

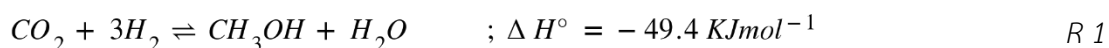
There are two methods for converting carbon dioxide to liquid fuels. The FT process begins with the conversion of CO_2 to CO via the reverse water gas shift (RWGS) reaction, and then transforms CO to hydrocarbons via the FT synthesis process. Regrettably, the distribution of hydrocarbon products via this pathway is always governed by the Anderson-Schulz-Flory (ASF) distribution [4]. As a result, it is incapable of accurately predicting or specifying any hydrocarbon %age. On the other side, the Hydrogenation route is the second mechanism for converting CO_2 to hydrocarbons. CO_2 was first converted to methane using an active metal catalyst, and then to hydrocarbons via the Dimethyl Ether intermediate route in collaboration with an acid zeolite catalyst. This technique may be used to choose desired hydrocarbon products such as LPG gasoline or long-chain hydrocarbons by selecting a zeolite with the appropriate properties.

Several hydrocarbon compounds have been utilized as fuel. For instance, gasoline and diesel are utilized in engines for transportation and generation of power. Additionally, LPG, or Liquefied Petroleum Gas, is a significant chemical raw material and a source of alternative clean energy with a wide range of applications. The combination of propane and butane results in a high consumption level due to its widespread use in transportation, cooking, industrial, and residential facilities (heating and cooking). There are, however, few research on generating from renewable sources [5].

As mentioned previously, there are numerous related processes for hydrogenation of CO_2 to a hydrocarbon, as illustrated in *R 1-R 4* [6]. Thus, two distinct types of catalysts are required for this reaction. The first is a metal catalyst for hydrogenation of CO_2 to methanol (see *R 1*), which is also referred to as a methanol synthesis catalyst. These catalysts have been studied extensively for a long period of time. There are several types of active metals with great potential, for example, cobalt- and iron-based catalysts. However, this work is intriguing because of the inexpensive

cost, excellent methanol selectivity, and great stability of the Copper/Zinc oxide base catalyst. In case of zeolite catalyst, zeolite was chosen according to the shape selectivity property of each zeolite type such as SAPO-5, SAPO-44, and HZSM-5 for the direct synthesis of hydrocarbons from CO₂ hydrogenation via methanol [7-10]

MeOH synthesis reaction (MS):



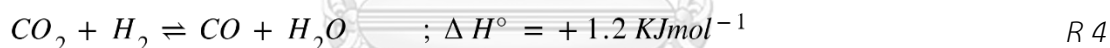
MeOH dehydration reaction (MD):



DME conversion to HCs:



Reverse water gas shift reaction (RWGS):



This research, according to the mansion above, was divided into two sections. The first section examined the influence of reaction parameters on the direct synthesis of LPG from CO₂ using a hybrid catalyst composed of Cu/ZnO/ZrO₂/Al₂O₃ (CZZA) and HY zeolite. The accomplishments of this section are intended to result in the identification of an optimal condition for CO₂ conversion that is compatible with LPG selectivity and will be used to syngas from biomass gasification in FTS. The second section examined the BTL process, which entails a biomass gasification unit and a FTS unit with the aim of producing hydrocarbons.

1.2. Objectives

1. To study the effects of reaction parameters of direct synthesis of LPG from CO₂ by using CZZA and HY zeolite as hybrid catalyst
2. To investigate long-term operation of biomass to liquid process which combined with biomass gasification unit and Fischer-Tropsch synthesis

1.3. Research methodology and Experimental procedures

1. Literature review
2. Prepare all tools, equipment, and chemical reagents required for the experiment.
3. Study the effects of reaction parameters of direct synthesis of LPG from CO₂ by using CZZA and HY zeolite hybrid catalyst on selectivity of LPG and CO₂ conversion
 - a. CZZA catalyst preparation
 - b. Na-Y zeolite preparation
 - c. Investigate the effect of reaction conditions following
 - i. Catalyst mixing method with Mix A, Mix B and Mix C
 - ii. Reaction temperature at 310 °C, 330 °C and 360 °C
 - iii. CZZA:HY zeolite mass ratio at 2:1, 1:1, 1:2, and 1:4
 - iv. Catalyst weight/feed flow rate (W/F) at 5, 10 and 15 gh/mol
 - d. Characterize the properties of catalysts by N₂ physisorption, X-ray diffraction (XRD), temperature programmed desorption (TPD), and energy dispersive X-ray spectrometer (EDX)
4. Study long-term operation of Biomass to Liquid Process which combined with biomass gasification unit and Fischer-Tropsch Synthesis
5. Write manuscripts and dissertation

Chapter 2

Theory and Literature Reviews

2.1. Hydrocarbon synthesis from CO₂ Hydrogenation

There are many methods for obtaining hydrocarbons from CO₂ hydrogenation (Figure 4). In general, the CO₂ hydrogenation process involves two concurrent processes: methanol synthesis (R 1) and reverse water-gas shift. (R 4, RWGS). Directly from syngas (CO + H₂) using FT synthesis (FTS) is one option, but industrial methanol syntheses and chemical modifications of methanol to a variety of hydrocarbons using MTH processes, which include the methanol-to-olefin (MTO) and methanol to propene (MTP) processes, are two other options that could be used (MTP). Methanol-to-gasoline (MTG) conversion is another option. Methanol and dimethyl ether have also been used to create aromatic or lower paraffin hydrocarbons (DME) [11-13].

CO₂ hydrogenation to methanol and MTH procedures may also generate a variety of hydrocarbons indirectly. An FTS-based direct approach (CO₂-FTS) has recently been discovered for converting CO₂ to hydrocarbons without the need of catalysts. CO₂ is reduced to CO through the RWGS reaction, followed by the FTS reaction, which converts CO to hydrocarbons. As a result, both the RWGS and FTS catalysts employed in the reactions must be active. As a result, it is feasible to achieve direct one-step hydrocarbon production from CO₂ hydrogenation by using both methanol catalysts and zeolites.

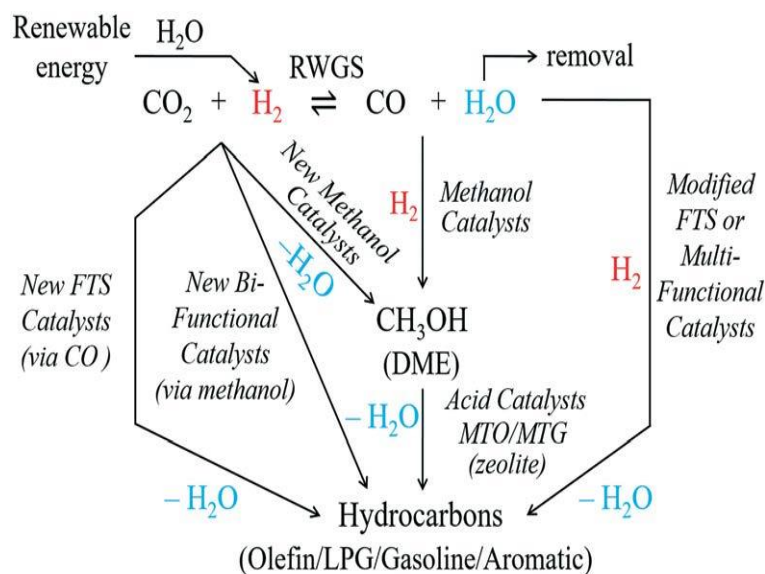


Figure 4 Production of Hydrocarbons via a variety of CO_2 hydrogenation techniques (olefins, LPG, gasoline, aromatics, etc). [14]

2.1.1. CO_2 hydrogenation to methanol

At pressures of about 6 MPa and temperatures of around 250 °C, the $\text{Cu}/\text{ZnO}/\text{Al}_2\text{O}_3$ catalyst system is utilized in the industrial synthesis of methanol. For almost 40 years, the industry has conducted significant study. CO_2 replacement as a feedstock for CO_2 usage in methanol synthesis is a feasible option. Unlike methanol synthesis from syngas, direct CO_2 hydrogenation produces water vapor, which significantly slows the process and causes substantial catalyst deterioration. Additionally, other byproducts such as CO and hydrocarbons are generated during the hydrogenation of CO_2 . It is therefore necessary to use an effective catalyst in order to enhance catalytic stability and decrease the formation of undesired by-products throughout the methanol synthesis process, which demands either constant tuning or the invention of a new catalyst system.

When methanol is synthesized industrially, the $\text{Cu}/\text{ZnO}/\text{Al}_2\text{O}_3$ catalyst combination is used at a pressure of approximately 6 MPa and a temperature of around 250 °C. The industry has been doing extensive research for over 40 years [15]. Methanol

synthesis using CO₂ as a feedstock is an approach that is viable. The direct CO₂ hydrogenation process, on the other hand, generates water vapor, which substantially slows down the process and deteriorates the catalytic material [16]. During the hydrogenation of CO₂, additional byproducts such as CO and hydrocarbons are produced. It is therefore necessary to use an effective catalyst in order to enhance catalytic stability and decrease the formation of undesired by-products throughout the methanol synthesis process, which demands either constant tuning or the invention of a new catalyst system.

These catalysts are divided into three categories: Cu-based catalysts, which are essentially methanol catalysts for CO hydrogenation, with Cu species serving as the major active component; noble metal-based catalysts, such as Pd and Pt; and oxygen-deficient catalysts. Unlike the In₂O₃/ZrO₂ catalytic system, this type of catalyst has a distinct reaction mechanism.

2.1.1.1. Cu-based catalysts.

Copper alone is inefficient in the synthesis of methanol from CO₂ because of its poor methanol selectivity, catalytic activity, and stability. Cu/ZnO and further modified catalysts that are used in industry as a catalyst for CO₂ hydrogenation into methanol or as a model catalyst for theoretical research are still being explored. Copper dispersion and stability can be improved with ZnO. A ZnO lattice has an open oxygen vacancy and an electron pair that can be used in the synthesis of methanol. Defects in the ZnO overlayer can have a significant influence on its stability [17]. As a result, Zn migration to the Cu surface is closely connected to the formation of stable Cu-ZnO interfaces and Cu-ZnO_x active sites during reduction and evaluation. A Cu-Zn active nanoalloy layer was produced on the Cu-ZnO nanoclusters, decreasing the activation energy for CO adsorption. To enhance the production of dimethyl ether

from syngas, the surface alloy layer and Cu–ZnO sites work in concert [18, 19]. A Cu–Zn surface alloy and a $\text{Cu}_x\text{Zn}_{(1-x)}\text{O}_y$ active phase are commonly accepted as the active sites for methanol synthesis.

For the methanol synthesis catalyst, zirconia has also been explored because of its excellent stability in reducing and oxidizing environments. To enhance surface area and improve dispersion, ZrO_2 can be added to Cu-based catalysts. In addition, the crystal morphologies of Zr have an impact on the catalyst's efficiency. Only the oxygen vacancy in t- ZrO_2 promoted copper atoms into the ZrO_2 lattice, resulting in stable Cu^+ . To increase yield and selectivity of methanol, the Cu/t- ZrO_2 interaction will result in a Cu– ZrO_2 interface containing oxygen vacancies.

A simplified approach for the catalyst surface and reaction channels is depicted in Figure 5 [20]. Adsorption of CO_2 on the surface of ZrO_2 results in the formation of a bicarbonate species, which is subsequently hydrogenated to create a formate intermediate species [21]. The hydrogen needed for the production of formate species may be provided by adsorption hydrogen overflow on Cu [22, 23].

X-ray diffraction (XRD) studies by Koepfel et al. indicated that active copper species exist mostly as Cu^0 rather than Cu/ZrO_2 [24]. Using static low-energy ion scattering studies, it was hypothesized that Cu^+ is the active component in a Cu/ZnO/ SiO_2 catalyst [25]. Cu metal, as well as low valence Cu, may all have an effect on the catalytic activity of Cu-based oxide catalysts [26, 27]. The first step in rationally constructing a high activity and selectivity catalyst is to determine the electrical and geometric properties of the active site [28].

The formate route, in which the rate-determining step is typically regarded to be intermediate HCOO production [23, 29-31]. Bidentate formate is the most stable adsorbed species on Cu, whereas monodentate formate is the most stable on ZnO [32]. The formate route is employed in the process, which results in the formation of HCOO, H_2COO (dioxomethylene), CH_3O (methoxy), and finally CH_3OH (Figure 6). The

high activity and selectivity of the Pd/b-Ga₂O₃ catalyst are due to the effective spillover of atomic hydrogen from the Pd surface to the carbonaceous species and the limited stability of methoxy species on Ga₂O₃. HCOO and H₂COO hydrogenation are both rate-determining processes, according to DFT studies on Cu(111) and Cu nanoparticles [33]. Cu nanoparticles exhibit higher methanol synthesis activity than Cu(111) due to active corner sites and structural flexibility, which stabilize the critical intermediates (HCOO, H₂COO, and CH₂O) and lower the barrier for the rate-determining steps.

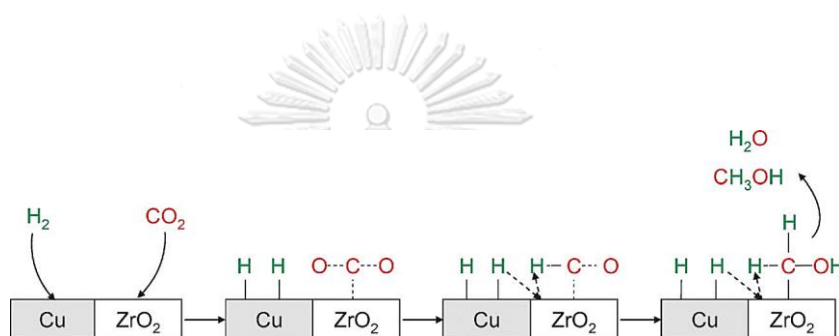


Figure 5 Proposed chemical method for producing methanol from CO₂ utilizing a Cu/ZrO₂ catalyst. [14]

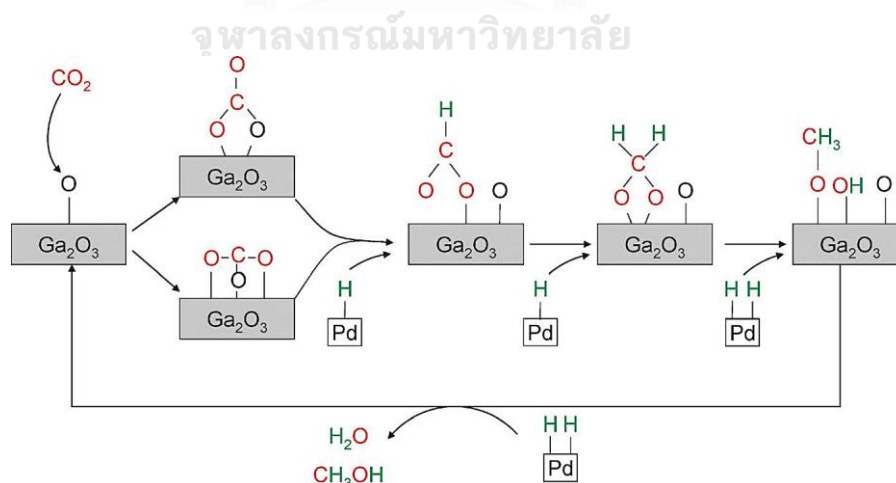


Figure 6 Pathways for producing methanol from CO₂/H₂ using a palladium/gallia catalyst. [14]

2.1.1.2. Noble metal catalysts.

Because of their high activity and selectivity for hydrogenation of CO₂ to methanol, Pd-based catalysts are the most commonly employed. The study of structure-activity relationships for CO₂ hydrogenation on a variety of Pd/ZnO catalysts. The results showed that the PdZn alloy produced during the reaction or high-temperature pretreatment significantly decreased CO generation during the RWGS process and served as the active site for methanol synthesis. Furthermore, the PdZn alloy's smaller particle size, lower surface metallic Pd concentration, and larger surface area all helped to increase methanol selectivity.

2.1.1.3. Other catalytic systems

In addition to classic copper and noble metal-based catalysts, several CO₂ hydrogenation catalysts based on novel reaction mechanisms and catalytic designs have been discovered in recent years. Using periodic DFT simulations, Ge et al. [34] explored the production of methanol from CO₂ hydrogenation on a malfunctioning In₂O₃(110) surface with surface oxygen vacancies (Figure 7). The technique for generating methanol on the D₄ surface with the O_{v4} oxygen defective site varies considerably from previous copper-based catalysts, and the O_{v4} oxygen defective site has been shown to be more beneficial for CO₂ activation and hydrogenation. The O_{v4} oxygen deficient site on the surface of In₂O₃(110) generally aids in the activation and hydrogenation of CO₂ as well as the stability of the critical intermediates involved in methanol production. To create and stabilize the most thermodynamically unstable O_{v4} oxygen deficient site cycle, ZrO₂ was introduced. In the hydrogenation of CO₂ to methanol, the catalysts exhibit high methanol selectivity (100%) and stability (1000 h).

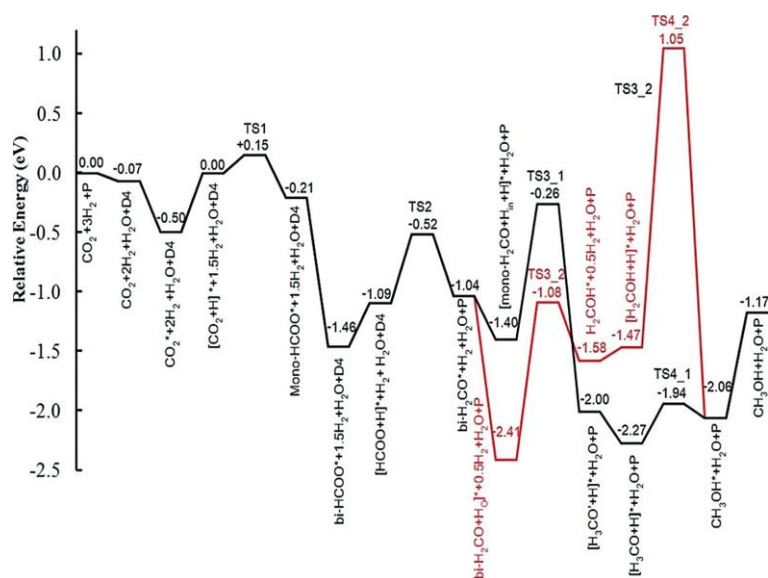


Figure 7 On the D_4 faulty $\text{In}_2\text{O}_3(110)$ surface, there are potential energy surfaces for CO_2 hydrogenation to methanol. [34]

2.1.2. Methanol to hydrocarbons

Methanol or its dehydration product, dimethyl ether (DME), can be utilized as a feedstock in the synthesis of a variety of hydrocarbons, including lower olefins, gasoline-range hydrocarbons, branched alkanes, and aromatics. The architecture of the zeolite, as well as the operating circumstances, dictate the selectivity for any of these chemical groups. The MTH method is based on the concept of controlling product selectivity and enhancing catalytic stability through the development of high-performance catalysts and the optimization of reaction conditions. In the next part, we will look at the catalyst and reaction mechanism of MTH.

2.1.2.1. Catalyst

Zeolite catalysts' behavior is influenced by their shape selectivity, three-dimensional structure, stability, and acidity characteristics, all of which may be altered under controlled circumstances. Medium-pore zeolite/microporous materials generate hydrocarbons in the $\text{C}_5\text{--C}_{11}$ range, whereas small-pore molecular sieves produce

hydrocarbons in the C_2 – C_4 range. A number of catalysts are employed, the most notable of which are the ZSM-5 (MTG-directed) and SAPO-34 molecular sieves (MTO directed).

2.1.2.2. *Synthesis of olefins*

Lower olefins are important carbon-based building blocks that are widely employed in the chemical industry. Historically, they were made by thermal or catalytic cracking of a variety of hydrocarbon feedstocks, including naphtha, gas oil, condensates, and light alkanes [35-37]. Inui et al. [38] explored the one-pass methanol synthesis of lower olefins from a $CO_2 + H_2$ mixture. The selective synthesis of olefin, according to the researchers, required a moderately acidic and tiny pore microporous crystalline catalyst, such as SAPO-34. A bifunctional catalyst made of In_2O_3 and SAPO-34 with high selectivity and activity may enable the direct synthesis of lower olefins via CO_2 hydrogenation. The selectivity of C_2 – C_4 olefins was around 76.9 percent, compared to a significantly lower CH_4 selectivity of 4.4 percent, although CO_2 conversion was greater than 34 percent [39].

2.1.2.3. *Synthesis of LPG*

LPG is an excellent fuel option for spark ignition engines, and it has the potential to replace aerosol propellants and refrigerants. As a result, direct LPG synthesis from CO_2 hydrogenation is an intriguing technique of turning the world's most plentiful carbon resource into extremely valued chemicals. Jeon et al. studied the catalytic performance of hybrid catalysts made up of methanol synthesis catalysts (such as $Cu/ZnO/ZrO_2$ and $Cu/ZnO/Al_2O_3$) and zeolites (such as SAPO-5, SAPO-44, and HZSM-5) for the direct synthesis of hydrocarbons from CO_2 hydrogenation via methanol. They observed that the most abundant product on hybrid catalysts, including SAPO-

44, was propane. Because of the differences in acidity and pore size between the two zeolites, isobutene was the dominant product on hybrid catalysts containing SAPO-5. Li et al. investigated the selective production of LPG using hybrid catalysts composed of a Zr-modified Cu–Zn–Al methanol catalyst and a Pd-modified zeolite (Pd-). The hybrid catalyst was shown to be active and stable for LPG synthesis at low temperatures (260 °C), with CO₂ conversion and hydrocarbon yields reaching up to 25.2 and 13.3 percent, respectively. Simultaneously, the selectivity of LPG was as high as 75%, with just 1% CH₄ generated, indicating that a methanol catalyst with zeolite was correctly utilized. The quantity of acid sites in the zeolite, according to Park et al., mainly determined hydrocarbon production. Furthermore, they discovered that in the case of the hybrid catalyst composed of Cu/ZnO/ZrO₂ and SAPO zeolite, the primary product was C₃ or C₄ hydrocarbons, showing that the SAPO zeolite functioned via the carbon pool mechanism [38, 39].

2.1.2.4. *Synthesis of gasoline*

Gasoline is an important transportation fuel that is used all over the world. Systems that combine methanol synthesis catalysts and zeolites can boost C₂₊ hydrocarbon yields by combining methanol synthesis with the MTG reaction. To obtain a gaseous fuel from CO₂ hydrogenation, a catalyst system consisting of a methanol synthesis catalyst (Pd–Na-modified Cu–Cr–Zn oxides) and a typical MTG catalyst (H-ZSM-5) was used, and the selectivity of C₂₊ hydrocarbons among the yielded hydrocarbons was up to 71.8 percent higher than the above composite catalysts. Fujiwara et al. used a Cu–Zn–Cr-oxide/zeolite composite catalyst system to study the hydrogenation of carbon dioxide (CO₂). Under reaction conditions of 400 °C, 0.5 MPa, H₂/CO₂ = 3, and 3000 ml.h⁻¹.gcat⁻¹, they discovered that Cu–Zn–Cr/HY performed the best for CO₂ hydrogenation, with CO₂ conversion and hydrocarbon selectivity of 39.9

percent and 12 percent, respectively, and a selectivity of C_{2+} hydrocarbons of up to 95.8 percent. It was also determined that the MTG reaction and methanol breakdown into CO were responsible for the production of C_{2+} hydrocarbons [39].

When oxygen vacancies on In_2O_3 surfaces combine with CO_2 and H_2 , methanol is generated, and further C–C coupling occurs inside the pores of the zeolite to produce gasoline-range hydrocarbons (Figure 8). The critical stages of methanol synthesis are more stable on the faulty In_2O_3 surface than on the Cu surface, considerably limiting CO production. As a result, at 340 °C, the CO selectivity over In_2O_3 integrated with the zeolite (45%) is significantly lower than the selectivity over conventional Cu-based catalysts (>90%). Furthermore, bringing the two components closer together (as seen in Figure 9) decreased CO selectivity while increased C_{5+} selectivity. When the distance between the two components was reduced further (mortar mixing), the number of extremely acidic sites on the spent catalyst fell significantly, resulting in severe deactivation and very poor C_{5+} hydrocarbon selectivity.

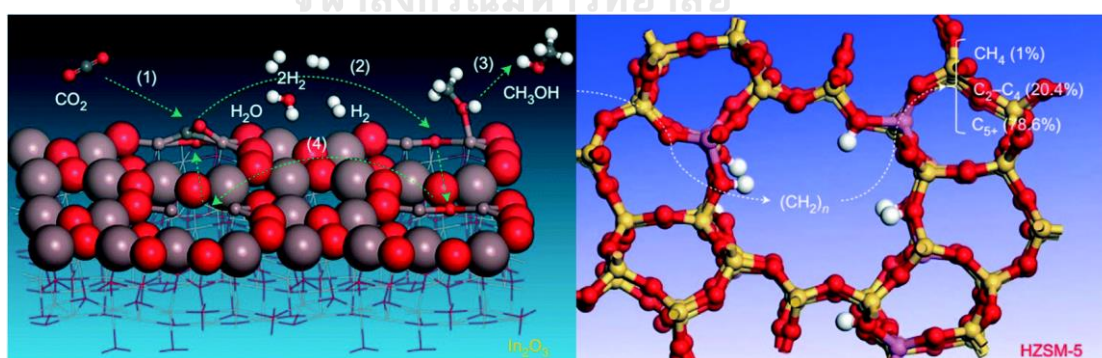


Figure 8 CO_2 hydrogenation into hydrocarbons at the molecular level using an In_2O_3 /HZSM-5 bifunctional catalyst. [39]

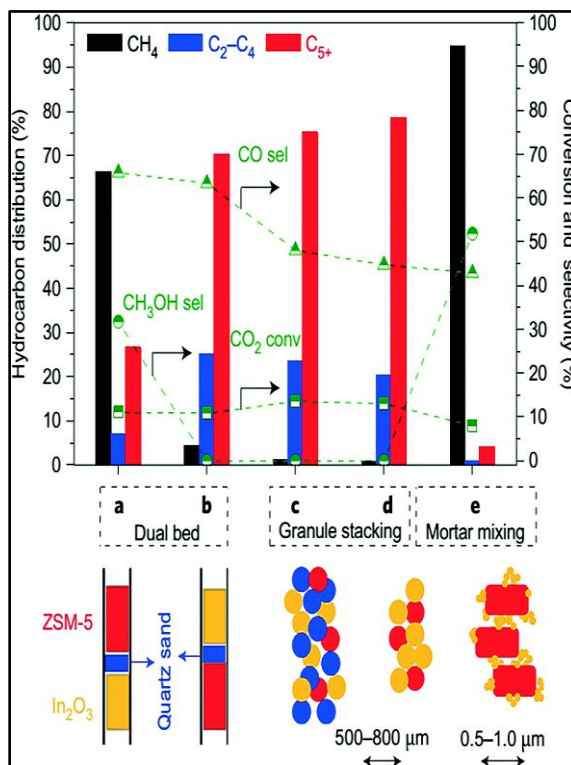


Figure 9 The effect of the active components' integration method[39]

2.2. Biomass to Liquid Process (BTL)

FTS is one method for creating synthetic transportation fuels. In 1925, Franz Fischer and Hans Tropsch invented this approach at Germany's Kaiser-Wilhelm Institut für Kohlenforschung. This method entails turning synthesis gas, which contains hydrogen and carbon monoxide, into long-chain (straight or branched) hydrocarbon products, essentially gasoline and diesel. This technique comprises of three main steps: (i) the generation of synthesis gas, (ii) the FT reaction, and (iii) product upgrading. Despite the fact that this technology has been around for a century, interest in it has recently increased owing to the depletion of fossil fuel sources, rising crude oil costs, and environmental concerns. Another element that adds to its appeal is the potential of the technique to use stranded and distant natural gas reserves. The net FT

technique consists of three steps. A typical process block diagram is shown in Figure 10.

2.2.1. Biomass Gasification to Produce Syngas

The biomass gasification process involves the partial oxidation of biomass at high temperatures (generally between 600 and 900 °C or higher) in the presence of a gasifying agent (for example, air, oxygen, steam, or CO₂, or mixtures of these components), resulting in the production of syngas or producer gas containing CO, H₂, CO₂, CH₄, and N₂. Because gaseous fuel requires air to be produced, it includes more N₂ and less CO, H₂, CO₂, and CH₄ than syngas [40]. Syngas, as opposed to producer gas, which is commonly used to generate power and/or heat, is used to manufacture fuels and chemicals. Syngas is created by purifying and conditioning the raw gases produced during biomass gasification. The major phases of a typical gasification process are depicted in Figure 11, which include fuel preparation, gasification, gas cleaning, and gas conditioning.

Biomass gasification entails a complex series of thermochemical reactions that are closely interconnected. The biomass gasification process may be characterized as follows, independent of the type of gasifier used: (i) drying of biomass particles, (ii) pyrolysis of dried biomass particles, also known as devolatilization, (iii) partial oxidation of pyrolysis gases and/or char, and (iv) reduction of char. This basic definition applies to the vast majority of gasification systems that operate at low pressures and obtain their energy from the burning of a portion of biomass-derived fuels. Figure 12 illustrates the interactions between the various stages of a typical biomass gasification process. Table 1 summarizes the key chemical processes involved in biomass gasification.

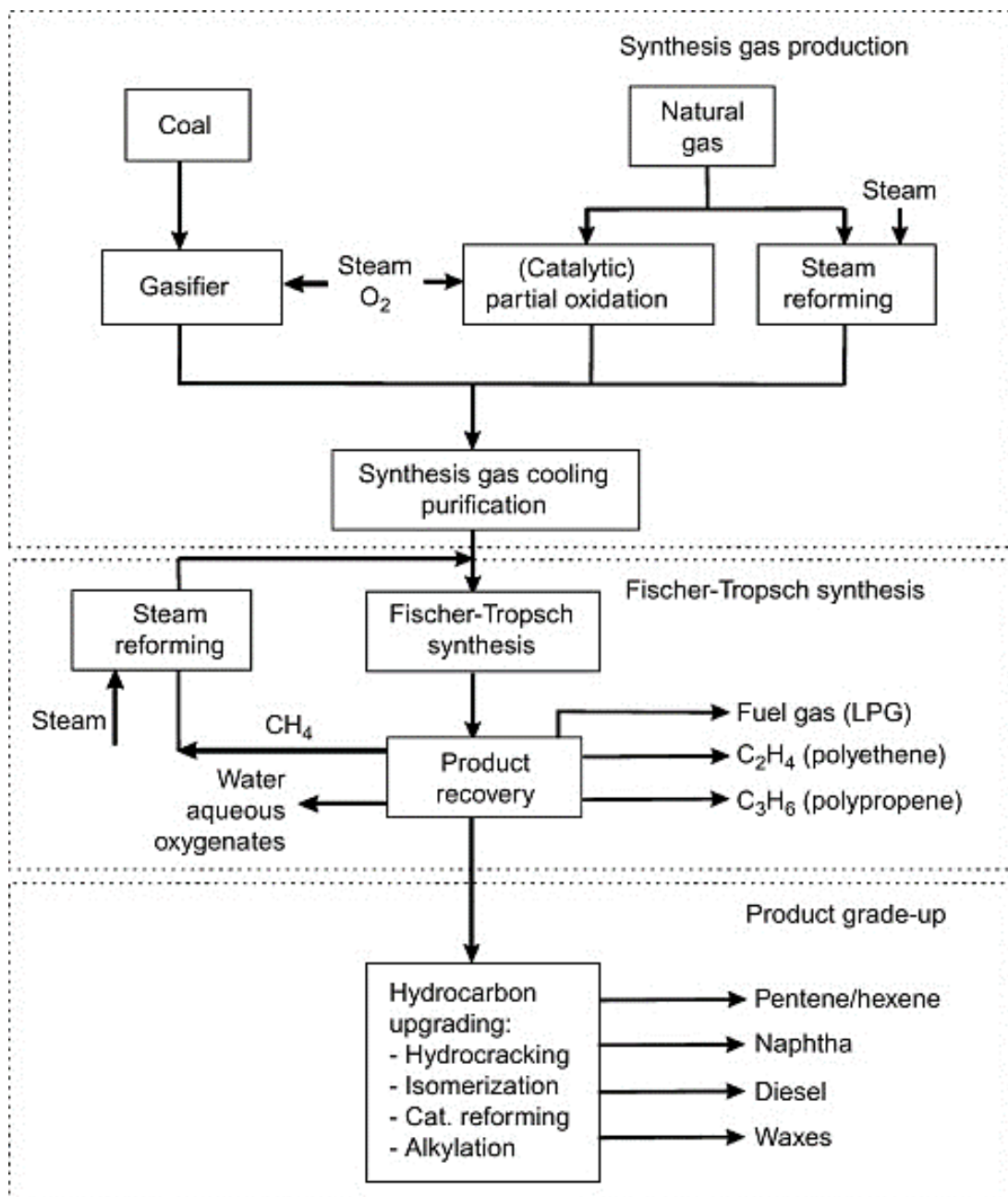


Figure 10 Overall process block diagram for the Fischer-Tropsch synthesis.[40].

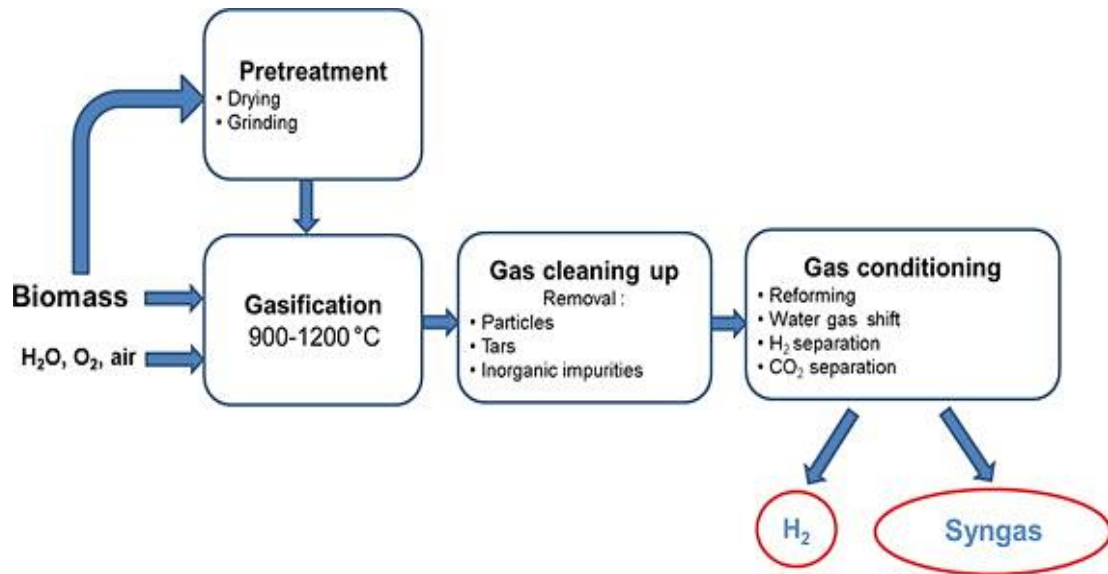


Figure 11 Schematic of the multistage production process of syngas or H₂ from biomass gasification. [41]

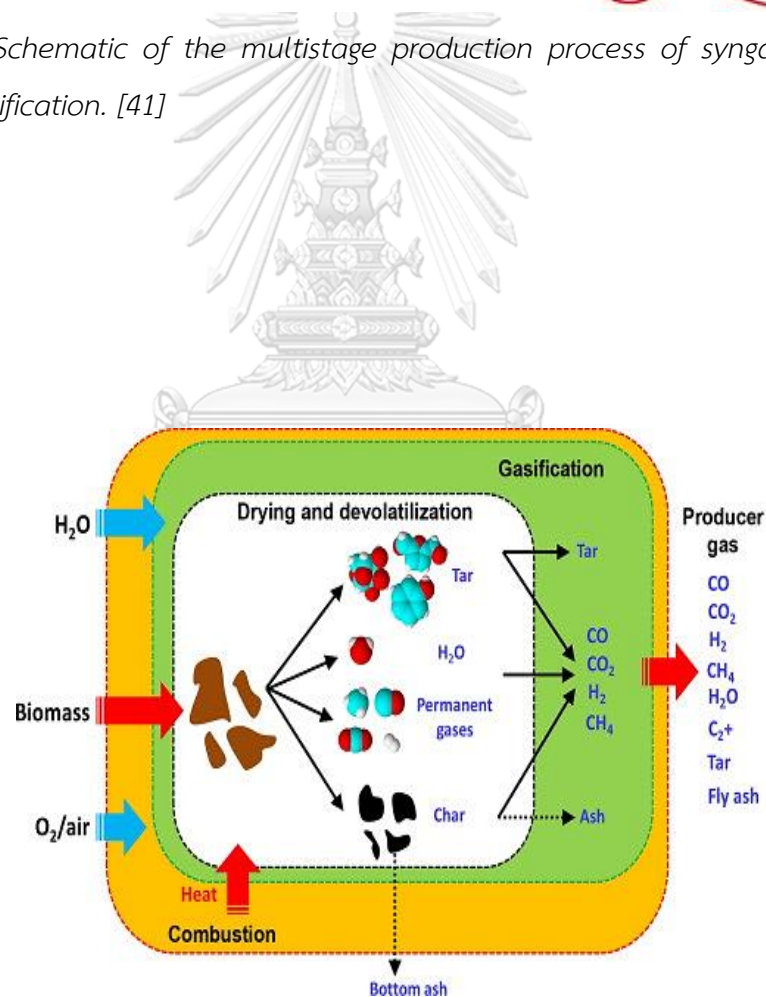


Figure 12 Schematic representation of the main processes involved in a biomass gasifier.[41].

The thermal breakdown of biomass feedstock into gaseous, liquid, and solid products without the need of an oxidant is known as pyrolysis (R 5). Methods of partial oxidation use less oxygen than is required for full combustion (R 6 and R 16). Steam gasification and reformation are the processes through which water interacts with biomass-derived fuel to produce carbon monoxide, carbon dioxide, and hydrogen (R 9 and R 17). The WGS reaction (R 14) and methanation are two more important reactions that occur during gasification (R 15). Numerous papers [39, 41, 42] have thoroughly investigated the chemistry and thermodynamics of biomass gasification.

The heat required to power the gasification reactions is generated in two ways: indirectly (or allothermal) gasification, which generates heat outside the gasifier and transfers it inside, or directly (or autothermal) gasification, which generates heat inside the gasifier via exothermic combustion and partial combustion reactions. The patent literature describes hundreds of distinct types of gasifiers. They may, however, be classified into two broad categories: fixed bed gasifiers and fluidized bed gasifiers, both of which have variants. The third type of gasifier, the entrained flow gasifier, was designed specifically for the gasification of finely split fuel particles (0.1-0.4 mm). This type of gasifier works well with coal particles. Its use in biomass begins with the conversion of biomass to easily pulverized material, such as rapid pyrolysis oil, char, or torrefied biomass particles [43].

Table 1 Main Chemical Reactions Involved in Biomass Gasification Process [41].

Reactions	Heat of reaction ΔH^0 (kJ mol ⁻¹)	Name	Number
Biomass \rightarrow char + tars + H ₂ O + light gases (CO + CO ₂ + H ₂ + CH ₄ + C _x H _y O _z + N ₂ + ...)	> 0	Pyrolysis or devolatilization	R 5
Char combustion			
C + ½O ₂ \rightarrow CO	- 111	Partial combustion	R 6
C + O ₂ \rightarrow CO ₂	- 394	Total combustion	R 7
Char gasification			
C + CO ₂ \rightleftharpoons 2CO	+ 173	Boudouard reaction	R 8
C + H ₂ O \rightarrow CO + H ₂	+ 131	Steam gasification	R 9
C + 2H ₂ \rightleftharpoons CH ₄	- 75	Hydrogene gasification	R 10
Homogeneous reactions			
CO + ½O ₂ \rightarrow CO ₂	- 283	CO oxidation	R 11
H ₂ + ½O ₂ \rightarrow H ₂ O	- 242	H ₂ oxidation	R 12
CH ₄ + 2O ₂ \rightarrow CO ₂ + 2H ₂ O	- 283	CH ₄ oxidation	R 13
CO + H ₂ O \rightleftharpoons CO ₂ + H ₂	- 41	Water-gas shift (WGS)	R 14
CO + 3H ₂ \rightleftharpoons CH ₄ + H ₂ O	- 206	Methanation	R 15
Tar conversion reactions			
C _n H _m + (n/2)O ₂ \rightarrow nCO + (m/2)H ₂		Partial oxidation	R 16
C _n H _m + nH ₂ O \rightarrow (m/2 + n)H ₂ + nCO ₂	Highly endothermic	Steam reforming	R 17
C _n H _m + nCO ₂ \rightarrow 2nCO ₂ + (m/2)H ₂		Dry reforming	R 18
C _n H _m \rightarrow (m/4) CH ₄ + (n-m/4)C		Thermal cracking	R 19

2.2.1.1. Fixed Bed Gasifiers

Fixed bed gasifiers were the first and most common type of syngas reactor. Fixed bed gasifiers have been widely utilized and investigated due to its ease of building and operation, as well as their relatively high thermal efficiency and little pretreatment of the supplied biomass. Based on the direction of airflow, fixed gasifiers are classed as updraft, downdraft, or cross-flow. While updraft and cross-flow are ideal for small-scale thermal applications, their use in power generation is limited due to the producing gas's high tar concentration. Downdraft gasifiers are suited for small-scale power generation because to the low tar and particle content of the output gas.

2.2.1.2. Downdraft Gasifier section.

A downdraft gasifier is a type of gasification reactor with four different zones: (a) an upper drying zone, (b) an upper-middle pyrolysis section, (c) a lower-middle oxidation section, and (d) a lower reduction zone. A downdraft gasifier is seen schematically in Figure 13 *Schematic of a downdraft gasifier.*

[9].. In the top portion, the feed biomass is dried. The dried biomass settles in the upper-middle zone, where it may undergo pyrolysis and tar conversion. Following that, unconverted tars and gases are transferred to the oxidation zone, where they burn at temperatures ranging from 1000 to 1400 degrees Celsius. Finally, the chemical species produced pass through a reduction zone, increasing the amounts of H₂ and CO. Because the majority of the tars are combustible in the oxidation zone, the produced gas has a low particle and tar concentration (1 g/Nm³). Downdraft gasifiers are suitable for producing clean syngas with low tar and particle content. However, this type of gasifier has drawbacks such as high moisture and ash content biomass and a low overall thermal efficiency.

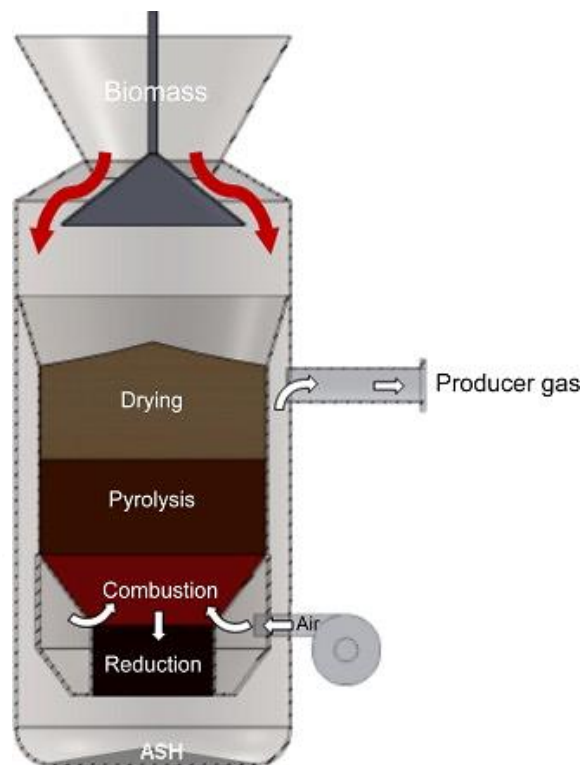


Figure 13 Schematic of a downdraft gasifier. [9].

2.2.1.3. Fluidized Bed Gasifiers

Fluidized beds appear to be the most appealing option for biomass gasification due to their flexibility and efficiency, particularly for large-scale applications. The fine particle size reduction of the biomass feedstock is the first step in these techniques, followed by the injection of air, steam, or oxygen at the reactor's bottom. The gas stream's tremendous velocity propels the biomass upward through a bed of valuable minerals. Drying, pyrolysis, homogeneous and heterogeneous oxidation all occur in the same zone of the reactor practically simultaneously. One advantage it has over fixed bed gasifiers is that it maintains a consistent temperature distribution in the gasification zone by circulating air over a bed of fine granular material (e.g., sand).

Fluidized bed gasifiers can handle a wide variety of fuels. Due to the intricacy of their construction and operation, these gasifiers are only suitable for large-scale applications. In addition, fluidized beds reach a typical intermediate tar level of 10

g/Nm^3 and a high particle loading, necessitating the deployment of specialist syngas cleaning equipment. Fluidized bed reactors are classified into two types based on their fluidization rate: (i) bubbling fluidized bed (BFB) gasifiers and (ii) circulation fluidized bed (CFB) gasifiers.

Bubbling Fluidized Bed Gasifier

The BFB gasifier consists of a vessel with a bottom grid into which the gasifying chemical is introduced (e.g., a combination of H_2O and air). A moving bed of fine-grained material is positioned above the grid, into which the prepared biomass feed is injected. The temperature of the bed is controlled between 700 and 900 °C by varying the air/biomass ratio. In the hot bed, the biomass is pyrolyzed, resulting in the formation of char, gaseous chemicals, and tar. The high molecular weight tar is transformed by contacting it with hot bed material, which may include a tar reforming catalyst, yielding a producer gas with a reduced tar concentration ($1\text{-}3 \text{ g/Nm}^3$). Furthermore, the BFB reactor enables the integration of several functions into the biomass gasifier via the bed materials and freeboard zone, with the goal of increasing process intensity (PI).



Dual Fluidized Bed Gasifier

Dual fluidized bed gasification (DFBG) is a technically mature process that has been shown at a demonstration scale and is acknowledged as a promising biomass gasification technology, particularly for the production of high-quality syngas. Several recent reviews and engineering studies [44] provide a detailed overview and analysis of DFBGs technology. DFBGs are composed of two linked fluidized bed (FB) reactors: an endothermal FB gasifier that employs steam as the gasifying agent and an exothermal FB combustor that provides heat to the gasifier via bed material circulation. Before the FB combustor burns the ungasified char, the FB gasifier first gasifies the

biomass. Separating fuel gas generation from char combustion in DFBGs enables the production of gas with a medium heating value that is not diluted by N_2 from the combustion air. Among the different DFBG configurations, the combination of a BFB for biomass gasification and a CFB for char combustion has been recognized as the optimum technological configuration for biomass gasification in terms of fuel conversion and tar generation. This DFBG biomass gasification technology has been demonstrated to be successful at the demonstration size [44, 45], and additional process design optimization has recently been reported to increase biomass gasification performance [46]. Figure 14 depicts a typical DFBG method in schematic form.

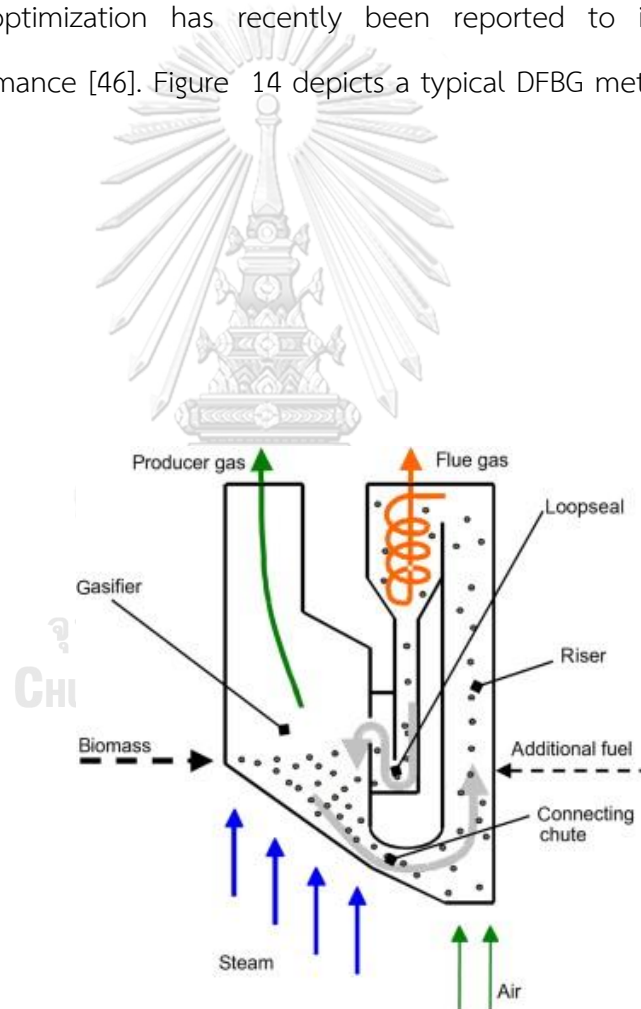


Figure 14 Schematic of the dual fluidized bed gasification process.[47] [21]

2.2.1.4. Syngas Cleaning

Figure 11 illustrates the many steps of biomass syngas generation, which include biomass preparation (drying and grinding), gasification, gas cleaning and conditioning (including particle, tar, and inorganics removal), WGS, CO₂ elimination, and perhaps H₂ purification. Gas purification and conditioning are critical steps in the conversion of biomass gasification into electricity, liquid biofuel, or hydrogen. Although CO, H₂, CH₄, CO₂, H₂O, and N₂ are the major byproducts of gasification (when air is used as the oxidizing agent), it also contains secondary products such as tars, inorganic compounds (alkali metals, nitrogen, sulfur, and chlorine compounds), and solid particles. Table 2 depicts the need for syngas in a variety of applications. These pollutants may have a negative influence on future syngas processing.

Nitrogen, sulfur, and chlorine-containing compounds (e.g., NH₃, HCN, H₂S, and HCl) are a source of worry due to their corrosive character and role as poisons for metal-based catalysts such as nickel or iron-based catalysts, as well as precursors of regulated emission products such as NO_x and SO₂. Because of fouling, corrosion, and erosion issues that, if not handled, result in lower efficiency and safety, the majority of syngas applications require more than 99 percent particle removal. Finally, tars are the most troublesome secondary pollutants found in biomass gasification raw gas. Tar removal is still a high priority for research and development. Tars also inhibit the activity of catalysts employed in downstream gasification processes [47-51].

Table 2 Examples of Syngas Specifications Required for Specific Applications, [51-56]

Final syngas application	Particles	Tar	Sulfur (H ₂ S, COS)	Nitrogen (HCN, NH ₃)	Alkali (Primarily K and Na)	Halides (Primarily HCl)
Steam-cycle power station	Minimal requirements	Of no importance, but condensation must be avoided ^a	Final SO _x emissions limited by regulation	Final NO _x emissions limited by regulation		
Gas engine	< 50 mg m ⁻³ N	< 100 mg m ⁻³ N	Final SO _x emissions limited by regulation	Final NO _x emissions limited by regulation	< 0.02 ppmV	< 1 ppmV
Gas turbine	< 30 mg m ⁻³ N	< 50 mg m ⁻³ N	< 20 ppmV	< 50 ppmV	< 0.02 ppmV	< 1 ppmV
Solid oxide fuel cell (SOFC)	< 1 ppmW	Several tens to few hundred ppmV	Few ppmV		1 ppmV	Few ppmV
Molten carbonate fuel cell (MCFC)	< 0.01 ηm	< 2000 ppmW	< 0.1 ppmV (H ₂ S)	< 0.1 ppmW (HCN) < 1 vol% (NH ₃)		< 0.1 ppmW
Proton exchange membrane fuel cell (PEMFC)		< 100 ppmV	< 1 ppm			
Methanol synthesis	< 0.02 mg m ⁻³ N	< 0.1 mg m ⁻³ N	< 1 mg m ⁻³ N	< 0.1 mg m ⁻³ N		< 0.1 mg m ⁻³ N
Fischer-Tropsch synthesis (F-T)	n.d. ^{ab}	< 1 ppmV	< 0.01 ppmV	< 0.02 ppmV	< 0.01 ppmV	< 0.01 ppmV

^a Tars are destroyed by combustion in the burner, thereby producing additional heat.

^b Not detectable

2.2.2. Fischer-Tropsch Synthesis

Several chemical techniques have been presented during the last few decades to explain the chemicals produced during the FTS. In the scientific community, the four most well-known mechanisms are the alkyl mechanism, the alkenyl mechanism, the enol mechanism, and the CO-insertion mechanism. The most significant (and well-known) mechanism for the FT reaction on iron catalyst is the Alkyl mechanism.

2.2.2.1. FT mechanism

FTS is a technique of surface polymerization. When the monomers generated in situ from the gaseous reactants (hydrogen and carbon monoxide) are adsorbed onto the catalyst surface, the FT reaction begins. Like any other polymerization process, the FTS comprises of three steps: (i) reaction start via chain initiator production; (ii) chain propagation via chain growth; and (iii) product desorption by chain growth termination.

Alkyl mechanism

According to this mechanism (Figure 15), the FT reaction begins with the dissociative adsorption of CO on the surface of the catalyst, resulting in the formation of surface-bound carbon and oxygen. Water is formed when surface-bound oxygen interacts with adsorbed hydrogen. Surface oxygen also interacts with carbon monoxide to create CO₂. As a result, surface oxygen levels decline, causing water and CO₂ to be produced. After hydrogenation of the surface carbon, CH, CH₂, and CH₃ intermediates are generated in the alkyl mechanism reaction scheme, with CH₂ acting as the monomer and CH₃ functioning as the chain initiator. The process for chain formation is assumed to involve the sequential inclusion of the monomer, CH₂ surface species. The product is formed during the desorption process either by hydrogen elimination or by hydrogen addition, with the primary products being olefins and n-paraffins. The

primary disadvantage of this technique is that it does not explain how oxygenated products are produced. However, Johnston and Joyner proposed that the production of oxygenated compounds is caused by the surface hydroxyl group. Furthermore, tiny amounts of branched-chain hydrocarbons cannot be accounted for by the alkyl process. Olefin resorption is the most important process in the synthesis of branched-chain hydrocarbons. Schulz et al. presented a technique for generating branched-chain hydrocarbons as a result. This extra chemical route is not part of the alkyl mechanism, but it is necessary to explain the synthesis of branched-chain hydrocarbons [57].

Alkenyl mechanism

The alkyl (Figure 15) and alkenyl (Figure 16) processes begin similarly, with the exception that the chain is initiated by a (CHCH_2) surface vinyl molecule. The surface vinyl species is formed when methylidyne (CH) and methylene react (CH_2). Surface alkyl species are formed by reacting surface methylene with vinyl species. Finally, H is added, resulting in the desorption of an olefinic species as the final product. This technique has a significant disadvantage in that it does not account for n-paraffin products.

Enol mechanism

Figure 17 illustrates this process, which was first shown in 1950. In this process, the interaction of chemisorbed CO with adsorbed hydrogen results in the formation of a surface enol species. The condensation of two neighboring enol species with the removal of water results in chain propagation. Desorbing and hydrogenating olefinic species on the surface yields the product. Paraffins are byproducts of the hydrogenation of olefins.

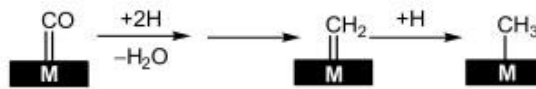
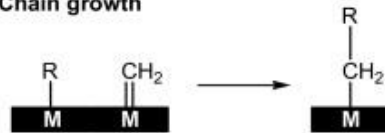
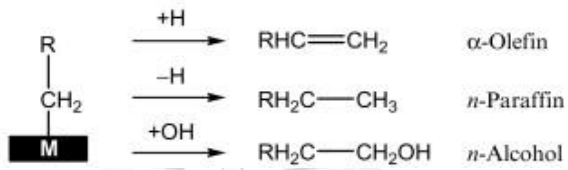
Initiation**Chain growth****Chain termination**

Figure 15 Alkyl mechanism [4]

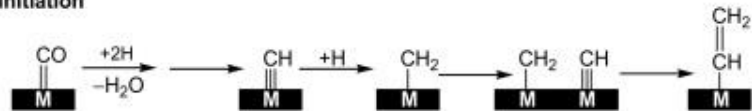
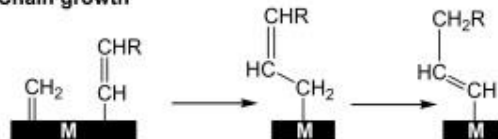
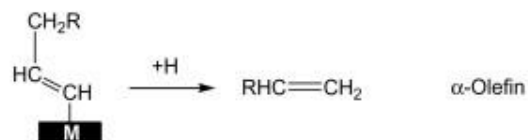
**Initiation****Chain growth****Chain termination**

Figure 16 Alkenyl mechanism [4]

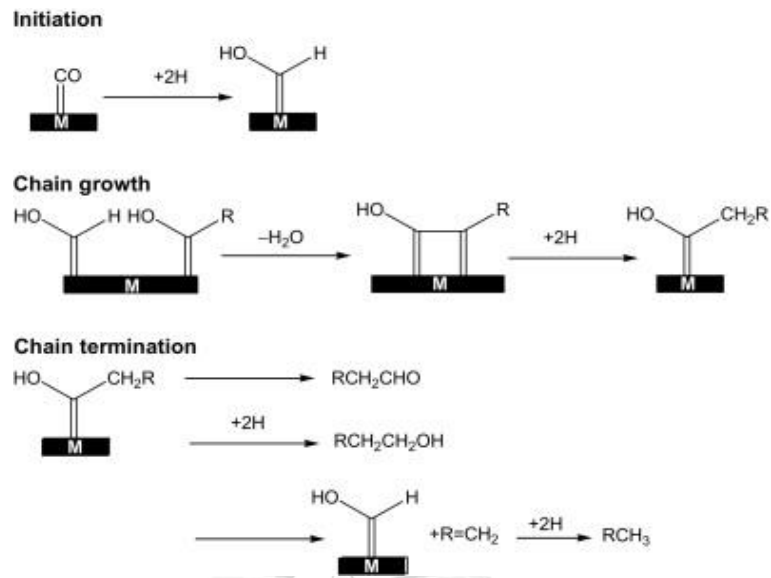


Figure 17 Enol mechanism [4]

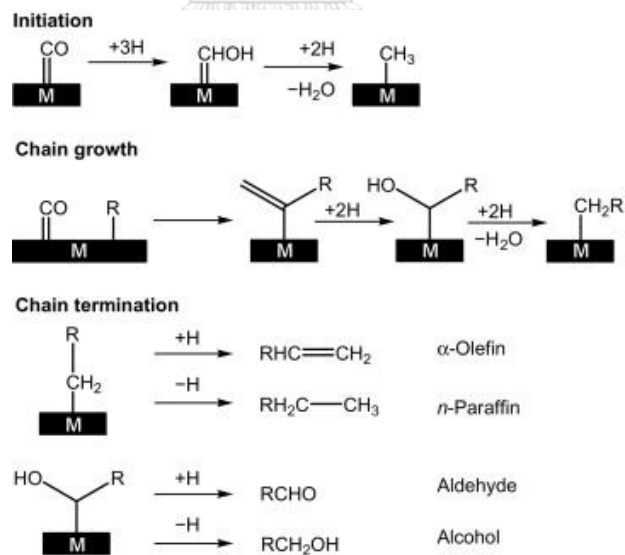


Figure 18 CO-insertion mechanism [4]

CO-insertion mechanism

The chemisorbed CO is hydrogenated in this process to create surface methyl species (Figure 18). CO is injected into the metal alkyl bond of the surface methyl species during the propagation stage. The major effect of removing or adding hydrogen is the formation of olefin or n-paraffin. Chain termination can also be accomplished by introducing hydrogen into the oxygenated intermediate produced during the chain propagation phase, resulting in the formation of both alcohol and aldehyde species.

2.2.2.2. The Profile of FT Products

Because the FT technique is a polymerization reaction, it generates a wide range of products with varying carbon chain lengths, including n-olefins, n-paraffins, oxygenated compounds, and branched-chain hydrocarbons. A range of reaction factors, such as temperature, pressure, catalyst type, and reactor design, influence product selectivity. Chain growth occurs in the FT reaction, as described in the mechanism section, by adding a monomer unit to the chain initiator. The likelihood of chain growth is defined as the probability of chain formation by adding a monomer to the initiator. It is believed that unidirectional chain growth occurs, and that chain growth up to carbon has the potential to evolve. Chain growth up to carbon (n-1) is C_{n-1} is α^{n-1} . The probability of chain termination (X_n) at C_n will be

$$X_n = \alpha^{n-1} (1 - \alpha) \quad \text{Eq. 1}$$

where, X_n is the mole fraction of the hydrocarbon product with carbon number n.

This equation for the weight fraction of different hydrocarbons was developed by Schulz and Flory. Steyberg and Dry investigated Schulz and Flory's model critically.

When plotted logarithmically, the following equation produces straight lines [57]. The above equation may be expressed as follows:

$$\log X_n = \log \frac{(1-\alpha)}{\alpha} + n \log \alpha \quad \text{Eq. 2}$$

These are referred to as Anderson-Schulz-Flory (ASF) plots (Figure 19a) (Friedel and Anderson, 1950). The average degree of polymerization, denoted by the letter 'D,' is provided by

$$D = \frac{1}{(1-\alpha)} \quad \text{Eq. 3}$$

The weight fraction W of C_n is given by

$$W_n = \frac{nW_n}{D} \quad \text{Eq. 4}$$

$$W_n = n(1-\alpha)^2 \alpha^{n-1} \quad \text{Eq. 5}$$

The ASF polymerization equation is commonly referred to as Eq. 5. Figure 19b depicts the FT product distribution using the ASF model. It is obvious that only gaseous methane has a selectivity of 100% with $\alpha = 0$. The maximum hydrocarbon yield in the gasoline range is 48%, whereas the maximum hydrocarbon yield in the diesel range is 30%. In an FT reaction, the ASF model predicts the product distribution. However, due to secondary processes such as hydrocarbon product reinsertion into the chain building process, hydrogenation, and hydrogenolysis, the actual product profile will always differ from the typical ASF distribution. These secondary reactions have a

significant impact on the final FT reaction products and should be thoroughly investigated if the required selectivity of the products is to be attained.

2.2.2.3. FT Catalyst

Since the process's inception, iron and cobalt have been the most commonly used catalysts. FT is generally active in transition group VIII metals. Only four have a greater hydrogenation activity than carbon monoxide and are hence suitable for commercial FTS (Fe, Co, Ni, and Ru).

Ni has a stronger selectivity for methane at high temperatures. Ru is the most active FTS catalyst, but its high cost and scarcity prohibit it from being extensively employed. Even at the higher temperatures employed in the Synthol process, iron has a lower methane selectivity.[57].

Iron catalysts are inexpensive and straightforward to produce. In FTS, both fused and precipitated catalysts are employed. Because of its porous nature, precipitated iron catalysts have a greater surface area than nonporous fused iron catalysts and are more commonly employed in industrial applications. To improve the activity of iron catalysts, metals such as K and Cu are added. Furthermore, SiO₂ or Al₂O₃ is utilized as a structural promoter to increase the material's attrition resistance. Iron appears in a variety of phases in iron-based catalysts exposed to FTS. Metallic iron (α -Fe), iron oxides (hematite, α -Fe₂O₃, magnetite, Fe₃O₄, and Fe_xO), five different iron carbides (ϵ -Fe₂C, ϵ -Fe_{2.2}C, and Fe_xC), and TP carbides (carbides having carbon atoms in trigonal prismatic interstices (χ -Fe_{2.5}C and Fe₃C) are among them. Iron catalysts, on the other hand, are useful because they can generate low molecular weight gaseous

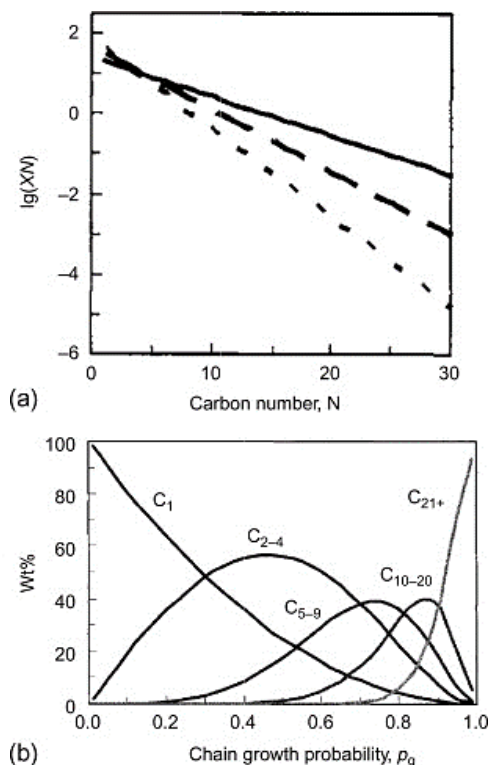


Figure 19 (a) Anderson-Schulz-Flory (ASF) plot and (b) FT product distribution in wt% as a function of chain growth probability α for ideal ASF kinetics. Reproduced with permission from Elsevier BV, Amsterdam. [4]

hydrocarbons at high temperatures and high molecular weight liquid hydrocarbons at low temperatures. Because of their high WGS activity, iron catalysts have the potential to create CO-rich syngas from coal or biomass gasification. The water generated during FTS reacts with the iron and deactivates it during the oxidation process, which is a major operational issue with iron catalysts [58-61].

Because of its increased activity and selectivity for long-chain paraffins utilized as synthetic diesel, the cobalt-based catalyst performs significantly better in FTS with stoichiometric syngas. When combined with wax hydrocracking, cobalt catalysts may achieve more than 80% selectivity toward diesel fuel. Metallic cobalt is frequently widely dispersed by putting a cobalt salt on a large surface area support, such as Al_2O_3 or SiO_2 , and then reducing it. Because of its high mechanical characteristics and flexible

surface features, alumina is one of the most commonly used supports for cobalt FT catalysts. On the other hand, the strong interaction between the supported cobalt and Al_2O_3 frequently results in a product profile with limited reducibility. [62].

2.3. Literature Review

H. Ahouari et al. [63] explored a one-step CO_2 hydrogenation process to form HCs utilizing a bifunctional system composed of a $\text{Cu}/\text{ZnO}/\text{Al}_2\text{O}_3$ (CZA) methanol synthesis catalyst and a zeolite (HZSM-5). The effect of the configuration of the catalyst bed on activity, selectivity, and HCs yield has been studied. The findings obtained at $T = 623 \text{ K}$, $P = 3.0 \text{ MPa}$, and $\text{WHSV} = 6000 \text{ h}^{-1}$ indicate that the closeness of the oxide and zeolite had a significant effect on CO_2 hydrogenation and hydrocarbon selectivity. Indeed, the greatest conversion and yields of hydrocarbons (mostly C_2) were achieved using dual-bed bifunctional catalysts with the smallest oxide/zeolite proximity. This is due to the hydrogen spillover phenomena from the oxide catalyst to the zeolite surface, which increases the reducibility of oxide catalysts but does not stimulate the development of carbon chains.

Peng Gao et al. [64] asserted that direct conversion of CO_2 to lower olefins ($\text{C}_2 =$ - $\text{C}_4 =$) via a bifunctional catalyst composed of indium/zirconium composite oxide and SAPO-34 zeolite is highly attractive as a sustainable production route due to its significant contribution to greenhouse gas reduction and fossil fuel substitution; however, such a route typically exhibits low selectivity toward olefins. At greater than 35% CO_2 conversion, a bifunctional catalysis process was proven to have a $\text{C}_2 =$ - $\text{C}_4 =$ selectivity of up to 80% and a C_2C_4 selectivity of about 93 %. CO_2 activation and selective C-C coupling are carried out by the oxide composite and zeolite, respectively. Both the exact management of oxygen vacancies on the oxide surface and the method in which the components are integrated are critical in the direct synthesis of lower

olefins via CO_2 hydrogenation. It was discovered that mortar mixing deactivated the zeolite from which the In-Zr/SAPO-34 was produced. Due to the fact that excessive contact between bifunctional active sites resulted in indium migration during the reaction, followed by ion exchange of indium ions with zeolite protons, as confirmed by TEM-DEX, which significantly decreased the number of strongly acidic sites, resulting in severe deactivation with very low $\text{C}_{2=}$ - $\text{C}_{4=}$ selectivity.

Jiayang Wang et al. [6] demonstrated effective integration of methanol synthesis and methanol to hydrocarbons conversion using a bifunctional catalyst component composed of $\text{In}_2\text{O}_3\text{-ZrO}_2$ and SAPO-34 and SAPO-5. At $T=300$ °C, these tandem reactions display a high relative selectivity for $\text{C}_2\text{-C}_4$ (83%) and a reduced relative selectivity for CH_4 of less than 3%. According to a thorough investigation, the partly reduced indium oxide surface ($\text{In}_2\text{O}_3\text{-ZrO}_2$) is more effective at activating CO_2 and promoting the production of methanol than In_2O_3 alone. Additionally, the hydrocarbon distributions for SAPO-34 and SAPO-5 were summarized. $\text{In}_2\text{O}_3\text{-ZrO}_2\text{/SAPO-34}$, with its smaller 8-member-ring (MR) channels, demonstrated a higher relative selectivity to CH_4 (38%) and then decreased monotonically from C_1 to C_6 , with the total relative selectivity to $\text{C}_2\text{-C}_4$ accounting for 51%. In stark contrast, $\text{In}_2\text{O}_3\text{-ZrO}_2\text{/SAPO-5}$ demonstrated a total selectivity to $\text{C}_2\text{-C}_4$ of 83 %, which was much greater than the SAPO-34-supported catalyst.

Young Kwon Park et al. [65] explored direct hydrocarbon synthesis from CO_2 hydrogenation using hybrid catalysts composed of a methanol synthesis catalyst (CuZnOZrO_2) and zeolites (HZSM-5 and SAPO). The reactions were carried out at a temperature of 400 °C, a pressure of 28 atm, and a concentration of W/F of 20 $\text{g}_{\text{cat}}\cdot\text{h}\cdot\text{mol}^{-1}$. The results indicated that the yield of hydrocarbons was significantly dependent on the number of acid sites in the zeolite, but the product distributions were little impacted by the acidity variation. In the case of the HZSM-5 hybrid catalyst,

the primary product was ethane; in the case of the SAPO hybrid catalyst, the primary product was a C₃ or C₄ hydrocarbon.

Congming Li et al. [5] performed CO₂ hydrogenation over a hybrid catalyst to produce LPG. The catalyst consisted of a metal phase including copper (Cu), zinc (Zn), zirconia (Zr), and aluminum (Al₂O₃), a CZZA, and a modified zeolite containing Pd. Mechanical mixing was used to combine the catalysts. Numerous variables affecting catalyst activity were found, including reaction temperature, space velocity, pressure, and the H₂/CO₂ ratio. The results indicated that the hybrid catalysts maintained activity for 100 hours and had a high selectivity for LPG synthesis, with a conversion of CO₂ and a yield of hydrocarbon of 25.2% and 13.3%, respectively, and a selectivity for LPG and CH₄ of 75% and 1%, respectively, at low temperature (260 °C) and low pressure (2 MPa). Additionally, the chemical pathway explained how CO₂ hydrogenation happened by direct hydrogenation of CO₂ to methanol on the metal phase of the catalyst, followed by conversion of methanol to DME and direct conversion to hydrocarbon on the acid sites of Pd-zeolite.

Xiaoxing Wang et al. [66] created a core-shell catalyst having a core of Fe–Zn–Zr and a shell of zeolite (HZSM-5, Hbeta, and HY). The catalysts shown excellent activity in the direct production of iso-alkanes via CO₂ hydrogenation. The author observed that a single-zeolite shell, Fe–Zn–Zr@HY with a weight ratio of 2 : 1, exhibited strong iso-alkane selectivity, whilst Fe–Zn–Zr@Hbeta with a weight ratio of 2 : 1 exhibited superior HC selectivity. In the case of double-zeolites, Fe–Zn–Zr@HZSM-5–Hbeta with a weight ratio of 4 : 1 demonstrated the best iso-alkanes selectivity (81.3 %), and the hydrocarbon distributions are inversely proportional to the weight ratio of the two zeolites.

Kim et al. [67] investigated the long-term operation of the biomass-to-liquid (BTL) process with the goal of producing bio-syngas that meets the Fischer–Tropsch (FT) process purity requirements. The integrated BTL system included a 20-kWth

bubbling fluidized bed (BFB) gasifier, a gas cleaning unit, a syngas compression unit, an acid gas removal unit, and an FT reactor. In the gas cleaning unit, the syngas was cleaned using cyclones, a gravity dust collector, a two-stage wet scrubber (packing-type), and a methanol absorption tower. The cleansed syngas contained no sulfur compounds (less than 1 ppmV) and met all FT process criteria. The BTL process proved successful after 500 hours of long-term manufacturing, and the data obtained may be utilized to build the larger one.

Kim et al. [68] investigated a biomass-to-liquids (BTL) system that included a dual fluidized bed gasifier (DFBG), a methanol absorption tower, and an F-T synthesis process. The feasibility of producing clean biodiesel for use in automobiles was examined. The results indicated that a DFBG, an efficient indirect gasifier, is capable of producing syngas with a high calorific value while reducing nitrogen in the output gas. The syngas contained a majority of H₂ (35% by volume) and CO (21.3 by volume). Due to the cooled methanol cleaning procedure, the H₂S and COS contents in the syngas were less than 1 ppmV. Additionally, a fully integrated BTL system was successfully operated for over 500 hours. The results indicated that the BTL diesel may be utilized as a substitute for diesel in automobiles.

Chapter 3

Experimental

3.1. Material and Reagents

3.1.1. Preparation of CZZA catalyst

The starting materials were Copper (II) nitrate trihydrate [$\text{Cu}(\text{NO}_3)_2 \cdot 3\text{H}_2\text{O}$, A.R. Grade, FUJIFILM Wako Pure Chemical Corporation], Zinc nitrate hexahydrate [$\text{Zn}(\text{NO}_3)_2 \cdot 6\text{H}_2\text{O}$, A.R. Grade, FUJIFILM Wako Pure Chemical Corporation], Zirconium(IV) oxynitrate hydrate [$\text{ZrO}(\text{NO}_3)_2 \cdot 2\text{H}_2\text{O}$, A.R. Grade, FUJIFILM Wako Pure Chemical Corporation], Aluminum nitrate nonahydrate [$\text{Al}(\text{NO}_3)_3 \cdot 9\text{H}_2\text{O}$, A.R. Grade, FUJIFILM Wako Pure Chemical Corporation], Sodium carbonate [Na_2CO_3 , A.R. Grade, FUJIFILM Wako Pure Chemical Corporation]

3.1.2. Preparation of synthesis Na-Y zeolite

Na-Y zeolite synthesis methods were investigated by several experimental which different chemicals and techniques. The chemical started with Ludox SM-30 colloidal silica [SiO_2 , 30 wt.%, Sigma Aldrich], Aluminium isopropoxide [$\text{Al}[\text{OCH}(\text{CH}_3)_2]_3$, AIP, A.R. Grade, FUJIFILM Wako Pure Chemical Corporation], 25% Tetramethylammonium Hydroxide in water [$(\text{CH}_3)_4\text{N}(\text{OH})$, $(\text{TMA}_2)\text{O}$, A.R. Grade, FUJIFILM Wako Pure Chemical Corporation], Sodium Hydroxide [NaOH , A.R. Grade, FUJIFILM Wako Pure Chemical Corporation], Sodium Metasilicate Nonahydrate [$\text{Na}_2\text{O}_3\text{Si} \cdot 9\text{H}_2\text{O}$, A.R. Grade, FUJIFILM Wako Pure Chemical Corporation], Sodium Aluminate [AlNaO_2 , A.R. Grade, Kento chemical Co.], Na-Y zeolite [FUJIFILM Wako Pure Chemical Corporation]

3.1.3. Biomass feedstock for gasification

The rotary kiln gasifier unit was tested with two different biomass types: rubberwood pellet and dried Eucalyptus wood chips. The wood pellet was cylinder shape with 8 mm in diameter and 30 - 80 mm in length. The size and shape of wood chips were proved by testing the behavior of biomass in the feed system, including channeling formation and movement downward in hopper and obstruction in screw feeder. Sieving should help to control the size and shape of wood chips and beneficial for homogeneity in biomass. The average size of wood chips used was 5 - 10 mm.

3.2. Catalyst Preparation

3.2.1. Preparation of CZZA catalyst

The CZZA mixed metal phase catalyst was produced using the co-precipitation technique (seen Figure 20) [5] and comprised of Cu/Zn/Zr/Al at a molar ratio of 4.0/3.0/1.5/1.5. To begin, an aqueous solution of copper nitrate, zinc nitrate, zirconium oxynitrate, and aluminum nitrate was dissolved in deionized (DI) water to a concentration of 1 M total cation. Following that, a dropwise addition of sodium carbonate Na_2CO_3 solution (1 M) was made to the cation solution while vigorously stirring and maintaining the solution at 65 °C and less than pH 7.5. The precipitate was maintained at 65 °C with stirring for 1 hour, then aged at room temperature for 24 hours before being filtered and washed multiple times with DI water at 60 °C to completely eliminate the remaining sodium ions. The precipitate was then dried for 12 hours and calcined for four hours at 450 °C.

3.2.2. Na-Y zeolite Synthesis Observation

The CO₂ hydrogenation process was investigated using a commercial H-Y zeolite (com-HY). However, syn-NaY was synthesized for the purpose of comparing catalytic characteristics. Syn-NaY was synthesized utilizing an organic solvent-free approach at a molar ratio of 5 Na₂O: 1.17 Al₂O₃: 15.70 SiO₂: 322 H₂O. As seen in Figure 21, sodium aluminate (Wako) and sodium hydroxide (Wako) were combined and agitated in a polypropylene container until the solution became transparent. Following that, Ludox MS-30 colloidal silica (30 wt. %, Sigma Aldrich) was gently added and mixed for an additional 1 hour before being aged at room temperature for 72 hours. The gel solution was then transferred to a 100 mL autoclave and maintained at 100 °C for 72 hours, followed by 30 minutes centrifugation at 8,000 rpm. The pellet was washed 34 times with distilled water, dried overnight at 60 °C, and then calcined at 500 °C for 8 hours at a heating rate of 1 °C/min [69].

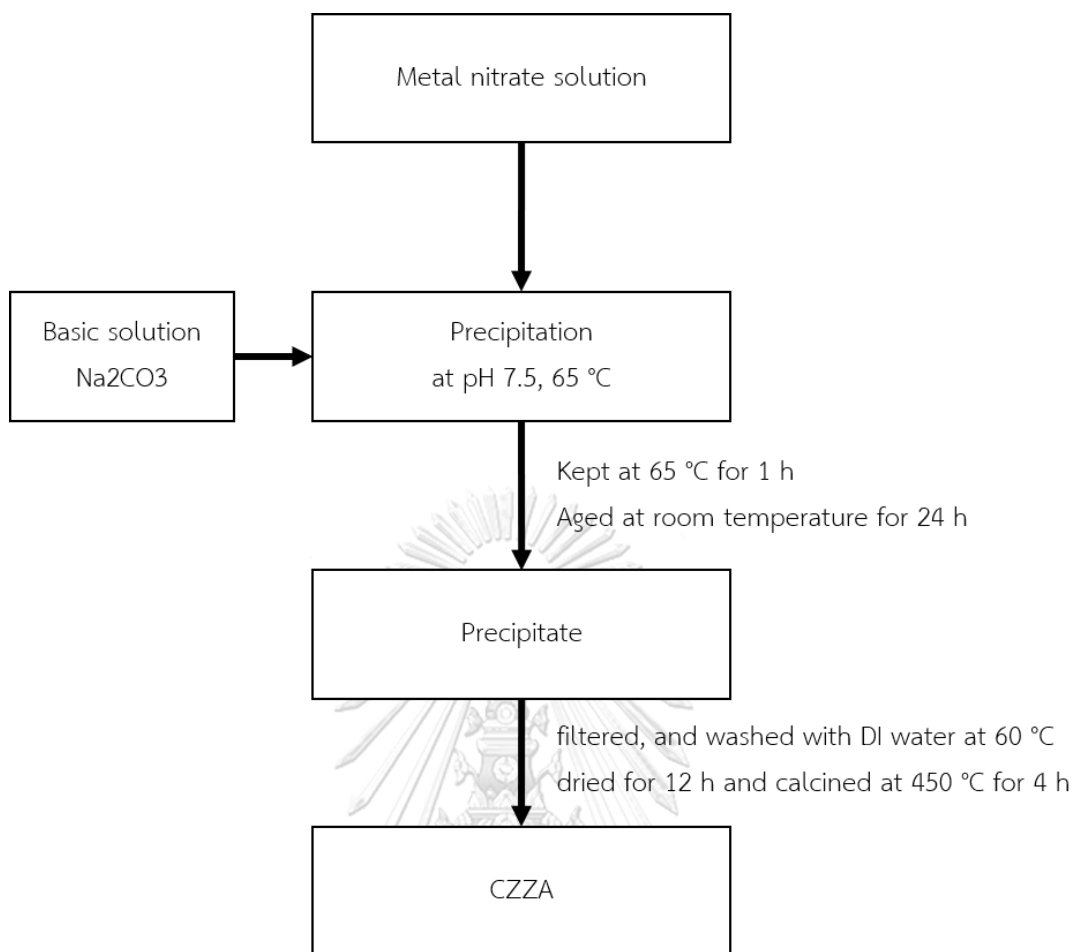


Figure 20 Schematic flow chart of CZZA catalyst preparation by co-precipitation method

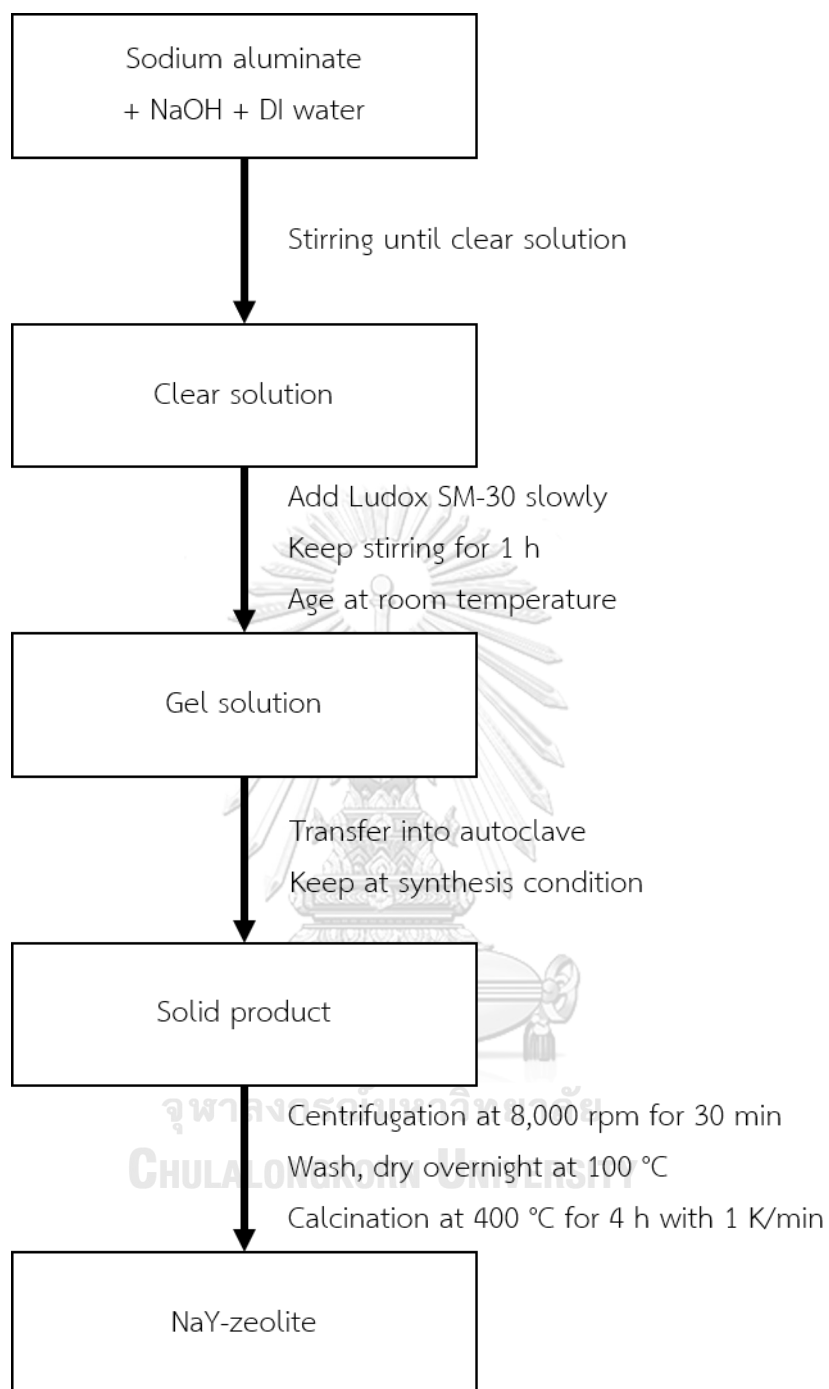


Figure 21 Schematic flow chart of NaY zeolite

3.3. Characterization

3.3.1. Catalyst characterization

3.3.1.1. X-ray Diffraction (XRD)

The crystalline phases of the prepared catalyst (CZZA, NaY zeolite) as well as com-HY zeolite were analyzed by using a Rigaku RINT2000 X-ray powder diffractometer instrument with a monochromatic Cu-K α radiation source ($\lambda = 0.154$ nm) operated at 40 kV and 20 mA in the 2θ rang of 0 - 90 degrees.



Figure 22 X-ray Diffraction (XRD), Rigaku RINT2000

3.3.1.2. The Brunauer-Emmett-Teller (BET)

The Brunauer-Emmett-Teller (BET) specific surface area (S_{BET}), average pore size (Pore_{BET}), and total pore volume (V_{BET}) of the catalysts were determined by nitrogen (N_2) adsorption-desorption isotherms with a Quantachrome Nova 2200e automated analyzer. Before the analysis, samples were degassed at 200 °C for six h.



Figure 23 N_2 adsorption-desorption, Quantachrome Nova 2200e



Figure 24 Ammonia Temperature-Programmed Reduction (NH_3 -TPD)

3.3.1.3. Ammonia Temperature-Programmed Reduction (NH_3 -TPD) and N_2O -titration measurements

Ammonia Temperature-Programmed Reduction (NH_3 -TPD) was used to analyze acid strength of the catalyst by using BELCATII-T-SP as analyzer (shown in Figure 24). As the same instrument, the copper surface area (SCU) and dispersion (DCU) of the CZZA catalyst were determined using a single-pulse N_2O titration at 90 °C using a BELCAT-II-T-SP analyzer equipped with a thermal conductivity detector (TCD). The CZZA was decreased in situ at 300 °C for one hour using a 100 mL/min H_2 stream, followed by 15 minutes of flushing with N_2 carrier flow at 300 °C. The CZZA was then cooled to 90 °C for the measurement. The S_{Cu} and D_{Cu} values were computed using a $\text{Cu}:\text{N}_2\text{O}$ titration stoichiometry of 2:1 and a surface atomic density of $1.461019 \text{ Cu}_{\text{at}}/\text{m}^2$,

with Cu particles having a spherical form. The average particle size (d_{Cu}) was calculated using the standard formula $d_{Cu} \text{ (nm)} = 104/D \text{ (}\%)$. [70]

3.3.1.4. Energy dispersive X-ray spectrometry (EDX)

Energy dispersive X-ray spectrometry (EDX) was also employed to analyze the catalysts' element composition using a SHI-MADZU EDX-700 instrument.

3.3.2. Biomass characterization

The physical and chemical properties of biomass feedstock were analyzed, including Proximate analysis was determined using ASTM D3172-3175 standard procedure method, Ultimate analysis was measured by element analyzer (Leco - CHNS 628) and followed ASTM D5373 standard procedure method and heating value was determined using Leco - AC500 with ASTM D5868 standard procedure method.



Figure 25 Energy dispersive X-ray spectrometry (EDX)

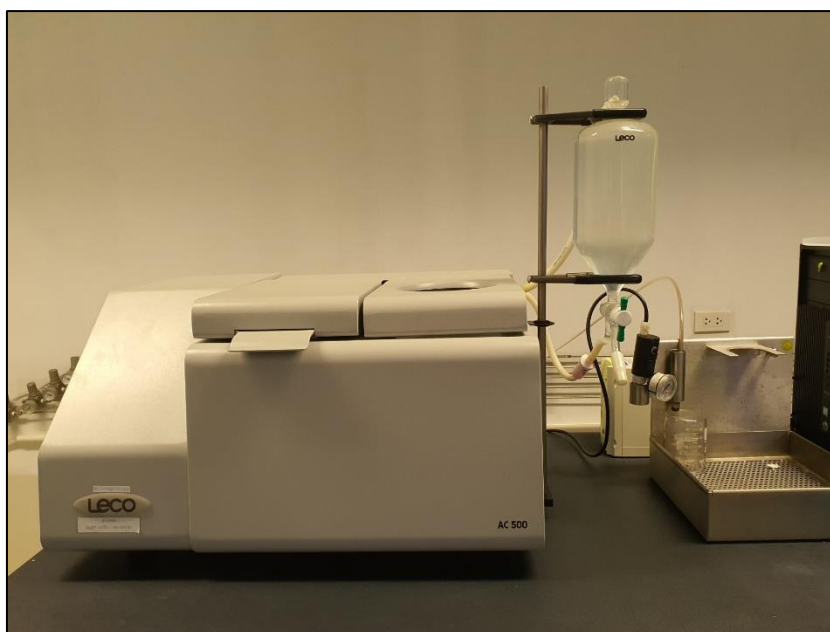


Figure 26 Heating value analysis, Leco - AC500

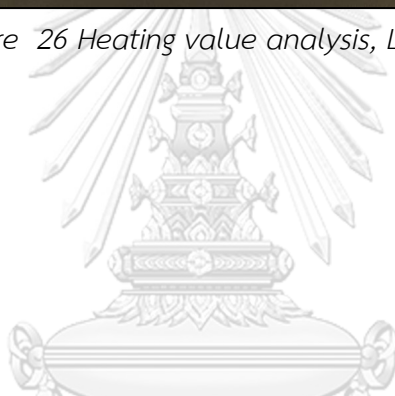


Figure 27 Ultimate analysis, element analyzer (Leco - CHNS 628)

3.4. CO₂ hydrogenation investigation

The hydrogenation of CO₂ to LPG was carried out in a fixed bed reactor equipped with mass flow controls (MFC) and gas chromatography (GC) units, as schematically seen in Figure 31, with the reactant gas entering the reactor from the top and exiting at the bottom. After the exit, a back pressure (BP) valve was installed to regulate the pressure in the reactor and lower the gas pressure before to GC analysis. 0.5 g of catalyst was mixed with 2.0 g of inert quartz grains in a typical run, and the catalysts were reduced for four hours in a flow of 5% H₂/N₂ at 250 °C. The reactions were then carried out at 4 MPa with four different parameters: reaction temperature (310 °C, 330 °C, and 360 °C), CZZA:com-HY mass ratio (2:1, 1:1, 1:2, and 1:4), and W/F (5, 10, and 15 gh/mol). The input gas was a mixture of H₂/CO₂/CO/Ar at a ratio of 68.00/25.70/3.18/3.12 (v/v). All items were GC examined. The Ar, CO, CH₄, and CO₂ were evaluated using a gas chromatograph (GC) equipped with a thermal conductivity detector (TCD), whilst the HCs were studied using a second gas chromatograph equipped with a flame ionization detector (FID).



Figure 28 Gas chromatograph equipped with TCD



Figure 29 Gas chromatograph equipped with FID

The CZZA mixed metal phase and com-HY zeolite catalyst were mixed in three different physical mixing methods as follows (Figure 30):

- *Mix A*: two catalysts were independently crunched and pelletized into a granule shape of 20~40 mesh size. Subsequently, the granules were randomly mixed before being used in the reaction.
- *Mix B*: the two catalyst powders were premixed and then crunched and pelletized into a granule shape of 20~40 mesh size before being used in the reaction.
- *Mix C*: the independent granule-shaped (20~40 mesh size) catalysts were filled into the reactor in separate stages. The upper stage contained the CZZA mixed metal phase, and the bottom stage the com-HY zeolite catalyst.

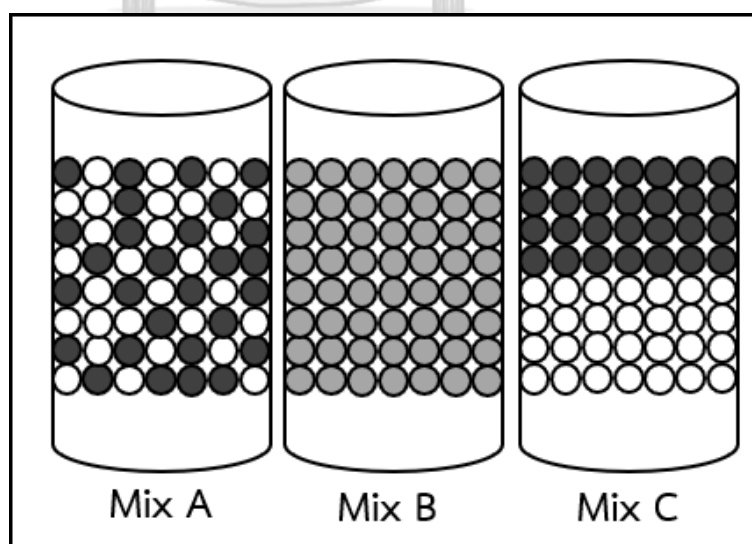


Figure 30 Physical mixing methods for CZZA catalyst(●) and HY zeolite (○)

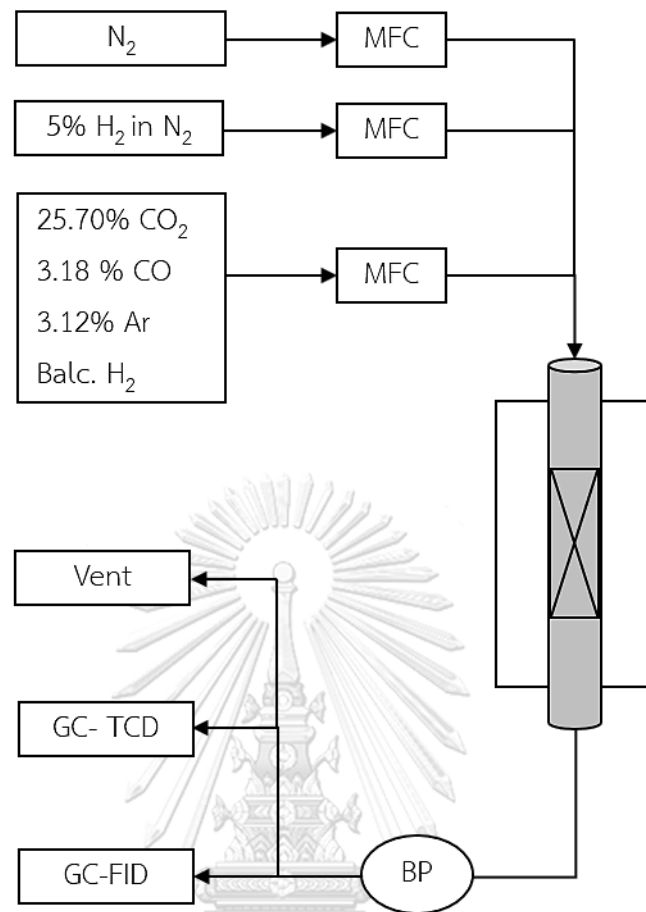


Figure 31 Schematic flow chart of LPG synthesis fixed bed reactor

3.5. BTL Process

จุฬาลงกรณ์มหาวิทยาลัย
CHULALONGKORN UNIVERSITY

3.5.1. Gasification Process and System Configuration

The purpose of this research is to evaluate a pilot horizontal gasifier that utilizes rubberwood pellets and eucalyptus wood chip to generate syngas with a specified H_2/CO ratio. The research was separated into two sections. The first was a series of tests conducted in a laboratory-scale reactor to investigate the influence of temperature on the composition and tar %age of gas products. The second section examined the operation of a pilot horizontal gasifier that had been carefully adjusted to the proper gasification temperature based on the data from the first part.

3.5.1.1. Laboratory scale gasification

Fine particle biomass combustion of rubberwood and eucalyptus wood with a screen size of 0.5 - 0.71 mm was carried out in a laboratory-scale batch fixed bed gasifier, as seen in Figure 32. The primary equipment for the system consists of a steam generator, a flow controller, an electric furnace, and an ice trap. The flow controller was utilized to modify the rate of N₂ flow, which was set to 100 mL/min. The fixed bed gasifier reactor was made of stainless steel tubes with an inner diameter of 27 mm and a length of 893 mm. The reactor was heated by an electric furnace and fueled by steam generated by a steam generator, which saturated vapor at a pressure of 1 atm. Three ice traps were used to gather the experiment's data to ensure that all tar was condensed.

3.5.1.2. Pilot scale gasification

The pilot horizontal gasification plant and associated facilities were developed and placed at the Chulalongkorn University Saraburi campus in Saraburi Province, Thailand. The schematic view of the gasification unit is shown in Figure 33. It is made up of the following components: a feeding system, a gasifier, a steam generator, a tar reformer, a gas purification unit, a gas compression unit, and a gas storage unit. The gasifier was designed to burn wood pellets at a rate of 4.0 kg/h. Additionally, this gasifier may be used with different biomass forms. As a result, the FT process was the downstream process. Because the produced gas required a high caloric value to avoid contamination of inert gas due to the use of air as the gasifier agent, this study employed steam as the gasifier agent. Additionally, due to the variety of pollutants present in generated gas, syngas purifying machines were required. Following is a detailed description of each sub-unit of the gasification unit.

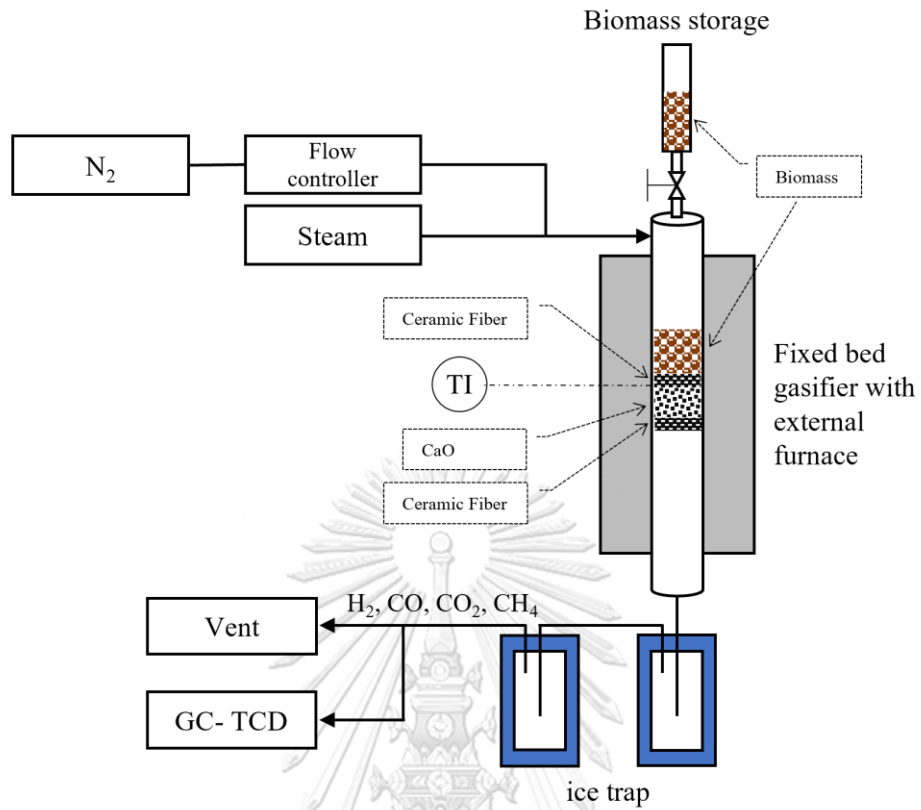


Figure 32 Schematic flow chart of laboratory-scale batch fixed bed gasifier

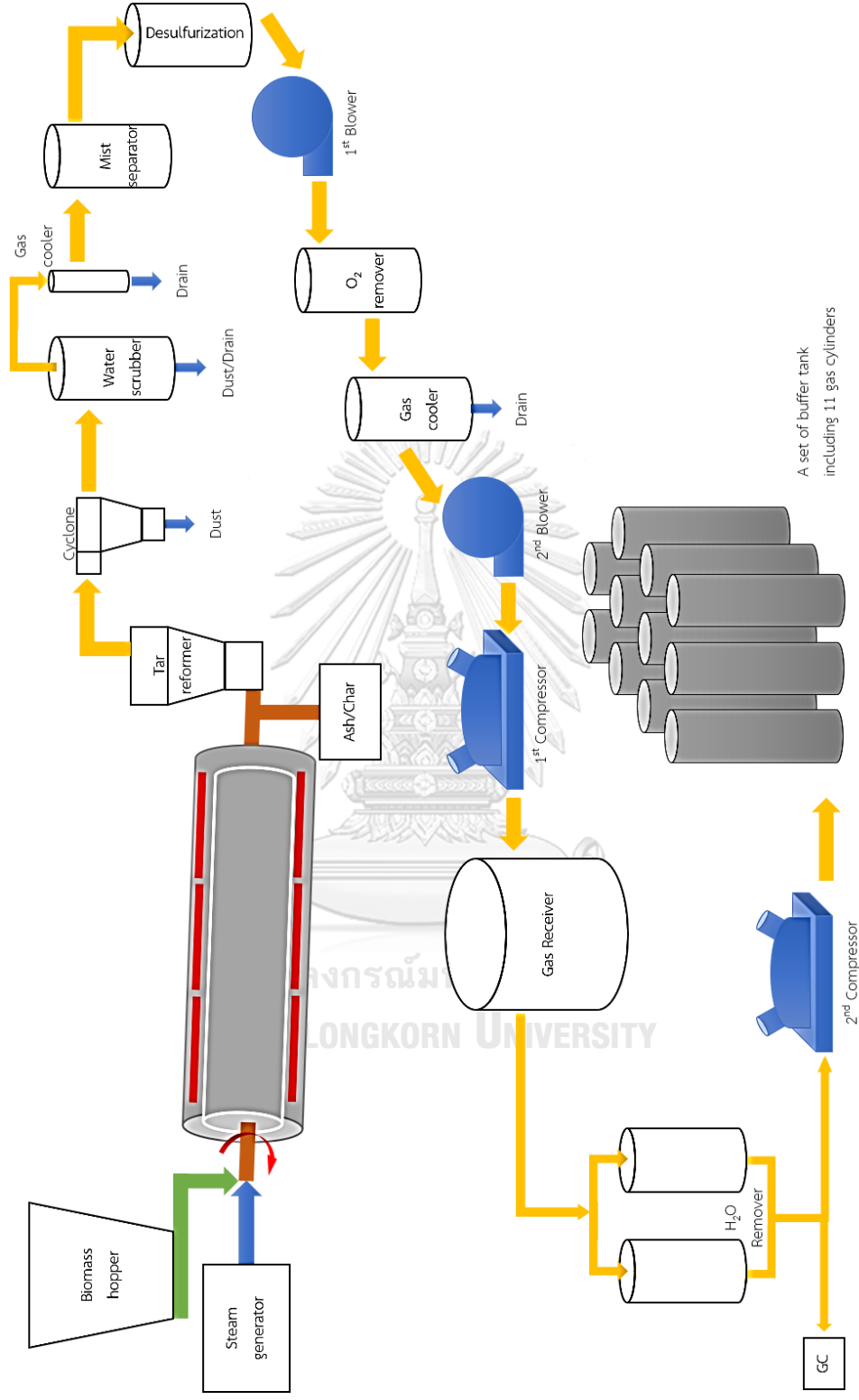


Figure 33 The schematic view of pilot horizontal gasification unit

3.5.1.2.1. Feeding system

A biomass feedstock hopper with a capacity of 200 L was positioned above the screw feeder. The screw feeder was a twin screw design used to feed biomass into a gasifier. It had an adjustable feed rate of up to 10 kg/h.

3.5.1.2.2. Gasifier Reactor

The gasifier is the primary equipment used in gasification systems that convert biomass to syngas. The Pilot Horizontal Gasifier was utilized in this study (Rotary Kiln Reactor). Three zones of the gasifier reactor are connected to three electric heaters to maintain a temperature of 900 °C. The gasifier has a 2.5 m length, 0.2 m inner diameter, and a 2 degree decline. The physical gasifier's form, with a 1.0 m external diameter, was completed by wrapping the heating coil and ceramic insulating wall around the reactor. The connection to the feedstock feeding system was terminated at the junction to the Tar reformer for gas and the char box for solid product.

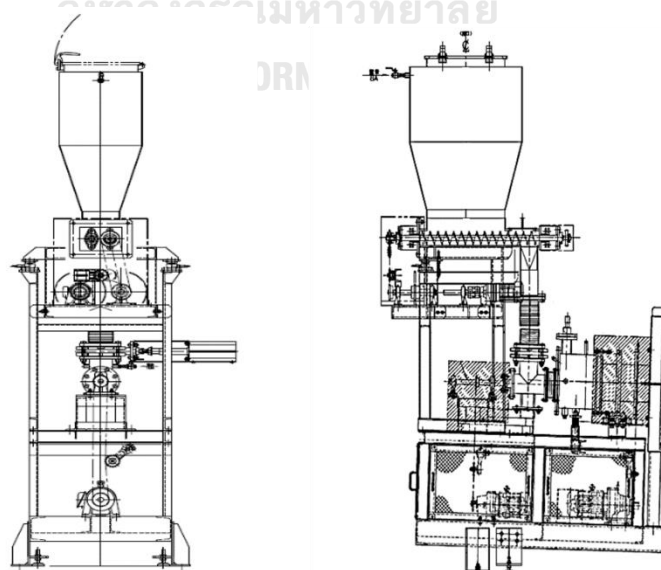


Figure 34 Feeding system

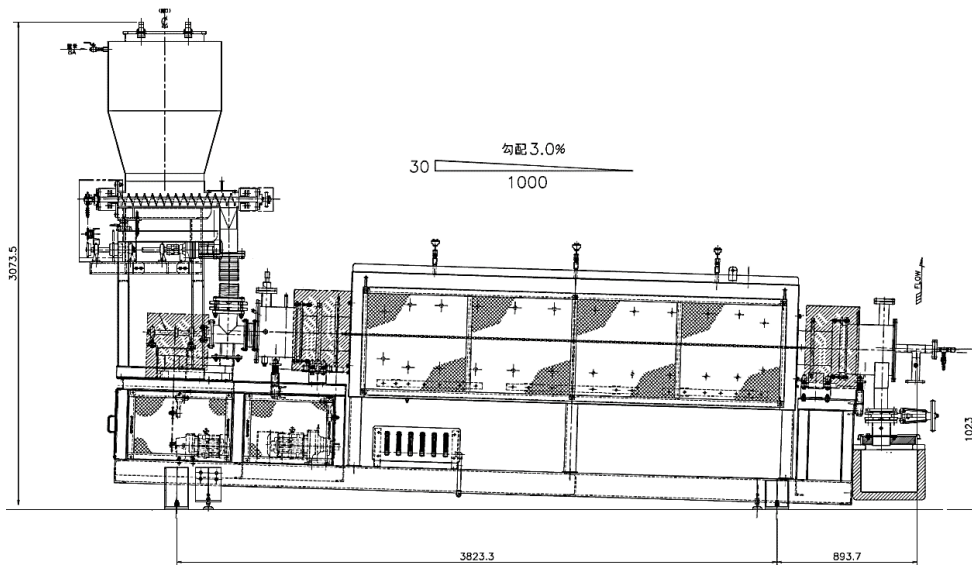


Figure 35 Horizontal gasifier

3.5.1.2.3. Steam generator

Steam was supplied for this gasification unit by an electric steam generator that was linked to the gasifier and flowed into the gasifier along with the biomass. The steam generator was composed of a water tank, a pump, a reverse osmosis membrane, and a water softener with a maximum rate of 5.5 kg/h and a maximum temperature range of 200 °C to 600 °C depending on the set setting.

3.5.1.2.4. Tar reformer

Tar Reformer was located adjacent to the gasifier and operated at the same temperature of 900 °C as the gasifier's syngas. The fine CaO (0.25 - 1.00 mm particle size) acts as a catalyst inside the Tar reformer's approximately 10 - 15 kg capacity and also acts as a bubble fluidized bed with the heater set to a maximum temperature of 900 °C. Cao reaction should be minimized in order to preserve the tar produced when the syngas ascend from the bottom to the top.



Figure 36 Steam generator

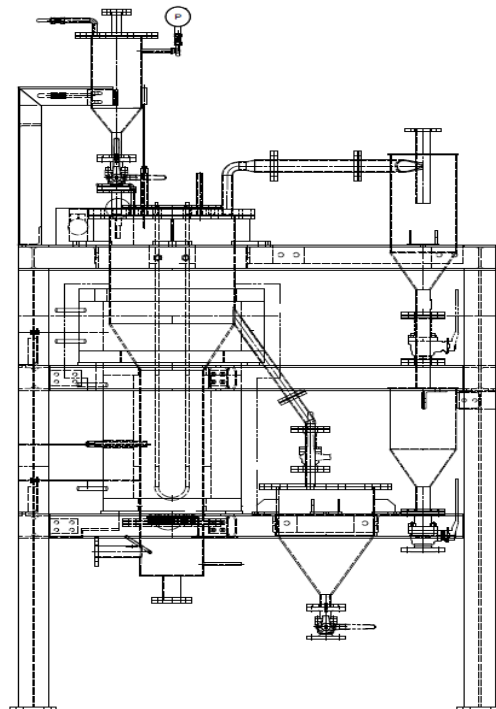


Figure 37 Tar reformer

3.5.1.2.5. Gas cleaning unit

Depending on the syngas requirements for the FT process, a gas cleaning unit may be required for the BTL process. The gas cleaning equipment used in this procedure includes a water scrubber, a mist separator for gas coolers, desulfurization, O₂ removal, and H₂O removal. In this BTL method, the gas cleaning process was divided into two stages based on the pressure level.

The first section was devoted to the low-pressure zone. This zone was linked following the completion of the tar reformer, which continued to operate at a high temperature and negative pressure level. There were several units of gas purification in this zone, each performing a specific function.

A water scrubber was the first purifying machine. The gas produced by the tar reformer may contain light tar that may be dissolved in water while preserving a high temperature. The earliest gas purification device was a water scrubber, which comprised of two stages of water spray nozzles (upper and lower). Each nozzle received 1.5 L/min of water to cool the syngas and remove some light tar before it passed through downstream purification.

Following the use of water scrubbers, syngas was decreased in tar content and temperature to less than 50 °C. However, it remained elevated, and syngas was used to lower the temperature in the second stage (gas cooler). Not only did syngas lower the temperature in this unit, but it also dried the gas by moisture condensation at low temperatures (below 30 °C).

Following that, cool gas went to the mist separator. A tank lined with strain-free steel wool provided a greater surface area for the mist to condense readily.

Due to the poisonous nature of sulfur compounds used in the FT process, desulfurization was used to remove sulfur compounds by adsorption using Ni and Mo on activated carbon. Two desulfurization vessels were installed in tandem for a total

operating duration of 2,000 hours at a concentration of 100 parts per million of H₂S and 50 parts per million of COS for maximum contamination.

O₂ impurity in syngas makes the catalyst inactive in the FT process by producing metal oxide. As a result, O₂ removal was required for the BTL procedure. Because this procedure required a high temperature (150 °C) for O₂ removal, an electric heater was put in this vessel, along with Pd/Al₂O₃ as an O₂ removal catalyst.

The pressure of syngas was raised to 0.8 MPa following the first compression stage. It was a zone of elevated pressure. High-pressure circumstances resulted in the condensing of residual water. As a result, the H₂O removal step was put after the first gas compression. Two containers were employed alternatively to remove H₂O using a molecular sieve, with one functioning and the other being regenerated by heating with N₂ flow.



Figure 38 Water scrubber

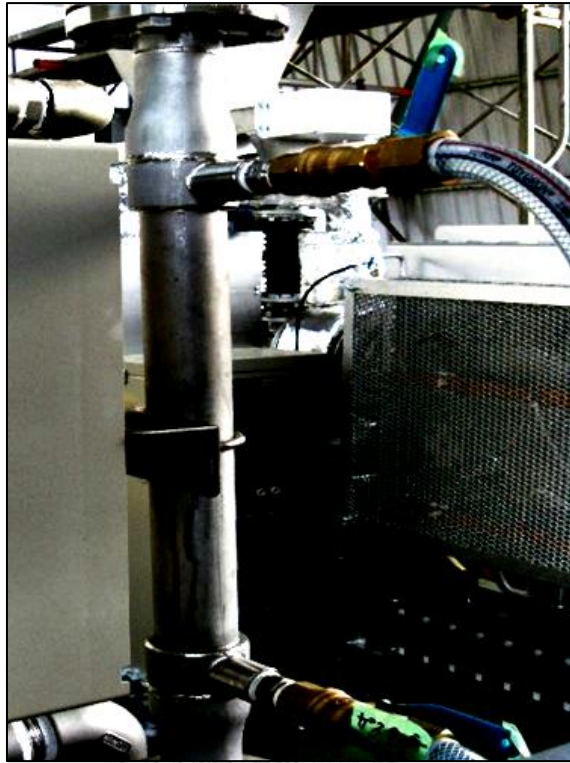


Figure 39 Gas cooler

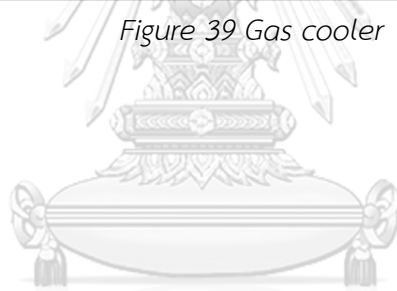


Figure 40 Set of Gas cleaning Unit a) Mist separator, b) Desulfurization, c) O₂ remover



Figure 41 H₂O remover

3.5.1.2.6. Gas compression unit

Syngas was stored at a pressure of 12 MPa in the storage tank, while the gasification process operated at a negative pressure (-10 kPa). Thus, syngas pressures should be raised in two stages. Syngas was compressed in the first stage from -10 kPa to 0.8 MPa using a reciprocating compressor equipped with a cooling water after cooler. The highest flow rate was 8 Nm³/h with an output pressure of 0.8-1 MPa and a cooling water flow rate of 15 L/min. Medium pressure syngas was injected into a tank that maintained a pressure of 0.8 MPa. Syngas was sampled to determine the composition and quality of the gas prior to being sent to the second compressor and stored in the storage tank. After cooler, the second compressor was an air-driven compressor with an air-cooling system. The highest flow rate was 6 Nm³/h, and the maximum output pressure was 14.7 MPa.



Figure 42 The first gas compression unit



Figure 43 The second gas compression unit



Figure 44 Gas storage tanks (Buffer Tank)

3.5.1.2.7. Gas storage tank

A buffer unit is a storage gas unit. There were seven sets of Buffer tanks with eleven cylinders for each set. The total volume capacity of all buffer tanks was 6.35 m³ (820 Nm³ at 14.7 MPa, 35 °C).

3.5.2. Experimental Setup

3.5.2.1. The Lab-scale Gasification

Seven grams of biomass were placed in biomass storage on top of the gasifier, away from the heater zone. N₂ was continually injected into the reactor. When the temperature reached the required level (600 °C, 800 °C, 900 °C, or 1,000 °C), the biomass storage valve was opened, and the biomass suddenly fell into the gasifier. Simultaneously, steam was supplied into the gasifier through co-current flow with

biomass for 1 minute, which was sufficient to provide surplus steam ambient in the reactor. Gas was collected in a gas bag, and tar condensed in an ice trap was collected continually for 10 minutes until full gasification, complete reaction time. The last experiment was performed to investigate tar removal via CaO, which was packed individually layer after biomass and operated at 900 °C. Following that, the gasifier reactor was withdrawn from the heater to fast cool, the remaining biochar and condensed tar were weighed, and the gas produced was evaluated by GC-TCD (Agilent technology, GC7820A).

3.5.2.2. *The pilot horizontal gasification*

After purging the gasification system with N₂ and heating the gasifier, biomass was manually loaded into the hopper. The screw-type feeder located beneath the hopper was used to regulate the gasifier's feed rate. At the hopper, four load cells were placed to monitor the feed rate. A superheated steam generator equipped with a feed controller was installed to deliver steam to the gasifier as a gasifier agent. The produced gas from the gasifier was sent to the tar reformer (TR) unit and then to the gas cleaning unit, while the biochar dropped into the char box at the gasifier's output. At the tar reformer, generated gas, which included tar and vapor, was forced through a CaO bubble bed. This section involved the conversion of tar to syngas. Syngas with no tar was transported to the cleaning section. Syngas was cooled in this section, and tar was condensed in a water scrubber. Freshwater was delivered to a water scrubber, and cooling water was treated with tar using a standard water treatment system. A gas cooler and mist separator were constructed adjacent to the water scrubber to remove any water that may have been generated by the gasifier process or the water scrubber. Although the sulfur level of biomass feedstock is quite low [ref.]. Nonetheless, the desulfurization (DS) unit is required since sulfur is a toxin to the FT catalyst. The DS

unit was installed after the mist separator unit and linked to the system's first induced draft (ID) fan, which was used to manage syngas flow and maintain system pressure balance. Due to the fact that the downstream process is the FT process, which is an exothermic and pressured process, the oxygen level in syngas was a major safety concern. As a result, an oxygen remover (OR) was applied and installed. In two stages of compression, cleaned syngas was compressed and stored in a system of buffer tanks. To begin, syngas was flowed from the OR to the first compressor through a second ID fan, which was used to generate gas pressure and store it in the receiver tank. After the buffer tank, an automated control valve was installed to maintain the pressure in the buffer tank at 0.8 MPa before sending the gas to the second step compression. Prior to the second compressor unit, syn gas with a pressure of 0.8 MPa could be moistened at high pressure by water saturation. Thus, an H₂O remover employing a molecular sieve was used to adsorb the moist and dry gas, and the gas humidity was determined in real time by dewpoint measurement (Michell Instrument) and the gas composition via Micro-GC (Agilent Technology: 490 Micro GC). A second gas compressor squeezed medium high-pressure gas to fill the buffer tank to a pressure of 12 MPa. This gas was immediately available for use in the downstream unit. K-type thermocouples were used to monitor the temperature of the gasifier and its downstream unit. Pressure was measured at each location and shown in the main monitor. All data and settings were saved in a computer.

To determine the optimal steam/biomass ratio that results in the desired H₂/CO ratio (1.75-2.25), two variations in the steam/biomass ratio were investigated in comparison to other similar factors. The gasification test was done continuously for 5 hours. Each ratio and generated gas were tested every 30 minutes to assess the gas composition, and the results of gasification are summarized in Table 9.

After determining the optimal steam/biomass ratio, other types of biomass were investigated. The properties of rubberwood and eucalyptus wood are listed in

Table 7. This process was conducted continuously for 10 days in order to completely fill seven sets of buffer tanks at a pressure of 12 MPa for each kind of biomass. Total production gas would be calculated for mass balance and gas yield calculations by the quantity of gas pressurized into a fixed volume of the buffer tank. This technique determined the precise amount of generated gas and its use for mass balance analysis, and the results of gasification were summarized in Table 10.

3.5.3. Fischer-Tropsch Synthesis and Process configuration

The FT synthesis in this investigation was carried out in a slurry-phase reactor. The FT unit flow chart was shown in Figure 45. A gas feeding controller was installed in the reactor, which included a regulator valve, a mass flow controller, and a pre-heater. The reactor zone consisted of a reactor chamber and oil cooling pipelines running the length of the reactor. At the reactor, electric heaters were placed on maintaining the temperature. Two condensers were installed adjacent to the reactor to condense the liquid product. The final element was the gas released unit, which contained a backpressure valve for pressure management within the reactor. Following the backpressure valve, low-pressure gas was released to the flare and split for composition analysis through GC-TCD.

After completing the FT reactor installation by adding 20 kg of Fe catalyst and a solvent with a high boiling point (n-hexadecane), the catalyst was reduced to activate it. H_2 was fed into the reactor at a rate of 50 L/min kg.cat at a temperature of 240 °C and a pressure of 2 MPa. The reduction step was carried out continuously for 8 hours. The catalyst was then prepared for FT synthesis following the reduction process. The temperature was set to 280° C, and then syngas was fed into the reactor at a rate of 20 L/min.kg.cat with a set pressure of 2 MPa. Following the reaction, the Fe-catalyst's performance was determined by Co conversion. The reaction is complete

when the CO conversion appears to have decreased by 20 %. Also, the buffer tank's syngas pressure was less than 3 MPa. Following that, liquid products were collected for weighing and composition analysis.



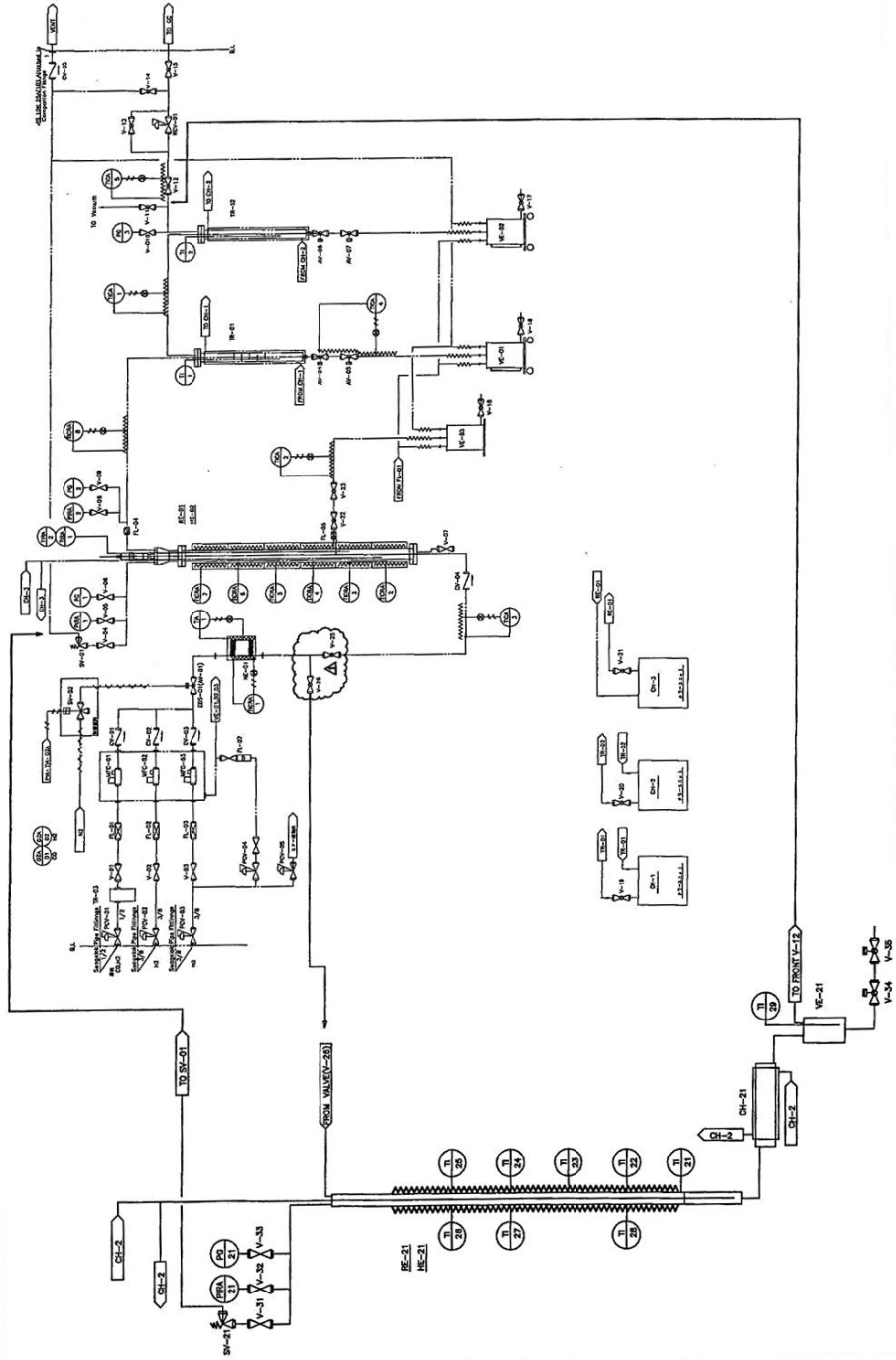


Figure 45 FT flow chart

Chapter 4

Results and Discussion

4.1. Catalyst characterization

4.1.1. CZZA catalyst

XRD analysis of the calcined CZZA catalyst obtained the findings shown in Figure 46. CuO and ZnO phases were assigned diffraction peaks at 35.5° and 38.5° and 48.0°, 56.6°, 62.8°, and 68.0°, respectively. The Al₂O₃ phase's diffraction peaks are obscured, most likely due to their integration into those of ZnO [71]. Due to ZrO₂'s low crystalline degree, no diffraction peaks were found [16]. Cu, Zn, Zr, and Al, on the other hand, were identified through EDX analysis, with their proportional amounts reported in Table 1. Calcined CZZA had a BET surface area (SBET) of 57.75 m²/g, with the remaining characteristics (pore size and volume) listed in Table 1.. Additionally, Table 2 summarizes the Cu surface area and dispersion of the decreased CZZA as measured by N₂O adsorption. which revealed a metallic Cu surface area of 30.45 m²g⁻¹ following reduction, a result comparable to the earlier work. Additionally, metallic characteristics of Cu revealed a high dispersion value of 11.36 % owing to the effect of ZrO₂ addition.

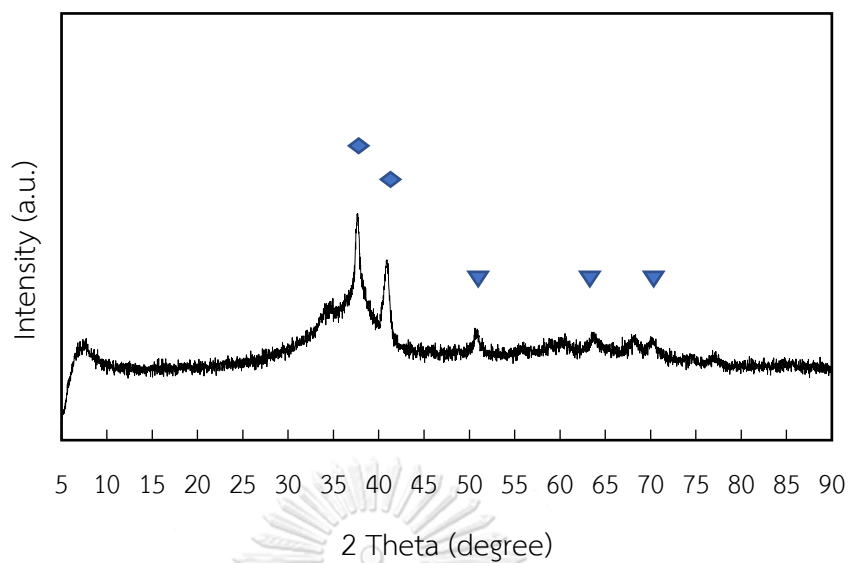


Figure 46 XRD pattern of calcined CZZA showing the peaks for CuO (◆) and ZnO (▼).

Table 3 The EDX results of the CZZA mixed metal catalyst

Catalyst	Calculated		EDX	
	metal	wt. %		wt. %
CZZA				
Cu	4	Cu	48.11	41.58
ZnO	3	Zn	28.99	25.59
ZrO ₂	1.5	Zr	13.35	14.10
Al ₂ O ₃	1.5	Al	9.55	18.73
total	10		100.00	100.00

Table 4 The BET surface area and pore characteristics of the catalysts

Catalyst	S_{BET} m^2g^{-1}	S_{micro} m^2g^{-1}	S_{external} m^2g^{-1}	V cm^3g^{-1}	D nm
Com-HY	552.46	549.24	3.21	0.28	2.56
Syn-NaY	592.67	571.31	21.36	0.28	2.04
CZZA	57.75	13.11	44.64	0.01	21.76

Table 5 Metallic properties of the reduced CZZA

Catalyst	Cu surface area ($\text{m}^2\text{g}_{\text{cat}}^{-1}$)	Cu particle size (nm)	Cu dispersion (%)
CZZA	30.45	9.19	11.36

4.1.2. NaY and HY Zeolite Characterization

XRD analysis of the syn-NaY and com-HY zeolites revealed similar diffraction peaks Figure 47, suggesting that the syn-NaY zeolite was effectively synthesized [72]. The textural characteristics of the com-HY as determined by N_2 adsorption-desorption revealed a typical I isotherm (Figure 48), suggesting that the com-HY exhibited a typical microporous structure [73], as shown by the S_{BET} area and pore volume (V) of $552.46 \text{ m}^2\text{g}^{-1}$ and $0.28 \text{ cm}^3\text{g}^{-1}$, respectively. Additionally, this data demonstrated that the SBET value and pore volume of syn-NaY ($592.67 \text{ m}^2\text{g}^{-1}$ and $0.28 \text{ cm}^3\text{g}^{-1}$, respectively) are comparable to those of com-HY. The acid sites of the various HY zeolites were assessed by temperature-programmed desorption of ammonia (NH_3 -TPD), with the TPD profiles of com-HY (Figure 49) exhibiting two main peaks at 150-250 and 300-450 °C, respectively, corresponding to weak and medium/strong acid sites. However, the profile of syn-NaY zeolite revealed a single peak between 150 and 250 °C, consistent with the presence of weak acid sites [74].

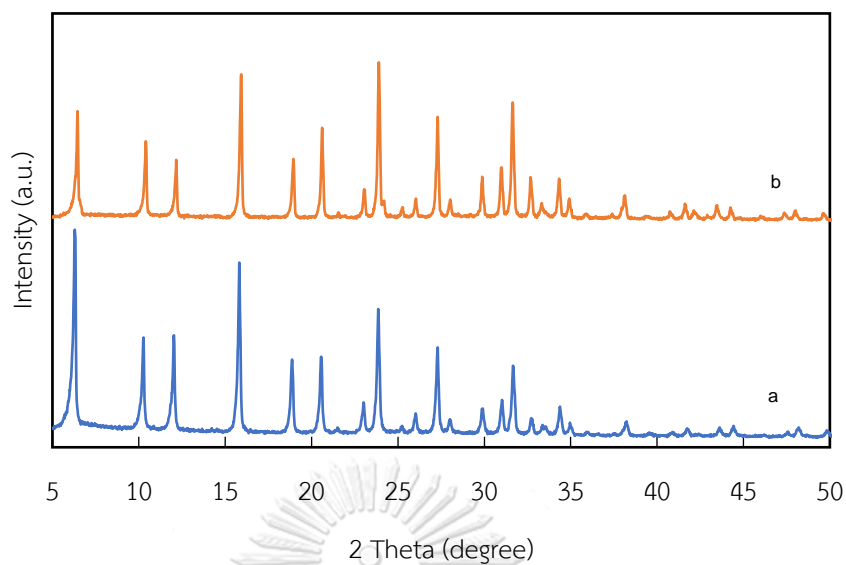


Figure 47 Representative XRD patterns of the (a) com-HY, (b) syn-NaY zeolites

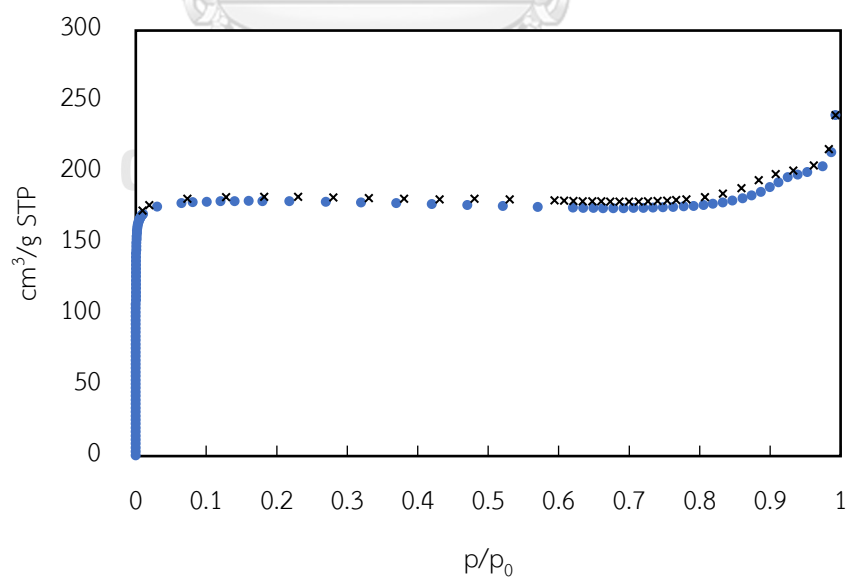


Figure 48 Representative N_2 adsorption (●) – desorption (x) isotherm of com- HY

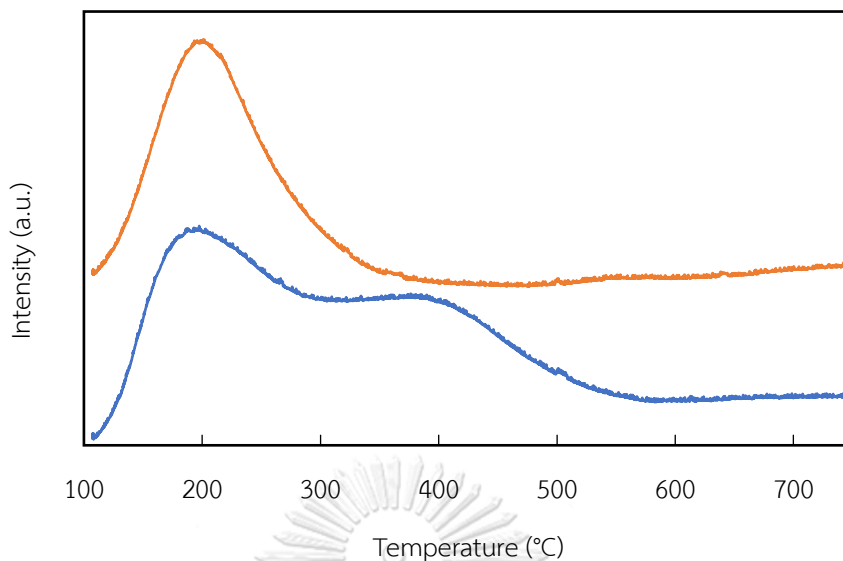


Figure 49 Representative NH_3 -TPD profiles of the (a) syn-NaY and (b) com-HY zeolites

4.1.3. Reaction conditions Investigation

4.1.3.1. Effect of the Mixing method

The influence of various catalyst mixing methods on the CO_2 hydrogenation process was tested at 310 °C, 4 MPa, and a W/F of 10 gh/mol, with the results shown in Figure 50 (conversion and product selectivity) and Figure 51. (carbon distribution in HCs product). Mix A had the highest CO_2 conversion and LPG selectivity, at 22.11 percent and 66.32 percent, respectively. Mix B had a CO_2 conversion level of 19.68 percent, which was essentially equivalent (slightly lower) to Mix A but had a substantially lower CO conversion level. It is probable that Mix A inhibited the RWGS reaction, resulting in poor CO conversion in Mix B. Furthermore, the major product (79.42 percent) exhibited a minimal HC selectivity (2.0 percent). The Mix B catalyst exhibited low catalytic activity for CO_2 dehydration due to the inactive zeolite catalyst. This is due to a closer contact between the CZZA and HY zeolites as a result of the Mix B method. Water generated during the MS and RWGS processes prevented MeOH

and DME from dehydrating to HCs, which quickly adsorbed on the HY zeolite and were not detectable in the product stream. Furthermore, a substantial CH₄ selectivity was seen in the HC distribution, indicating a restricted amount of active carbon on the zeolite's surface due to the acidic catalyst's poor CO₂ dissociation [75]. These findings are similar with a recent study [64] on the hydrogenation of CO₂ to lower olefins utilizing In₂O₃/SAPO-5 and various mixing methods. Combining the metal and zeolite catalyst particles prior to pelletization led in metal migration during the reaction, followed by ion exchange of metal ions with zeolite protons, greatly decreasing the amount of highly acidic sites and severely deactivating the zeolite.

The Mix C catalyst converted CO₂ at a rate equivalent to the Mix A and Mix B catalysts. It did, however, have a relatively low CO conversion level despite having the highest HC selectivity (99.98 percent) and contained no DME. Separating the two types of catalyst (CZZA and HY zeolite) resulted in the separation of CO₂ hydrogenation to MeOH, which happens on the CZZA mixed metal catalyst, and MeOH conversion to HCs, which requires the acid sites on the zeolite catalyst. As a result of the high concentration of MeOH on the surface of the CZZA metal catalyst, an equilibrium conversion of CO₂ hydrogenation to MeOH occurred, as indicated in *R 1*, halting the reaction. As a result, the RWGS became more dominant [76], and equivalent results were obtained employing a single CZZA catalyst in Figure 54.

As a result, zeolite contributes to RWGS suppression in the following ways: The MeOH and DME generated during the CO₂ hydrogenation process on CZZA are dehydrated on the HY zeolite to yield HCs and H₂O, and the H₂O formed increased the vapor concentration near the CZZA metal catalyst. As a result, the RWGS reaction was stifled. Furthermore, the Mix C catalyst generated no detectable DME and had the highest HC selectivity [77]. Despite this, C₅₊ was the dominating component in the HC distribution, indicating that virtually all MeOH was converted to DME. The DME was then completely converted to HCs in the zeolite phase. Separating the CZZA and HY

zeolite catalyst phases, on the other hand, increased the retention time of intermediate products that can be continually converted to higher HC products. As a consequence, the Mix A catalyst had the greatest catalytic activity.

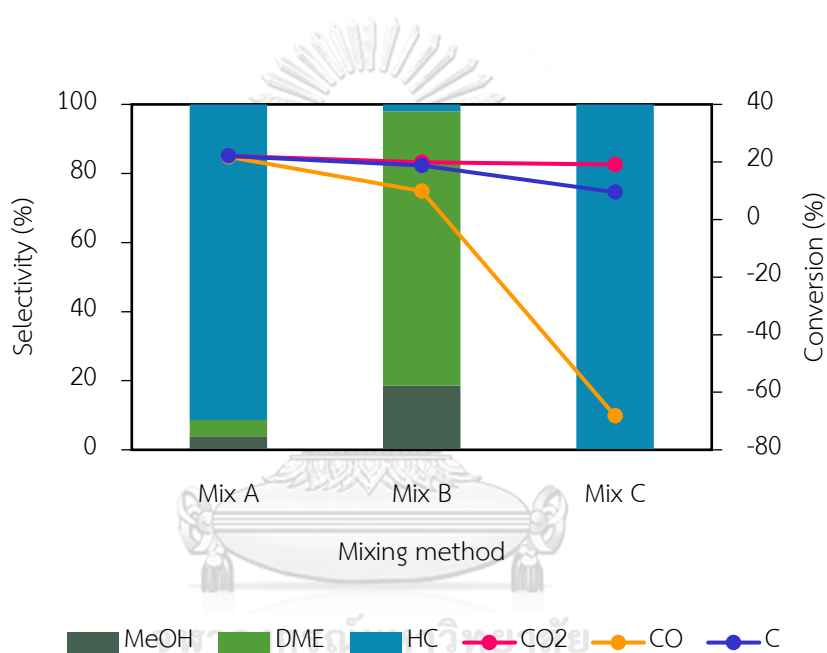


Figure 50 The influence of various catalyst mixing techniques on reaction results obtained at 310 °C, 4 MPa, 10 g mol^{-1} , and a CZZA: com-HY zeolite mass ratio of 1:1. Data are shown as CO₂, CO, C conversion and MeOH, DME, HC selectivity.

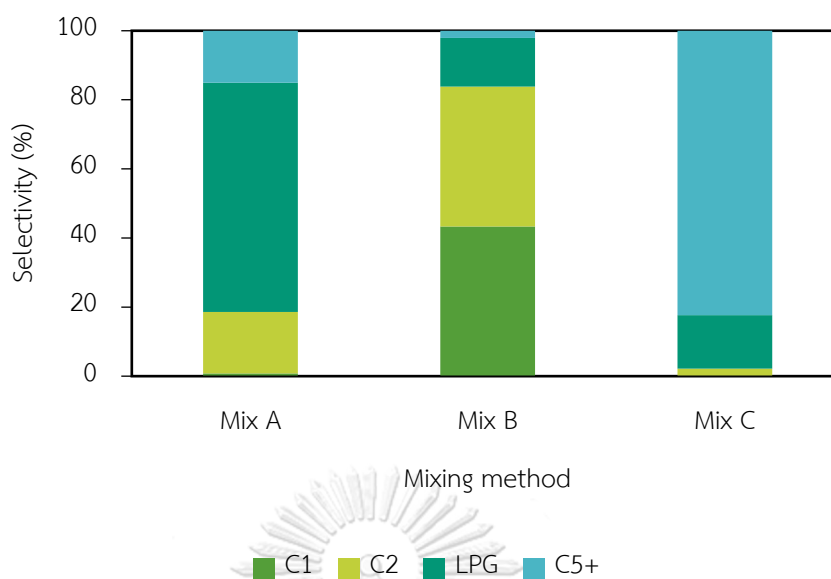


Figure 51 Carbon distribution in produced HC products using various catalyst mixing techniques at 310 °C, 4 MPa, 10 g_hmol⁻¹, and a CZZA: com-HY zeolite mass ratio of 1:1.

4.1.3.2. Effect of the reaction temperature

The hydrogenation of CO₂ to LPG was studied at several reaction temperatures (310–360 °C) with a W/F of 10 g_hmol⁻¹ under 4 MPa, and the results are shown in Figure 52 and Figure 53. Because the endothermic RWGS reaction was preferred, increasing the reaction temperature resulted in an increase in CO₂ conversion and a decrease in CO conversion [6]. These findings are consistent with a previous study on CO selectivity under different reaction conditions, which found that lowering the reaction temperature from 420 to 360 °C dramatically reduced CO selectivity from 91 percent to 51 percent, levels considerably below equilibrium [64].

The selectivity of MeOH and DME decreased as the reaction temperature increased in MeOH and DME dehydration processes. Because the DME conversion to HCs is endothermic, the selectivity improved considerably from 91.31 to 96.53 percent at 310 and 330 °C, respectively, and marginally to 98.76 percent at 360 °C. In contrast,

the selectivity for the desired LPG product was virtually same at 66-68 percent. As a consequence, the optimum temperature for LPG synthesis was determined to be 330 °C.

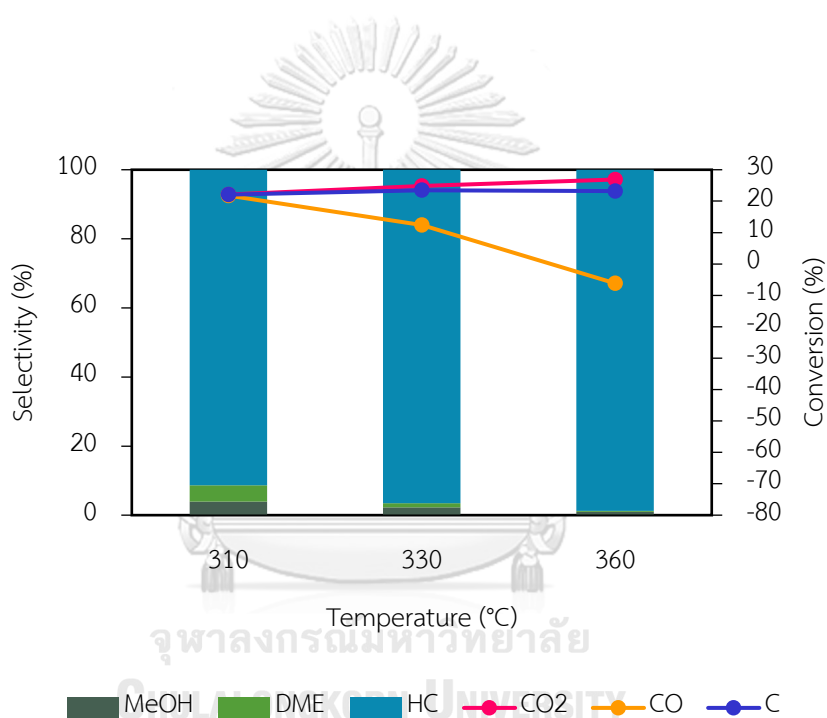


Figure 52 The influence of various Temperature on reaction results obtained at 4 MPa, 10 g_{mol}⁻¹, and CZZA: com-HY zeolite mass ratio of 1:1 using the Mix A catalyst. Data are shown as CO₂, CO, C conversion and MeOH, DME, HC selectivity.

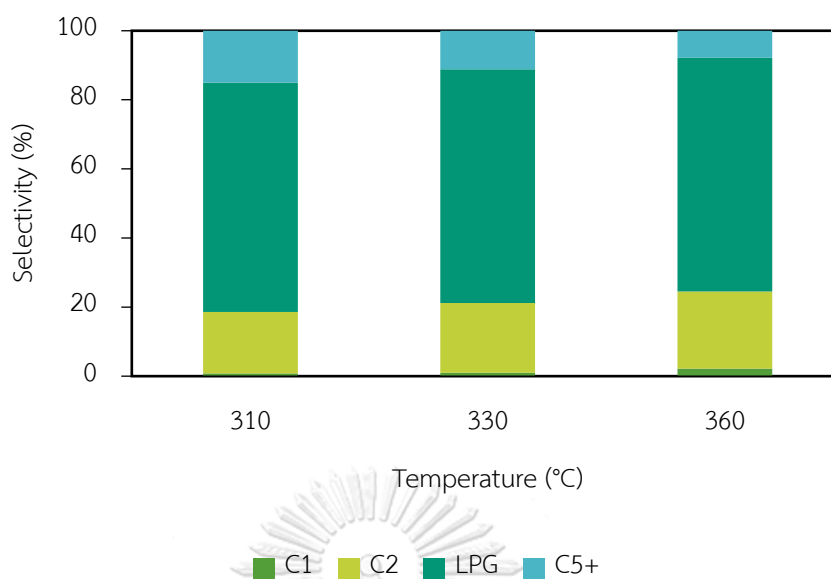


Figure 53 Carbon distribution in produced HC products using various different reaction temperatures at 4 MPa, 10 g mol^{-1} , and a CZZA: com-HY zeolite mass ratio of 1:1 using the Mix A catalyst.

4.1.3.3. Effect of the CZZA: HY zeolite mass ratio

The effect of the CZZA metal catalyst: HY zeolite mass ratio on catalytic performance was investigated (only CZZA, 2:1, 1:1, 1:2, 1:4, only HY), and the findings are shown in Figure 54 and Figure 55. Single CZZA or HY zeolite catalysts demonstrated low LPG selectivity. The metal catalyst to HY zeolite mass ratio had minimal influence on LPG selectivity but had a considerable effect on CO conversion level. The CZZA catalyst alone transformed CO at an exceptionally low rate of -145.59 percent due to the dominant RWGS reaction. Because the HY catalyst is not the active site for CO_2 conversion, it has extremely low CO_2 and CO conversion levels (near to 0 percent). When the CZZA:HY zeolite mass ratio was increased, the CO_2 conversion level climbed somewhat, reaching a maximum (27%) at a mass ratio of 1:2, while the CO conversion level was greatest (20.94%) at the same mass ratio. Furthermore,

increasing the mass ratio of CZZA to HY zeolite improved selectivity for HCs, since more HY zeolite contributes more to the conversion of MeOH and DME to HCs. As a consequence, the optimal CZZA to HY zeolite mass ratio was 1:2.

For HCs products synthesized only from CZZA and HY zeolite, a similar carbon distribution pattern was found. The inability of such a device to produce HCs might indicate a strong CH₄ selectivity. The LPG selectivity seen in the HY experiment, on the other hand, might be due to the zeolite's selective characteristic rather than the low rate of CO₂ hydrogenation (4.41 percent of CO₂ conversion). Furthermore, only the HY zeolite used in the method was unable to function as a CO₂ hydrogenation catalyst via the MeOH pathway. The reaction might, however, proceed via the FT pathway via CO₂ conversion to CO via RWGS. The CO was then hydrogenated at the acid sites of the zeolite, which explains why CO conversion was detected despite having a high level of CO selectivity. As a result, reactions via the FT pathway typically display the Anderson-Schulz-Flory (ASF) distribution [78]. Despite the fact that Figure 55 showed a similar carbon distribution pattern when just CZZA and HY zeolites were employed. In contrast, the correlative impact of the combination catalyst exhibited good CO₂ conversion and HCs selectivity. Because mixing HY zeolite with a methanol synthesis catalyst significantly improves CO₂ conversion and HCs generation [37]. When methanol and DME intermediates generated over a Cu-base catalyst are converted into HCs over a zeolite acid site, HCs are created [79].

Moreover, due to the collaboration of their catalysts, the hybridization of two catalysts increased the performance of HCs production. The HCs chain formation process was described as a carbon pool mechanism by Dalil and Kolboe [80]. A carbon pool such as (CH₂)_n exists on the zeolite surface and has been engaged in the sequential evolution of olefinic intermediates towards higher HCs. Oxide catalysts become more reducible as a result of hydrogen overflow from the oxide catalyst to the zeolite surface, and chain formation is inhibited [63].

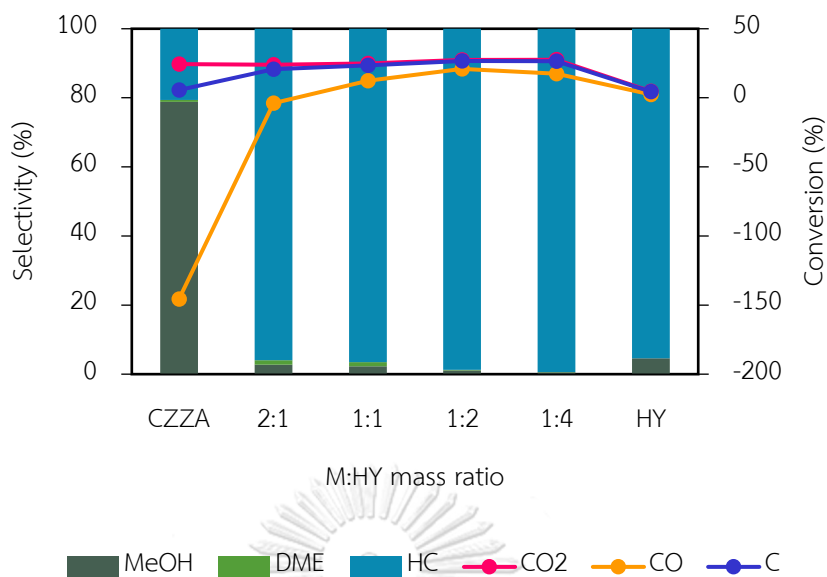


Figure 54 The influence of various CZZA: HY zeolite mass ratios on reaction results obtained at 330 °C, 4 MPa, and 10 ghmol⁻¹ using the Mix A catalyst. Data are shown as CO₂, CO, C conversion and MeOH, DME, HC selectivity.

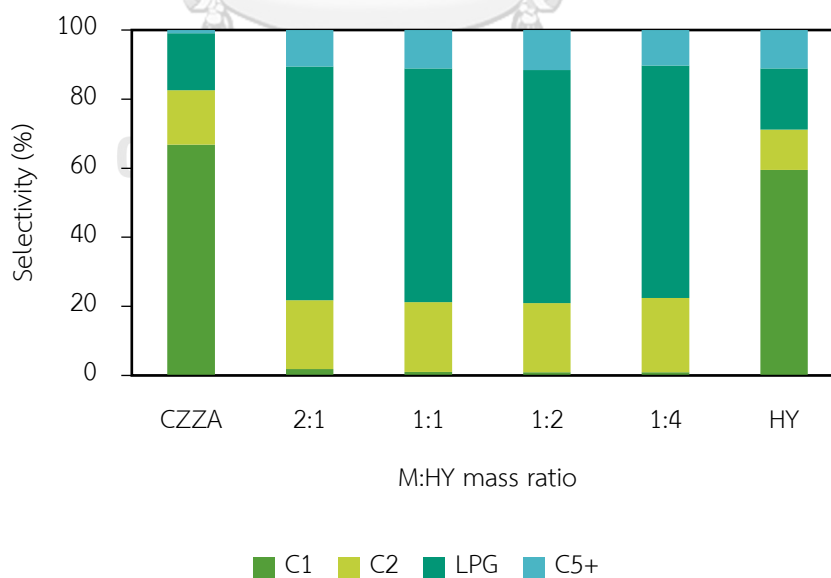


Figure 55 Carbon distribution in produced HC products using various different CZZA: HY zeolite mass ratios at 330 °C, 4 MPa, and 10 ghmol⁻¹ using the Mix A catalyst.

4.1.3.4. Effect of the W/F ratio

Figure 56 and Figure 57 show the hydrogenation of CO₂ to LPG at various W/F ratios (5, 10, and 15 ghmol⁻¹) at a reaction temperature of 330 °C and a pressure of 4 MPa. The catalyst transformed CO₂ at a rate of 25.06 percent and CO at a rate of -5.06 percent when the W/F ratio was 5 ghmol⁻¹. In comparison, the CO₂ and CO conversion levels increased with a W/F of 10 and 15 ghmol⁻¹, respectively, indicating that a high flow rate was not favorable for CO₂ conversion and that the RWGS reaction was favored. They did, however, show equivalent CO₂ conversion and CO selectivity when the reactions were carried out at W/F values of 10 and 15 ghmol⁻¹, showing that the reaction had reached its theoretical limit at W/F value of 10 ghmol⁻¹. Despite this, the distribution of HC products was largely consistent across all W/F ratios tested. Thus, a W/F ratio of 10 ghmol⁻¹ coupled with a higher flow rate is favorable for CO₂ hydrogenation-based LPG production.

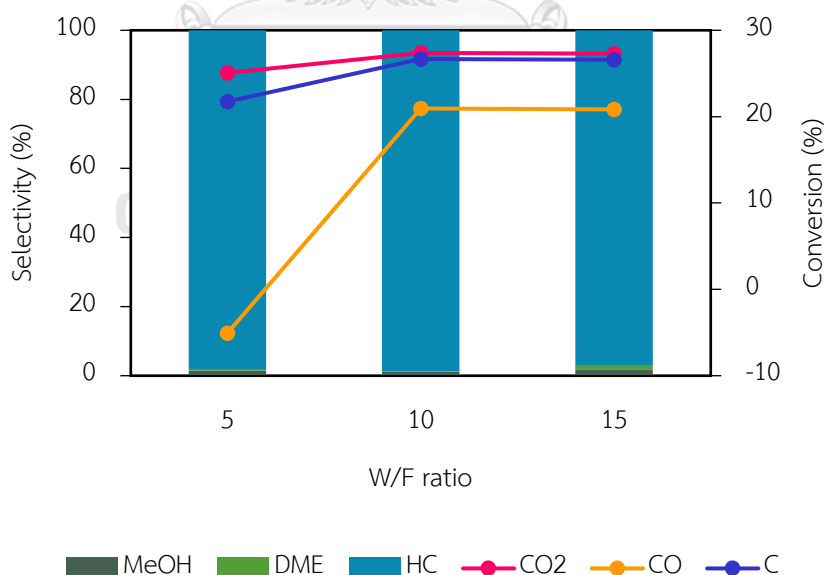


Figure 56 The influence of various W/F ratios on reaction results obtained at 330 °C, 4 MPa, and a CZZA: com-HY zeolite ratio of 1:2 using the Mix A catalyst. Data are

shown as CO_2 , CO , C conversion and MeOH , DME , HC selectivity.

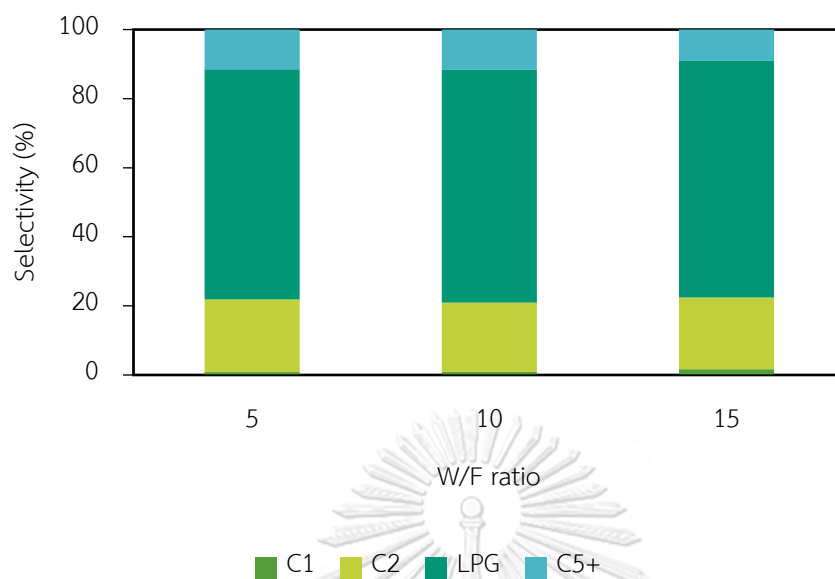


Figure 57 Carbon distribution in produced HC products using various different W/F ratios at 330 °C, 4 MPa, and a CZZA: com-HY zeolite ratio of 1:2 using the Mix A catalyst.

4.1.4. RWGS reaction Suppression

CO was added into the feeding gas, as specified in the experimental setup method, to suppress RWGS reaction, a prominent side reaction for this system. This was achieved by increasing the partial pressure of CO as a result of the RWGS reaction. In a reversible gas phase reaction, specifically a RWGS reaction, increasing the partial pressure of the product suppresses the forward motion and allows the reaction to occur in the reverse direction. Thus, the impact of CO in the input gas on product yield was examined in this part by comparing the findings from the prior section's optimal condition to those from two alternative feeding gases: $\text{H}_2/\text{CO}_2/\text{CO}$ (called RXN 1) and H_2/CO_2 with a molar ratio of 3/1 (designated RXN 2) [81-83].

Table 6 summarizes the results of RXN 1 and RXN 2. The degree of CO_2 conversion in RXN 2 (25.81%) was found to be lower than in RXN 1. (27.39 percent)

Furthermore, a significant CO yield (27.86 percent) was found in the RXN 2 product stream, and CO exhibited a high conversion level (20.94 percent) in RXN 1 due to the severe degree of RWGS reaction in RXN 2, validating the rationale for adding CO to the input gas for this research. Furthermore, the results showed that RXN 2 had an HCs yield of 18.07 percent, which was lower than the 26.33 percent found in RXN 1. The difference between the two experiments appears to be minimal in the case of LPG selectivity in HCs products.

The BET surface area of the CZZA catalyst was determined in this study and is shown in Table 4. CZZA has a smaller BET surface area than the standard [5, 16] synthesis technique. However, the active Cu surface area as determined by N₂O chemisorption was more than the reference due to the high degree of Cu dispersion, which led in a higher CO₂ conversion rate when compared to Cu-base catalys [5, 65, 75]. Additionally, the superior performance of CZZA and HY zeolite appears to have an effect on the reaction outcomes. Young-lawon Park and colleagues [84] reported that hydrocarbon yield was dependent on the amount of acid sites in zeolite, which was consistent with the findings of Since Inui and Jean et al. [85], who proposed that higher hydrocarbon yield and selectivity could be obtained using a zeolite catalyst with a moderate acid strength. The HY zeolite used in this work has favorable characteristics that promoted HCs formation. As seen in Figure 49, the medium acid strength with a broad base of the peak indicated a large amount of acid site [86]. Moreover, the crystallinity or particle size of HY zeolite may have an effect on its LPG selectivity. The carbon distribution synthesized from RXN 1 was analyzed by GC, and its chromatogram is shown in Figure 58. It revealed a high selectivity for propane and butane due to the intra- or inter-crystalline diffusion limitation of the micropore of HY zeolite [65], which was reported as type I of N₂ adsorption-desorption isotherm in Figure 48 and 2.56 nm of pore diameter in Table 4.

When compared to previous research, the results from this work indicated a high selectivity of the HCs product at 98.70 % or 26.33 % yield with 27.39 % CO₂ conversion and 20.94 % CO conversion. In Addition, the influence of the RWGS reaction appears to be diminished as a result of the appropriate contact distance between CZZA and HY zeolite, which results in a stable active site for the zeolite and CO in the feed. However, other research have documented the hydrogenation of CO₂ to light hydrocarbons or the synthesis of liquid hydrocarbons using a variety of methanol synthesis catalysts in combination with a variety of zeolite types. For example, Fujiwara and colleagues [75] reported reaction values of 36% CO₂ conversion, 56.5 % CO selectivity, and 34.3 % HCs selectivity using Cu-Zn-Cr and HY as the catalyst and zeolite, respectively, for MeOH synthesis. The finding appears to indicate a high CO₂ conversion rate, with a high CO selectivity from the RWGS reaction. Li and his colleagues published [5] CO₂ hydrogenation for LPG production in 2014. At low temperatures, the performance of CZZA coupled with Pd- beta zeolite was evaluated. The results indicated a high CO₂ conversion rate (26.2 %) with a low CO selectivity (11.9 %), and a similarly low HCs selectivity of 13.3 %. Thus, while the RWGS reaction was inhibited at low temperatures due to the endothermic nature of the reaction, the DME generated by MeOH dehydration required sufficient energy to convert to hydrocarbon on the acid site of the zeolite. As a result, the reaction resulted in a poor selectivity for HC and a high selectivity for DME (74-8 %). Additionally, in a prior research of CO₂ hydrogenation to HC, Tong M. and colleagues [87] reported successful synthesis utilizing Zn-ZrO₂ and modified Mn-SAPO-34. However, the findings indicated a high selectivity for CO in the product stream (42.2 %) and a CO₂ conversion rate of 21.3 %.

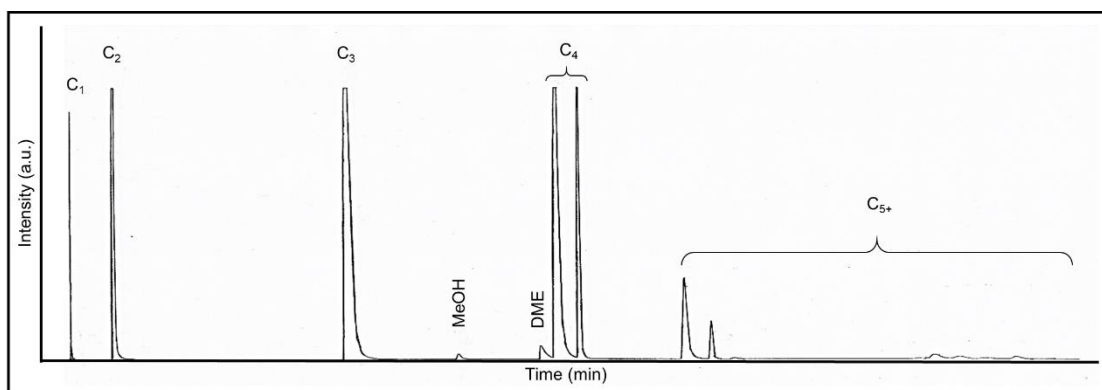


Figure 58 Chromatogram of products from LPG synthesis , conducted at 330 °C, 4 MPa, 10 g mol^{-1} , and a CZZA: com-HY zeolite ratio of 1:2 using the Mix A method



Table 6 Reaction results with difference inlet gas composition ^[a]

Inlet gas	denoted as	% Conversion			% Yield (% Selectivity)					Carbon distribution (%)				
		CO ₂	CO	C	CO	MeOH	DME	HCs	C ₁	C ₂	C ₃	C ₄	C ₅₊	LPG
H ₂ /CO ₂ /CO ^[b]	RXN 1	27.39	20.94	26.68	-	0.3	0.05	26.33	0.91	20.02	30.03	37.41	11.63	67.44
						(1.11)	(0.19)	(98.70)						
H ₂ /CO ₂ ^[c]	RXN 2	25.81	-	18.62	27.86	0.38	0.18	18.07	1.35	20.36	30.80	37.57	9.92	68.37
					(27.86)	(1.46)	(0.69)	(69.99)						

[a] conducted at 330 °C, 4 MPa, 10 ghmol⁻¹, and a CZZA: com-HY zeolite ratio of 1:2 using the Mix A method

[b] H₂/CO₂/CO = 68.00%/25.7%/3.18% balance with Ar

[c] H₂/CO₂ = 3/1 = 71.8%/24.5% balance with Ar

4.2. BTL Process.

4.2.1. Biomass Gasification

4.2.1.1. Feedstock characterization

Table 7 summarized the biomass properties of rubberwood pellets (RWP) and eucalyptus wood chips (EWC), including final analysis, proximate analysis, and low heating value. Although the milling procedures for both biomass feedstocks were different, the chemical and physical characteristics appear similar on a dry basis. For example, RWP had a low heating value of 18.37 MJ/kg, which was comparable to EWC's 18.39 MJ/kg on a dry basis. Furthermore, comparable characteristics may influence similar gasification results. The primary distinctions between these biomass feedstocks, however, were their form and moisture content. The form of biomass feedstock has an effect on bulk density, which may have implications for transportation and storage facilities [88]. The biomass milling process results in a variation in the moisture content of the feedstock, resulting in a range of biomass feedstock quality [89]. In other words, the wood pellet milling process requires a drying process. As a result, wood pellets are constantly less wet (8-10 wt. % of moisture). On the other hand, the wood chips milling process is a straightforward biomass conversion or size reduction process that consists solely of reducing the size of biomass from wood logs to tiny chips, without any drying. As a result, wood chips have a similar moisture content to new logs [90]. Due to the limitations of the gasification unit specification, wood chips were sun-dried prior to use in this investigation.

Table 7 Characteristics of Biomass

	RWP	EWC
Moisture content, MC	8.47	8.02
Proximate analysis (wt. %), d.b.		
Volatile matter, VM	79.47	81.42
Fixed carbon*, FC	17.98	17.90
Ash	2.55	0.68
Ultimate analysis (wt. %), d.b.		
C	49.70	47.80
H	5.98	5.78
N	0.31	0.28
O*	44.01	46.14
H/C	1.43	1.44
O/C	0.66	0.72
Heating value, MJ/kg		
LHV, d.b.	18.37	18.39

d.b.: dry basis

*by difference

จุฬาลงกรณ์มหาวิทยาลัย
CHULALONGKORN UNIVERSITY

4.2.1.2. Influence of temperature on tar yield in lab-scale reactor

The purpose of this study was to determine the effect of gasification temperature on the amount of tar produced using rubberwood and eucalyptus as raw materials. The temperature ranged between 600 and 1000 °C, with an abundance of water vapor. Table 8 summarizes the product yield and gas composition data. For rubber and eucalyptus wood, it was discovered that tar declined as temperature increased, but gaseous yield increased. The liquid yields of rubber and eucalyptus wood were reduced from 19.63 % to 1.01 % and 26.57 % to 1.96 %, respectively. Surprisingly, between 800 and 900 °C, the form of RWP and EWC decreased from 12.6

to 3.84 % and 16.02 to 5.32 %, respectively. While the component of the gas product was investigated as a function of temperature. A higher temperature promotes primary and secondary water gas reactions, secondary cracking and reforming of heavy hydrocarbons or tars, all of which are endothermic and enhance H₂ production [91-93]. While the CO was reduced with increasing temperature, Franco et al. [94] observed that during biomass gasification utilizing holm-oak and eucalyptus at temperatures ranging from 730 to 830 °C, lesser CO was generated owing to the water gas shift reaction. The CO₂ concentration was somewhat higher due to the dominance of secondary water gasification over water-gas shift, which was also found by Franco et al. While the CH₄ concentration dropped with increasing temperature due to further cracking and reforming processes. Furthermore, it has been observed that the influence of temperature on methane consumption is largely reliant on gasifying factors such as steam [94, 95]. CO and H₂ were critical in a gas product that requires an H₂/CO ratio of 1.75 - 2.25 for FT synthesis. It was discovered that this range ratio could be created between 900 and 1000 °C. However, when the liquid yield is considered, the temperature of 900 °C for both types of raw material was shown to be enough for generating syngas at the required ratio. Furthermore, tar removal via CaO at 900°C for RWP and EWC was studied. The efficiency of CaO for tar removal was observed. Tar content in both raw materials was less than 0.2 wt%. Tar reforming (R 20) and hydrocarbon reforming (R 21) were the primary tar removal processes. This experiment's catalytic reforming of tar not only decreases the quantity of tar in the produced gas but also increases the hydrogen and CO content, as reported by Tanksale et al. [96] and Balat et al. [97]. However, when the tar yield was taken into account, the temperature of 900 °C for both types of raw material was adequate to generate syngas at the required ratio. Thus, 900 °C was selected as the operating temperature for the pilot horizontal gasifier.

Table 8 Product yield and gas composition of variation temperature

Biomass	Temp. (°C)	Product yield (wt.%)			Gas composition (vol.%)				
		Tar	Char	Gas	CH ₄	CO ₂	H ₂	CO	H ₂ /CO
RWP	600	19.63	17.98	62.39	17.25	9.62	0	73.13	0
	800	12.68	12.71	74.61	14.57	10.32	38.7	36.41	1.06
	900	3.84	10.27	85.89	10.39	11.64	51.69	30.25	1.71
	1,000	1.01	8.25	90.74	1.27	11.94	60.01	26.78	2.24
	900*	0.01	9.23	90.76	8.35	9.54	52.89	29.22	1.81
EWC	600	26.57	18.7	54.73	18.81	9.11	0	72.08	0
	800	16.02	11.38	72.6	12.41	10.46	39.09	38.04	1.03
	900	5.32	9.73	84.95	8.08	10.3	52.68	28.94	1.82
	1,000	1.96	3.48	94.56	2.95	11.11	59.9	28.04	2.14
	900*	0.02	8.75	91.23	7.95	9.21	53.21	29.63	1.79

* Removal tar by CaO.

Tars reforming; $\text{Tars} + \text{H}_2\text{O} \rightarrow \text{Ca(OH)}_2 + \text{CO} + \text{Hydrocarbons}$ R 20

Hydrocarbons reforming; $\text{Hydrocarbons} + \text{H}_2\text{O} \rightarrow \text{H}_2 + \text{CO}_2 + \text{CO}$ R 21

4.2.1.3. Investigation of Steam to Biomass ratio

The change in the biomass ratio (S/B) was calculated, and the findings are summarized in Table 9. Table 9 displayed the reaction findings for the different S/B ratios based on the stated Operating Parameters: biomass feed rate (kg/h), steam feed rate (kg/h), steam to biomass ratio (kg/kg), and gas compositions. The first, called EXP1, demonstrated reaction outcomes with a lower S/B (0.52) while the second, called EXP2, demonstrated reaction results with a higher S/B (1.35). When more steam was added, the H₂ gas composition increased significantly from 49.97 % to 56.72 % for EXP1 and EXP2, respectively. Although the quantity of H₂ in the gas component increases, the

level of CO_2 also increases with increasing S/B, from 14.74 % to 16.70 %. On the other hand, the high value of S/B had a significant effect on the CO and CH_4 levels in gas compositions, lowering them from 24.14 to 17.11 % for CO and from 11.16 to 9.48 % for CH_4 , respectively, resulting in an increase in the mole ratio of H_2 to CO from 2.07 to 3.32 for EXP1 and EXP2, respectively.

The addition of steam to the biomass gasification process increased the reactivity of the steam with the biomass, resulting in increased gas output. However, the addition of steam to the feed influenced primary, secondary water gasification, and a high degree of WGS reaction, resulting in an increase in H_2 and CO_2 levels in the gas composition and a decrease in CO levels, resulting in a lower H_2/CO molar ratio. Additionally, increased steam expedited water methane reforming process, which resulted in a decrease in CH_4 levels.

According to the S/B inquiry, when a long-term operation is undertaken, an appropriate S/B should be established. The downstream process (FT) requires a value of H_2/CO of about 2 (1.75 - 2.25 of H_2/CO). Therefore, for long-term operation, the S/B ratio was advised to be regulated by about 0.52. However, in long-term operation, there were regulated and uncontrolled factors that may alter the gas composition. As a result, the S/B value can be changed to suit the scenario.

4.2.1.4. Investigation of long-term operation gasification

The pilot horizontal gasifier operated for seven days, filling 77 cylinders with syngas for FT synthesis. The optimal settings were 900 degrees Celsius for gasification and a steam/biomass ratio of 0.5, with RWP and EWC as input materials. The operation's objective was to generate syngas with an H_2/CO ratio of 1.75-2.25.

Table 9 Gasification results for two differences of Steam/Biomass

	EXP 1	EXP 2
<i>Operating Parameters</i>		
Operating time, h	5	5
Biomass feed rate, kg/h	3.95	1.68
Steam feed rate, kg/h	2.07	2.27
Steam/Biomass, kg/kg	0.52	1.35
<i>Gas compositions</i>		
H ₂	49.97	56.72
CO	24.14	17.10
CO ₂	14.74	16.70
CH ₄	11.16	9.48
H ₂ /CO, mole/mole	2.07	3.32

Average syngas composition

The gas composition of Eucalyptus wood chips (EWC) and Rubberwood pellet (RWP) gasification during seven days operation was illustrated in Figure 59 and Figure 60, respectively, for long-term operation study. These data indicated that the gas composition trended toward stability for long-term operation, with an average H₂/CO ratio of 1.93 and 2.05 for EWC and RWP, respectively. However, there were some gaps in the gas composition curve, which corresponded to the interval between compression of the full tank and transferring to the new empty tank. At this time, maintenance and inspections of all components were performed to ensure proper operation, and syngas was passed and purged to avoid contamination.

Additionally, low N₂ and O₂ concentrations were reported as a result of steam being used as a gasifier agent. The stability of the syngas composition may be attributed to the consistent temperature in the gasifier and tar reformer, which may impact the gasification reaction, as detailed in the next section.

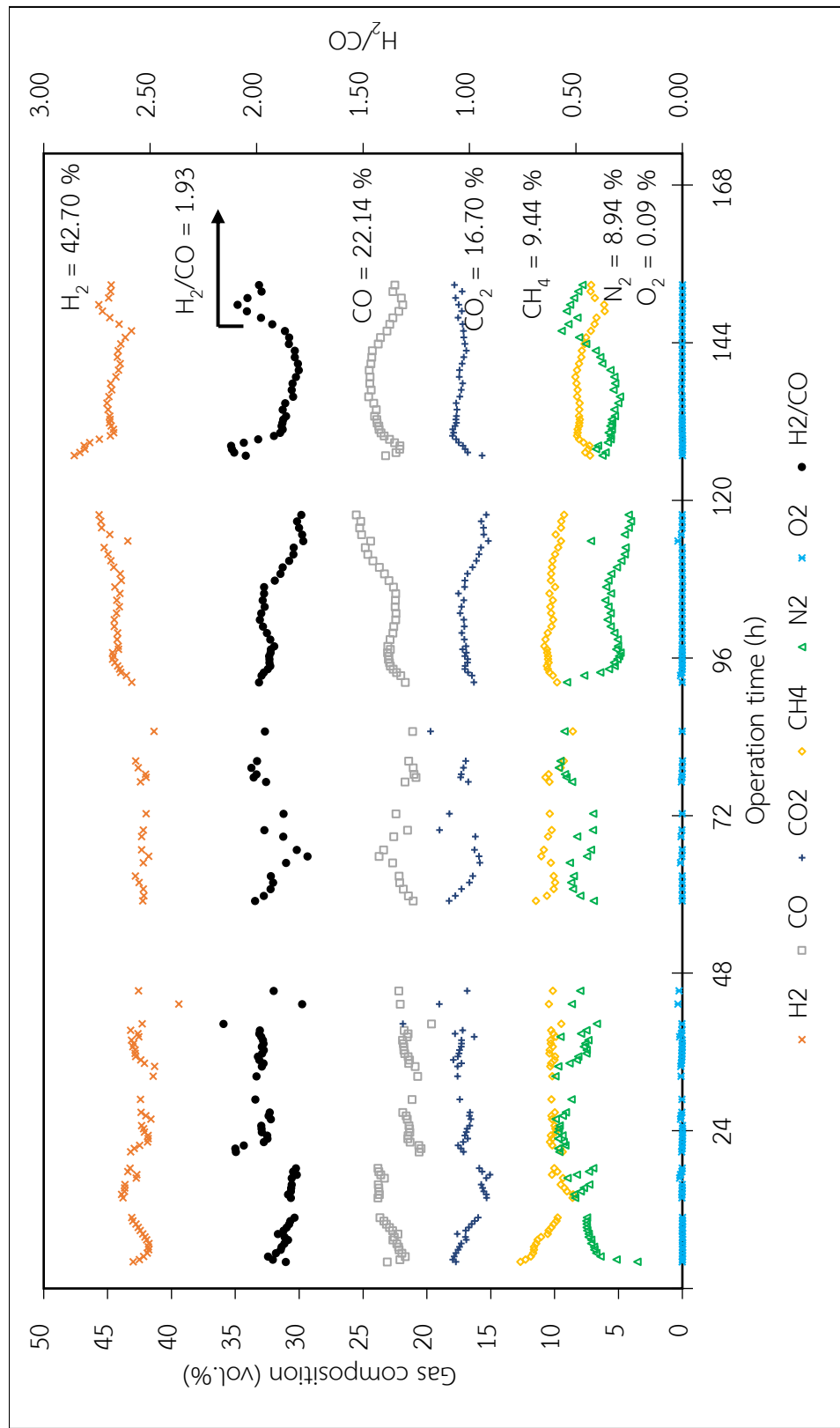


Figure 59 Overall gas composition of Eucalyptus gasification for 7 days operation

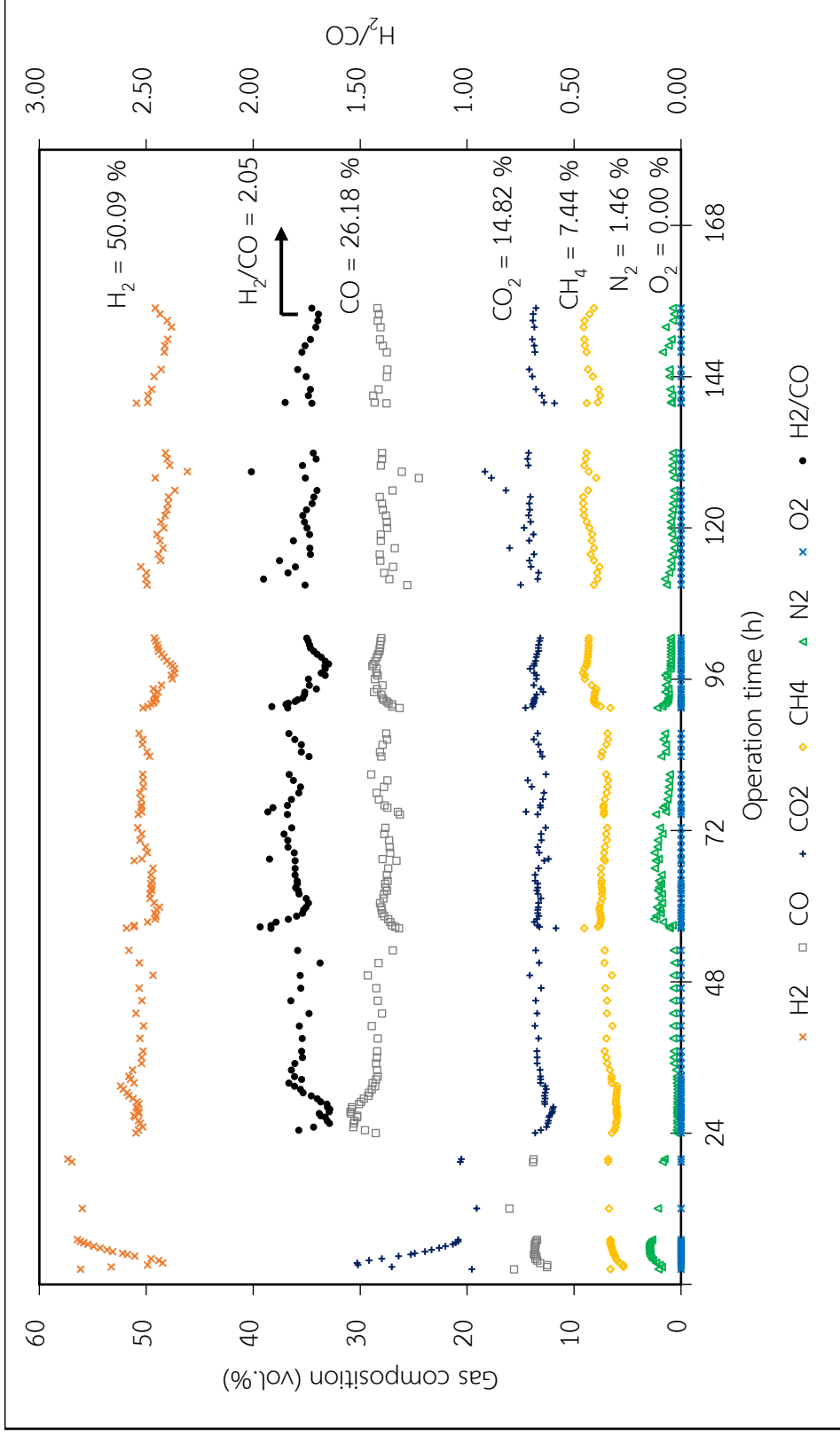


Figure 60 Overall gas composition of Rubber Wood gasification for 7 days operation

Temperature profile

The gasifier's temperature was illustrated in Figure 61, and the Tar Reformer's temperature was described in Figure 62 during the operational time. The gasifier's temperature was separated into three zones throughout its length, one for each heater. The temperature profile indicated that the temperature remained constant at 900 °C, whereas the output gas temperature remained steady at around 600 °C. The gasifier's consistent temperature ensured a steady reaction and had a direct effect on the gas composition. Moreover, the gasifier's consistent temperature made it easy to regulate the H₂/CO ratio. When the temperature remains constant, the temperature effect may be removed, leaving just the steam/biomass ratio to impact H₂/CO, which can be readily regulated and changed during operation. Additionally, at the tar reformer, the CaO was confined in the reactor's bottom zone (zone 1), the reaction zone. The tar-rich syngas flowed from the bottom up and caused CaO to behave as a bubble bed. According to Figure 62, when the syngas leaves the gasifier at a consistent temperature, the temperature of the tar reformer remains constant as well. The reaction happened at a temperature of 900 °C, and the gas exits the tar reformer at around 500 °C. Although the tar reformer was equipped with a heater to maintain and regulate the temperature at 900 °C, the CaO acted as a bubble bed. It had a high heat transmission rate and a high rate of heat loss. Thus, if the incoming gas temperature is not steady, temperature controlling would be difficult.

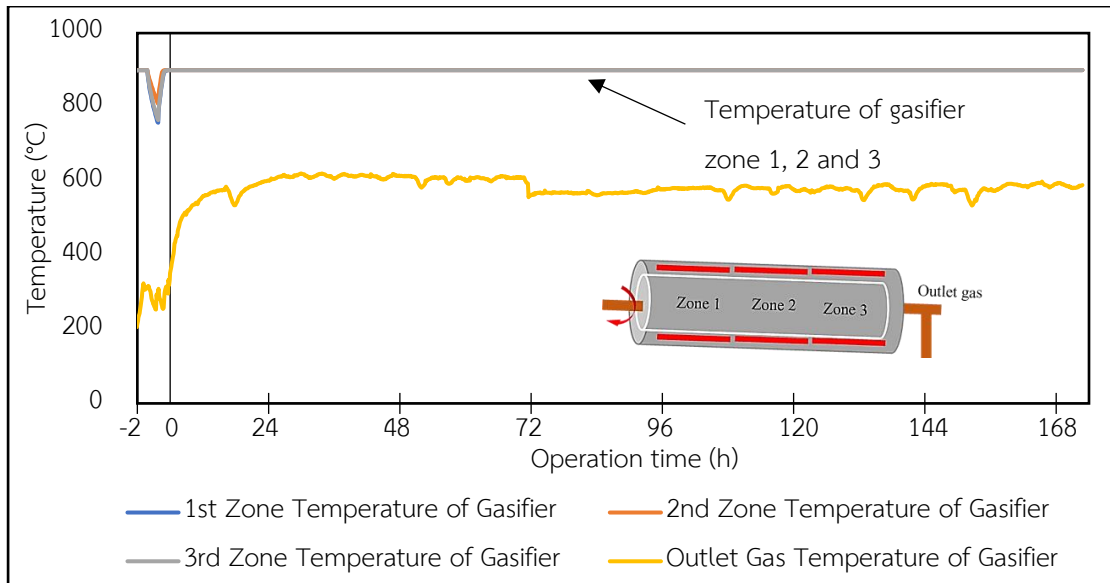


Figure 61 Temperature profile at gasifier zone for Eucalyptus gasification

Figure 63 displayed the pressure in the buffer tank since the feed began, and the gas was pressed into the tank until the pressure reached 12 MPa, a process that took approximately 27 hours. The slope of the curve in this image was constant, implying that gas was pumped into the tank constantly. The rate was reasonably constant, suggesting the gasification unit's reliability.

Additionally, the compressed gas was kept in a fixed-volume storage tank (0.9071 m³ of each set). This enables the precise determination of the quantity of moles of generated gas. As a result, the mole and mass of the generating gas could be determined precisely. As a result, system performance metrics such as cold gas efficiency and carbon conversion are calculated on a mass basis.

The gas generated by the gasification process was examined in real time every half hour and the results are shown in Figure 64, which includes the composition of the resultant gas and the molar ratio of H₂/CO produced by EW gasification. The gas composition was found to be very constant, containing 1.88 % H₂/CO, 44.65 % H₂, 23.69 % CO, 17.29 % CO₂, 7.54 % CH₄, 6.82 % N₂, and O₂ in trace amounts. Additionally,

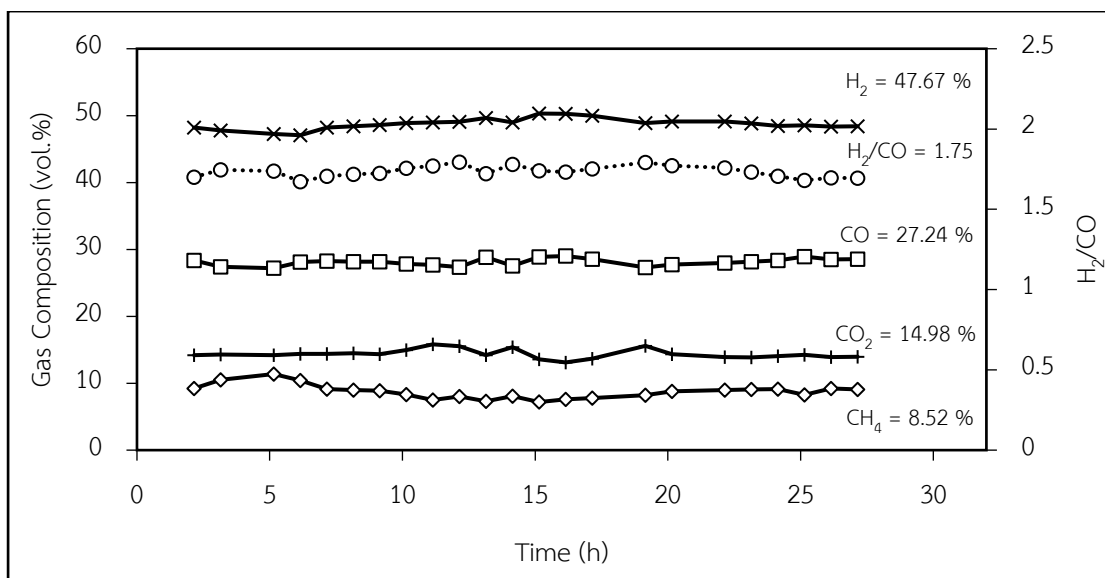


Figure 65 demonstrated a correlation between the RWP gasification value and the EWC result. H₂/CO was determined to be 1.75 with a very low O₂ concentration.

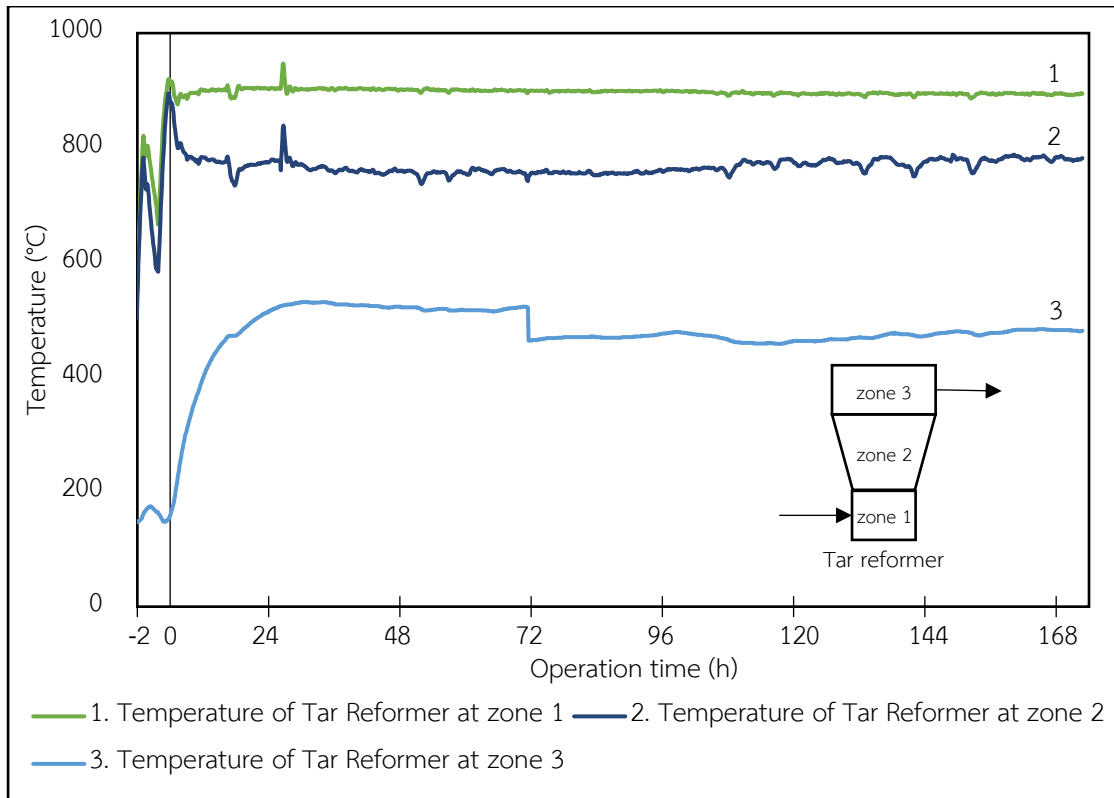


Figure 62 Temperature profile at tar reformer zone for Eucalyptus gasification

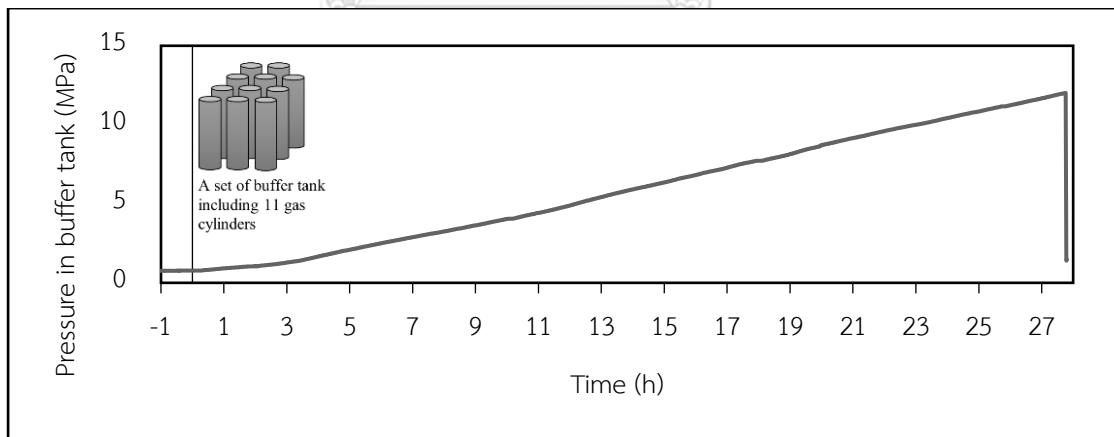


Figure 63 Pressure accumulation in Buffer Tank for Eucalyptus gasification

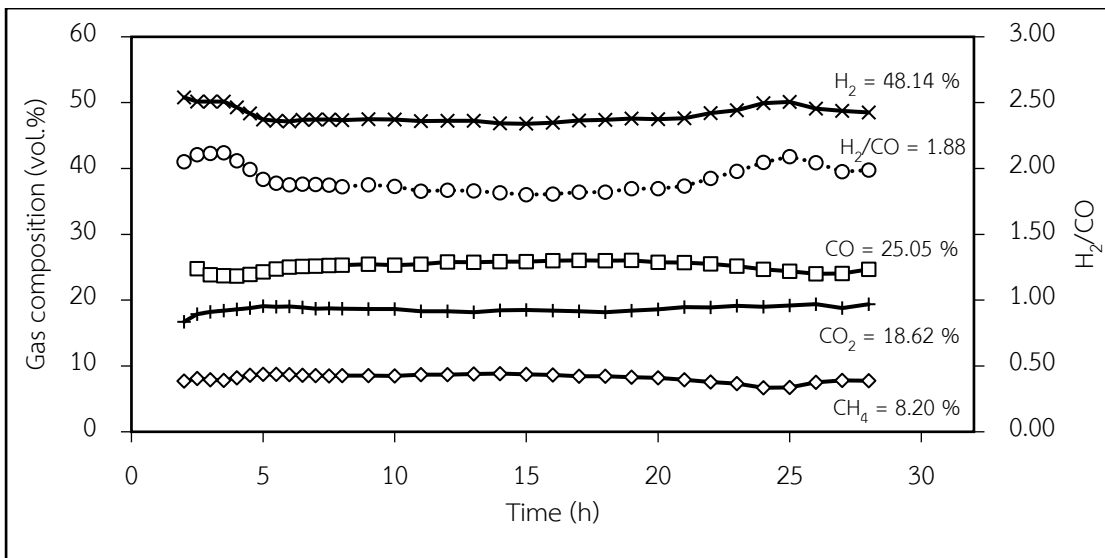


Figure 64 Gas composition for Eucalyptus gasification

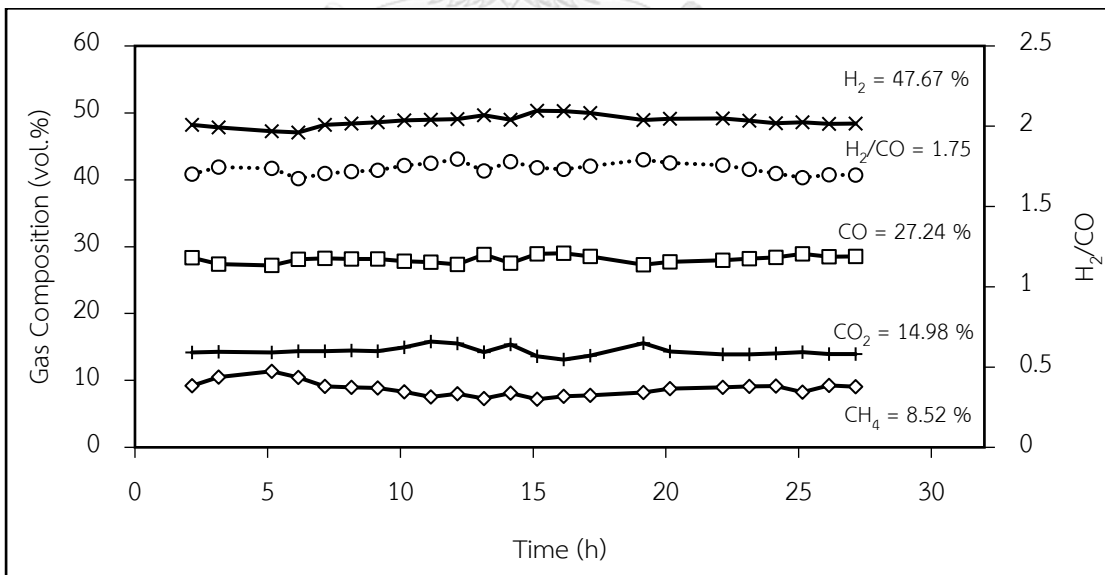


Figure 65 Gas composition for Rubber Wood gasification

Material balance of syngas production

The syngas production for seven days of operation was sufficient to fill seven sets of buffer tanks, each of which had 11 cylinders, or each set was filled daily. The pressure development shown in Figure 63 occurred during the filling of syngas into one set of the buffer tank, where the intended pressure was 120 MPa. The material balance was calculated for a single day of operation with a buffer capacity of 0.9071 m³, a pressure of 120 MPa, and a temperature of 30 °C. Table 10 summarized all of the data for RWP and EWC, including operating conditions, gas output, average composition of the gas, low heating value (LHV), and carbon conversion. RWP and EWC generated gas at rates of 2.48, 2.67 kg/h and 0.57, and 0.68 kg/kg, respectively. The biomass feed rates were 4.34 and 3.90 kg/h for RWP and EWC, respectively, but the steam feed rate of 2.02 kg/h for RWP was smaller than the EWC feed rate of 2.32 kg/h. It appeared as if the increased CO₂ and decreased CO content in gas products for EWC promotion via water gas shift reaction had a significant influence in boosting the production gas rate and lowering the LHV. LHV was calculated to be 12.88 MJ/Nm³ for RWP and 11.66 MJ/Nm³ for EWC. Additionally, the carbon conversion rate of RWP was 49.53 %, which was greater than the carbon conversion rate of EWC, which was 45 %. However, neither source material produced significantly different final gas properties. Among the byproducts was char, which could be recovered when the gasification process was completed. Carbon in char accounted for almost half of the total carbon in a feed measured for RWP and EWC. It discovered that RWP and EWC had a high carbon content of 83.06 and 88.76 wt. %, respectively, as indicated in Table 11. These charcoals behave similarly to activated carbon, with a BET surface area of 464,68 m²/g for RWP and 497.32 m²/g for EWC. EWC activated carbon has a greater BET surface area than RWC due to the higher steam feed rate used as the activating gas.

Table 10 Summary of gasification conditions and results for two types of biomass

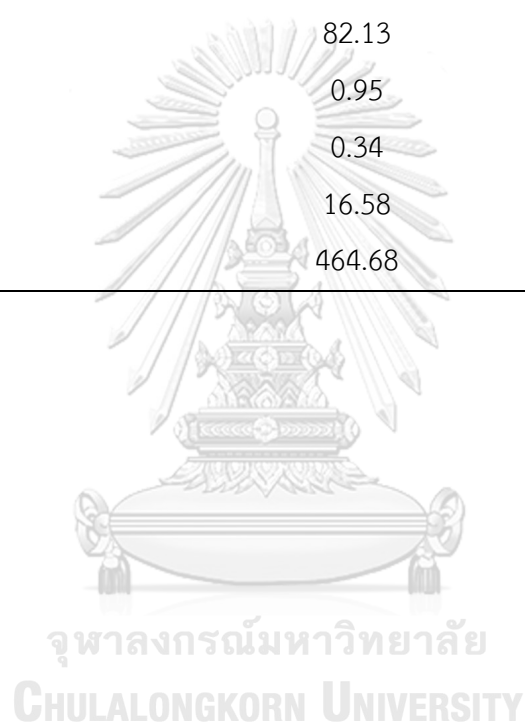
	RWP	EWC
Operating Parameters		
Operating time, h	30.5	27.77
Biomass feed rate, kg/h	4.34	3.90
Steam feed rate, kg/h	2.02	2.32
Steam/Biomass, kg/kg	0.47	0.59
Gas yield at constant volume of 0.9071 m³		
Produced gas rate, kg/h	2.48	2.67
Gas/Biomass, kg/kg	0.57	0.68
H ₂ /CO, mole/mole	1.75	1.89
Gas compositions		
H ₂	48.44	48.04
CO	27.68	25.42
CO ₂	15.22	18.53
CH ₄	8.66	8.01
Low Heating value, LHV		
MJ/Nm ³	12.88	11.66
Carbon balance, kg		
Feed stock	47.66	55.30
Produced gas	23.61	24.89
Char (solid)	24.05	30.41
Carbon conversion in gas product, wt.%, η_{carbon}		
	49.53	45.00

Table 11 Characteristics of Bio char

	Rubber Bio char	Eucalyptus Bio char
Moisture content, MC	13.48	13.85
<i>Proximate Analysis (wt.%), d.b.</i>		
Volatile matter, VM	3.51	3.60
Fixed carbon*, FC	83.06	88.76
Ash	13.43	7.64
<i>Ultimate Analysis (wt.%), d.b.</i>		
C	82.13	89.63
H	0.95	0.98
N	0.34	0.42
O*	16.58	8.97
B.E.T. (m^2/g)	464.68	497.32

d.b.: dry basis

* by difference



4.2.2. FT synthesis

For FT synthesis, monitor parameter was CO conversion. As shown in Figure 66, CO conversion was track since the syngas was feed into the reactor. At the initial of the period, CO conversion was driven to a higher level and likely constant at 46 - 48 %. At that time, the process was at steady-state condition. After 40 h passed, CO conversion level seems to decrease due to the inactive of catalyst. Until the conversion decreased to 20%, the FT synthesis was stopped due to a low CO conversion level and less pressure in the syngas tank that was insufficient for supporting to desire pressure condition. The operation was paused and collected liquid product.

Liquid products from FT synthesis were collected, weigh, and analyzed their composition. The liquid product's composition that determined by SimDis was shown in Table 12. Liquid product from condenser 1 showed a high level of diesel composition due to the higher controlled temperature of condenser 1. Condenser 2 showed naphtha rich in composition. Moreover, the total liquid of FT synthesis was 25.05 L, divided into 15.03 L for condenser 1 and 10.02 L for condenser 2.

The summary of production yield was shown in Figure 67. Mass conversion of syngas to the liquid product was 28.45 %. For the total conversion of the BTL process, biomass conversion to Liquid product was 16.28.

Table 12 Composition of liquid products from FT synthesis

Liquid Compositions	Diesel Production
Naphtha	1.7
Kerosene	2.8
Diesel	93.6
Residue	1.9

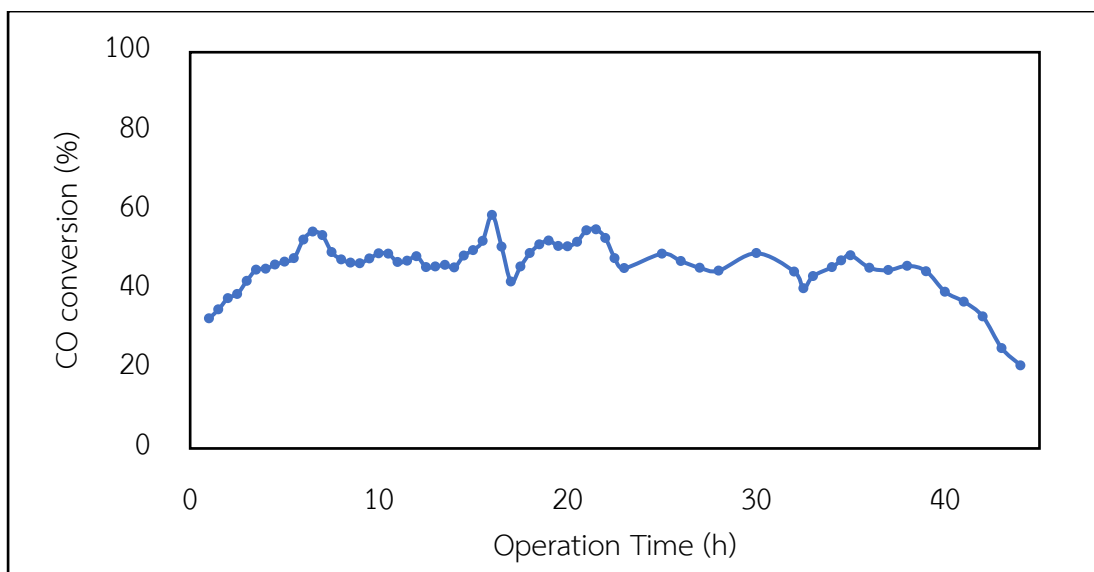


Figure 66 CO conversion from FT synthesis

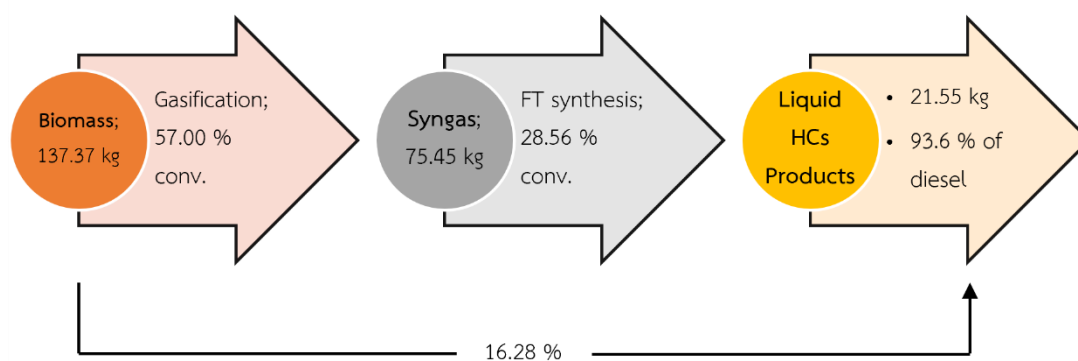


Figure 67 Mass conversion summary chart of BTL process

Chapter 5

Conclusions and Recommendations

5.1. Conclusions

5.1.1. The effects of reaction parameters of direct synthesis of LPG from CO₂ by using CZZA and HY zeolite as hybrid catalyst

CO₂ hydrogenation to LPG synthesis was investigated systematically in this research using a hybrid catalyst composed of CZZA metal and com-HY zeolite. The Mix A technique showed a high CO₂ conversion level of 27.39 % with a significantly reduced RWGS side reaction at 330 °C, 4 MPa, and a CZZA: com-HY zeolite ratio of 1:2 at 10 g_{mol}⁻¹. Furthermore, adding CO into the input gas affected the RWGS reaction barrier, resulting in a high LPG and HC selectivity of 66.56 % and 98.70 %, respectively. The excellent reaction outcomes from appropriate reaction conditions using conventional catalysts with no modification will significantly contribute to the development of LPG synthesis from CO₂, which is critical for energy recycling and environmental protection. Furthermore, the simple and common catalyst, CZZA/HY, examined in this research, shown selective function and a high potential LPG production, which may be an alternative method to promote people's access to cheap, dependable, sustainable, and contemporary energy in accordance with the SDGs.

5.1.2. The long-term operation of biomass to liquid process which combined with biomass gasification unit and Fischer-Tropsch synthesis

The goal of this study was to run a pilot horizontal gasifier with RWP and EWC to create syngas with an H_2/CO ratio of 1.75-2.25 for FT synthesis. The optimum gasifying temperature of 900 °C was determined in a lab-scale gasifier using both source materials. This temperature was set in a pilot horizontal gasifier. The tar removal system, gas purification system, and gas pressurized buffer tank system were all part of the pilot gasifier. The composition of gas products and the H_2/CO ratio are affected by the steam/biomass ratio. It was discovered that the steam/biomass ratio resulted in an H_2/CO ratio of 1.75-2.25. The output of syngas and the gas composition of both raw materials were stable for 7 days. For RWP and EWC, the gas production rates were 2.48 and 2.67 kg/h, respectively, with H_2/CO of 1.75 and 1.89. The external heat source was controlled to keep the gasifying temperature stable, resulting in a stable gas composition. In conclusion, the horizontal gasifier is another well-designed gasifier that has demonstrated good performance. After combination with FT synthesis the results showed 28.56 wt.% of syngas that converted to liquid fuels. For overall conversion of biomass to liquid fuels was 16.28 wt.%.

5.2. Recommendations

5.2.1. The effects of reaction parameters of direct synthesis of LPG from CO₂ by using CZZA and HY zeolite as hybrid catalyst

To enhance CO₂ conversion and LPG selectivity, an alternate hybrid catalyst such as an In₂O₃ base catalyst should be investigated. Moreover, this study employs a physical approach to combine the hybrid catalyst. This hybrid catalyst (CZZA/HY) may be used as the core-shell catalyst to improve the efficiency of synthesis. Further, the performance of core-shell catalysts should be evaluated and compared, with an emphasis on RWGS suppression. Additionally, the details of gas products such as i-C₄ should be studied in greater depth. That might be a more valuable product.

5.2.2. The long-term operation of biomass to liquid process which combined with biomass gasification unit and Fischer-Tropsch synthesis

This section reported on the high-performance generation of liquid fuels from biomass. However, before commercial use and business establishment, economics should be explored, and given the process's environmental benefits, life cycle analysis (LCA) may be performed.



EXPENDIX I

Calculation for Catalyst preparation

Reagents and Molecular weight

Reagents	Purity	Molecular weight	Metal (wt.%)
$\text{Cu}(\text{NO}_3)_2 \cdot 3\text{H}_2\text{O}$	100.00%	241.60	26.30
$\text{Zn}(\text{NO}_3)_2 \cdot 6\text{H}_2\text{O}$	99.00%	297.51	21.99
$\text{ZrO}(\text{NO}_3)_2 \cdot 2\text{H}_2\text{O}$	97.00%	267.26	34.13
$\text{Al}(\text{NO}_3)_3 \cdot 9\text{H}_2\text{O}$	98.00%	375.13	7.19

Calculation for the preparation of CZZA catalyst via co-precipitation method, comprised of mass ratio of 4.0/3.0/1.5/1.5 of Cu/ZnO/ZrO₂/Al₂O₃, respectively.

Basis, 10 g of CZZA

Substance	Weight (g)	Molecular weight	Metal (wt.%)
Cu	4.0	63.546	100.00
ZnO	3.0	81.408	80.35
ZrO ₂	1.5	123.223	74.03
Al ₂ O ₃	1.5	101.961	52.93

Weight the precursor

For example, weight the Cu precursor (Cu_{pre})

$$\text{Cu}_{\text{pre}} = \text{wt. Cu in cat.} / (\text{wt.}\% \text{ Cu in Precursor}) \times (\text{Purity})$$

$$\text{Cu}_{\text{pre}} = (4 \text{ g}) / (26.30\% \times 100\%)$$

$$= 15.2091 \text{ g}$$

EXPENDIX II

Experimental Data For direct synthesis of LPG from CO₂ by using CZZA and HY
zeolite as hybrid catalyst

Effect of Mixing Method

Fixed Parameters

Pressure	4 MPa
Temperature	310 °C
CZZA:HY	1:1
W/F	10

Mixing Method: A

TCD	1	2	3	4
CO ₂	141,143	149,810	151,369	151,647
CO	27,760	18,624	16,905	17,066
Ar	20,500	22,559	22,697	22,509
C1	109	215	197	191
FID	1	2	3	4
MeOH		25,738		24,427
DME		33,751		28,201
C ₁		5,100		4,483
C ₂		106,450		103,110
C ₃		157,256		162,780
C ₄		229,704		232,143
C ₅₊		83,064		94,948

Mixing Method: B

TCD	1	2	3	4
CO ₂	142,198	148,180	148,268	148,058
CO	26,379	20,072	18,895	18,814
Ar	20,474	21,324	21,671	21,689
C1	82	142	124	111
FID				
MeOH		65,019		70,759
DME		285,094		295,167
C ₁		3,442		2,769
C ₂		3,349		2,495
C ₃		722		369
C ₄		766		277
C ₅₊		361		0

Mixing Method: C

TCD	1	2	3	4
CO ₂	134,175	135,955	135,438	134,795
CO	34,631	31,991	32,569	33,138
Ar	19,275	19,566	19,465	19,509
C1	0	90	91	88
FID	1	2	3	4
MeOH		45		0
DME		0		0
C ₁		0		0
C ₂		1,391		1,889
C ₃		14,254		1,069
C ₄		17,671		0
C ₅₊		75,655		59,007

Effect of Temperature

Fixed Parameters

Pressure;	4 MPa
Mixing Method;	Mix A
CZZA:HY;	1:1
W/F;	10

Temperature; 310 °C

TCD	1	2	3	4
CO ₂	134,434	132,214	131,726	134,199
CO	31,860	33,183	33,444	33,685
Ar	19,212	19,399	19,456	19,489
C1	0	0	0	0
FID	1	2	3	4
MeOH		115,497		118,558
DME		14,006		9,898
C ₁		1,505		1,588
C ₂		161		162
C ₃		151		0
C ₄		314		315
C ₅₊		0		0

Temperature; 330

TCD	1	2	3	4
CO ₂	136,671	144,710	148,663	146,002
CO	27,901	20,021	19,886	19,275
Ar	20,913	22,656	22,696	22,774
C1	121	332	239	262
FID				
MeOH		15,902		14,489
DME		8,669		7,269
C ₁		6,923		5,923
C ₂		135,140		124,985
C ₃		192,938		189,223
C ₄		248,008		239,977
C ₅₊		68,369		75,178

Temperature; 360

TCD	1	2	3	4
CO ₂	136,967	141,706	142,604	142,527
CO	30,742	24,193	23,540	23,941
Ar	21,173	22,831	22,538	22,683
C1	242	579	588	630
FID	1	2	3	4
MeOH		7,869		5,162
DME		1,909		1,376
C ₁		14,048		13,844
C ₂		151,863		137,757
C ₃		229,859		212,254
C ₄		221,352		211,204
C ₅₊		51,408		49,219

Effect of CZZA:HY

Fixed Parameters

Pressure;	4 MPa
Mixing Method;	Mix A
Temperature;	330 °C
W/F;	10

CZZA:HY; 1:2

TCD	1	2	3	4
CO ₂	138,252	146,382	148,987	147,662
CO	26,325	18,594	18,333	18,848
Ar	22,363	23,890	23,743	23,487
C1	128	393	326	278
FID	1	2	3	4
MeOH		8,166		9,542
DME		1,109		1,840
C ₁		7,688		6,751
C ₂		166,404		150,492
C ₃		245,329		229,552
C ₄		310,943		281,092
C ₅₊		102,428		82,188

CZZA:HY; 1:1

TCD	1	2	3	4
CO ₂	136,671	144,710	148,663	146,002
CO	27,901	20,021	19,886	19,275
Ar	20,913	22,656	22,696	22,774
C1	121	332	239	262
FID	1	2	3	4
MeOH		15,902		14,489
DME		8,669		7,269
C ₁		6,923		5,923
C ₂		135,140		124,985
C ₃		192,938		189,223
C ₄		248,008		239,977
C ₅₊		68,369		75,178

CZZA:HY; 2:1

TCD	1	2	3	4
CO ₂	135,621	142,977	142,517	143,777
CO	29,329	22,889	22,217	22,676
Ar	20,839	21,902	21,997	21,835
C1	258	468	441	447
FID	1	2	3	4
MeOH		16,613		14,954
DME		8,099		6,590
C ₁		10,633		9,868
C ₂		114,319		106,020
C ₃		173,872		165,152
C ₄		208,048		199,809
C ₅₊		57,817		59,145

CZZA:HY; 1:4

TCD	1	2	3	4
CO ₂	136,681	145,766	146,430	147,074
CO	29,129	19,591	18,764	19,458
Ar	21,735	23,545	23,706	23,419
C1	160	306	280	316
FID	1	2	3	4
MeOH		4,431		3,586
DME		507		484
C ₁		6,903		6,245
C ₂		163,853		152,930
C ₃		219,456		213,525
C ₄		284,669		271,902
C ₅₊		72,621		78,726

CZZA only

TCD	1	2	3	4
CO ₂	121,127	120,777	122,066	121,612
CO	45,857	45,482	45,643	45,671
Ar	18,873	18,805	18,640	18,704
C1	0	182	192	166
FID	1	2	3	4
MeOH		33,500		28,557
DME		205		176
C ₁		5,254		5,544
C ₂		1,302		1,248
C ₃		840		775
C ₄		564		487
C ₅₊		83		70

HY only

TCD	1	2	3	4
CO ₂	143,192	142,357	14,569	14,632
CO	17,056	16,846	17,002	16,854
Ar	17,542	17,404	17,436	17,485
C1	0	0	0	0
FID	1	2	3	4
MeOH		54		63
DME		0		0
C ₁		661		635
C ₂		130		125
C ₃		0		0
C ₄		196		193
C ₅₊		124		128

Effect of W/F

Fixed Parameters

Pressure;	4 MPa
Mixing Method;	Mix A
Temperature;	330 °C
CZZA:HY;	1:2

W/F; 5

TCD	1	2	3	4
CO ₂	132,524	141,088	144,061	141,482
CO	32,210	23,361	22,352	23,438
Ar	20,686	22,307	22,249	21,807
C1	0	125	150	145
FID	1	2	3	4
MeOH		9,147		7,415
DME		2,408		2,821
C ₁		4,785		4,115
C ₂		122,365		110,758
C ₃		163,136		155,973
C ₄		215,913		201,510
C ₅₊		56,062		71,004

W/F; 10

TCD	1	2	3	4
CO ₂	138,252	146,382	148,987	147,662
CO	26,325	18,594	18,333	18,848
Ar	22,363	23,890	23,743	23,487
C1	128	393	326	278
FID	1	2	3	4
MeOH		8,166		9,542
DME		1,109		1,840
C ₁		7,688		6,751
C ₂		166,404		150,492
C ₃		245,329		229,552
C ₄		310,943		281,092
C ₅₊		102,428		82,188

W/F; 15

TCD	1	2	3	4
CO ₂	136,022	145,603	148,824	148,205
CO	28,495	19,730	18,052	17,933
Ar	20,930	23,407	23,853	23,703
C1	239	550	620	502
FID	1	2	3	4
MeOH		19,031		9,344
DME		12,827		2,894
C ₁		12,999		12,132
C ₂		156,540		159,720
C ₃		240,733		251,844
C ₄		266,953		285,998
C ₅₊		65,121		73,543

At Optimum condition

Conditions

Inlet Gas;	H ₂ /CO ₂ /CO
Pressure;	4 MPa
Temperature;	330 °C
Mixing Method;	Mix A
CZZA:HY;	1:1
W/F;	10

TCD	1	2	3	4
CO ₂	138,252	146,382	148,987	147,662
CO	26,325	18,594	18,333	18,848
Ar	22,363	23,890	23,743	23,487
C1	128	393	326	278
FID	1	2	3	4
MeOH		8,166		9,542
DME		1,109		1,840
C ₁		7,688		6,751
C ₂		166,404		150,492
C ₃		245,329		229,552
C ₄		310,943		281,092
C ₅₊		102,428		82,188

Conditions

Inlet Gas;	H ₂ /CO ₂ ; 3/1
Pressure;	4 MPa
Temperature;	330 °C
Mixing Method;	Mix A
CZZA:HY;	1:1
W/F;	10

TCD	1	2	3	4
CO ₂	118,671	121,589	123,063	122,538
CO	20,842	16,217	15,968	15,981
Ar	27,620	29,263	29,267	29,071
C1	153	309	287	260
FID	1	2	3	4
MeOH		9,909		10,914
DME		4,054		5,168
C ₁		7,441		6,890
C ₂		111,966		104,660
C ₃		164,569		162,977
C ₄		202,600		196,992
C ₅₊		53,422		52,032

EXPENDIX III

Calculation

Direct synthesis of LPG from CO₂ by using CZZA and HY zeolite as hybrid catalyst

The CO₂, CO, C conversion and products selectivity were calculated as the following formulas:

$$\text{CO}_2 \text{ conversion, } X(\text{CO}_2), \% = \frac{\text{mole of CO}_{2, \text{ in}} - \text{mole of CO}_{2, \text{ out}}}{\text{mole of CO}_{2, \text{ in}}} \times 100 \quad (\text{S1})$$

$$\text{CO conversion, } X(\text{CO}), \% = \frac{\text{mole of CO}_{\text{ in}} - \text{mole of CO}_{\text{ out}}}{\text{mole of CO}_{\text{ in}}} \times 100 \quad (\text{S2})$$

$$\text{Carbon conversion, } X(\text{C}), \% = X(\text{CO}_2) \times \left(\frac{a}{a+b} \right) + X(\text{CO}) \times \left(\frac{b}{a+b} \right) \quad (\text{S3})$$

where, a = concentration of CO₂ in feeding gas

b = concentration of CO in feeding gas

$$\text{CO selectivity, } \% = \frac{\text{mole of CO}_{\text{ out}} - \text{mole of CO}_{\text{ in}}}{\text{mole of CO}_{2, \text{ in}} - \text{mole of CO}_{2, \text{ out}}} \times 100 \quad (\text{S4})$$

$$\text{Product selectivity, } \% = \frac{\text{mole of product}_i}{\sum_{i=1}^n \text{mole of product}_i} \times 100 \quad (\text{S5})$$

$$\text{Product yield, } \% = \text{CO}_2 \text{ conversion} \times \text{Product selectivity} \quad (\text{S6})$$

BTL Process

To evaluate the performance of this gasification system, common gasification indexes was calculated. Therefore, total mole and composition of produced gas was precisely known, calculation of gas yield, carbon conversion as well as gas efficiency was based mass basis and followed:

$$\text{Gas yield, wt.\%} = \frac{\text{total mass of produced gas}}{\text{total mass of fed biomass}} \times 100 \quad (\text{S7})$$

$$\text{Carbon conversion, wt.\%} = \frac{\text{mass of carbon in produced gas}}{\text{mass of carbon in total fed biomass}} \times 100 \quad (\text{S8})$$

$$\text{Gas/Biomass} = \frac{\text{total mass of produced gas, kg}}{\text{total mass of fed biomass, kg}} \quad (\text{S9})$$

$$\text{Cold gas efficiency, } \eta_{\text{cold}} = \frac{M_{\text{syngas}} \times \text{LHV}_{\text{syngas}}}{M_{\text{biomass}} \times \text{LHV}_{\text{biomass}}} \times 100 \quad (\text{S10})$$

M_{syngas} = total mass of produced gas, kg

M_{biomass} = total mass of fed biomass, kg

$\text{LHV}_{\text{syngas}}$ = lower heating value of produced gas, MJ/kg

$\text{LHV}_{\text{biomass}}$ = lower heating value of biomass feed stock, MJ/kg

EXPENDIX IV

Gasification Experimental Data

GC data (GC-TCD) of produced gas from Eucalyptus gasification

Time	H ₂	CO	CH ₄	CO ₂
11/11/2019 2:00 PM	50.80	24.77	7.71	16.72
11/11/2019 2:30 PM	50.18	23.84	8.10	17.89
11/11/2019 3:00 PM	50.16	23.72	7.89	18.23
11/11/2019 3:30 PM	50.15	23.66	7.78	18.41
11/11/2019 4:00 PM	49.26	23.92	8.21	18.60
11/11/2019 4:30 PM	48.37	24.28	8.57	18.78
11/11/2019 5:00 PM	47.45	24.73	8.75	19.07
11/11/2019 5:30 PM	47.26	25.02	8.71	19.01
11/11/2019 6:00 PM	47.16	25.13	8.67	19.03
11/11/2019 6:30 PM	47.38	25.18	8.57	18.87
11/11/2019 7:00 PM	47.46	25.27	8.55	18.72
11/11/2019 7:30 PM	47.43	25.31	8.49	18.77
11/11/2019 8:00 PM	47.34	25.44	8.54	18.68
11/11/2019 9:00 PM	47.51	25.32	8.53	18.64
11/11/2019 10:00 PM	47.45	25.44	8.46	18.64
11/11/2019 11:00 PM	47.20	25.82	8.67	18.32
12/11/2019 12:00 AM	47.26	25.76	8.66	18.32
12/11/2019 1:00 AM	47.26	25.82	8.75	18.16
12/11/2019 2:00 AM	46.86	25.83	8.84	18.46
12/11/2019 3:00 AM	46.79	25.98	8.75	18.49
12/11/2019 4:00 AM	46.96	26.02	8.63	18.40
12/11/2019 5:00 AM	47.27	25.97	8.46	18.30
12/11/2019 6:00 AM	47.39	26.03	8.43	18.15
12/11/2019 7:00 AM	47.57	25.75	8.27	18.41
12/11/2019 8:00 AM	47.47	25.71	8.21	18.61
12/11/2019 9:00 AM	47.63	25.53	7.92	18.93
12/11/2019 10:00 AM	48.41	25.14	7.55	18.90
12/11/2019 11:00 AM	48.85	24.69	7.32	19.14

12/11/2019 12:00 PM	49.92	24.41	6.69	18.98
12/11/2019 1:00 PM	50.10	23.98	6.72	19.20
12/11/2019 2:00 PM	49.09	24.03	7.49	19.39
12/11/2019 3:00 PM	48.74	24.66	7.82	18.78
12/11/2019 4:00 PM	48.51	24.40	7.73	19.36
AVG	48.14	25.05	8.20	18.62



GC data (GC-TCD) of produced gas from Rubber wood gasification

Time	H ₂	CO	CH ₄	CO ₂
25/7/2019 2:55 AM	48.46	28.10	9.17	14.27
25/7/2019 3:53 AM	48.32	28.16	9.23	14.29
25/7/2019 4:57 AM	48.23	28.35	9.22	14.19
25/7/2019 5:59 AM	47.81	27.39	10.50	14.31
25/7/2019 7:57 AM	47.26	27.19	11.37	14.17
25/7/2019 8:57 AM	47.07	28.13	10.43	14.37
25/7/2019 9:57 AM	48.22	28.28	9.11	14.40
25/7/2019 10:59 AM	48.40	28.17	8.97	14.46
25/7/2019 11:54 AM	48.59	28.17	8.89	14.35
25/7/2019 12:54 PM	48.89	27.84	8.31	14.96
26/7/2019 1:54 PM	48.98	27.69	7.51	15.82
27/7/2019 2:54 PM	49.08	27.35	8.02	15.55
28/7/2019 3:54 PM	49.65	28.84	7.30	14.21
29/7/2019 4:54 PM	48.99	27.53	8.09	15.39
25/7/2019 7:55 PM	50.31	28.90	7.19	13.60
25/7/2019 9:00 PM	50.26	29.01	7.61	13.11
25/7/2019 10:00 PM	49.99	28.54	7.77	13.69
26/7/2019 12:01 AM	48.91	27.31	8.19	15.59
26/7/2019 1:09 AM	49.13	27.74	8.78	14.34
26/7/2019 3:54 AM	49.15	27.97	8.98	13.91
26/7/2019 4:55 AM	48.83	28.19	9.10	13.88
26/7/2019 5:57 AM	48.44	28.38	9.14	14.03
26/7/2019 6:54 AM	48.57	28.92	8.26	14.25
26/7/2019 7:53 AM	48.35	28.49	9.24	13.93
26/7/2019 8:53 AM	48.40	28.56	9.08	13.96
AVG	48.73	28.13	8.78	14.36

EXPENDIX V

Gasification Gas yield calculation

Calculation total mole of produced gas

Parameters	Value
V_{tank} , [m ³]	0.9071
P_{tank} , [MPa]	11.25
T_{tank} , [K = °C+273]	303
R [Pa.m ³ .K ⁻¹ .mol ⁻¹]	8.314

$$\begin{aligned}
 \text{Mole of gas} &= PV/RT \\
 &= [(11.25 \text{ MPa}) \times (0.9071 \text{ m}^3)] / [(1 \times 10^6) \times (8.314 \text{ Pa.m}^3.\text{K}^{-1}.\text{mol}^{-1}) \times (303 \text{ K})] \\
 &= 4050.93 \text{ mole}
 \end{aligned}$$

Gas Composition	MW [g/mole]	% mole	mole	mass [kg]	wt.%
H ₂	2.016	48.14	1808.74	3.65	5.50
CO	28.010	25.05	959.67	26.88	40.57
CO ₂	44.010	8.20	700.41	30.82	46.53
CH ₄	16.042	18.62	305.44	4.90	7.40
Total		100.00	4050.93	66.25	100.00

REFERENCES

1. *The Sustainable Development Goals*. The United Nations, 2017.
2. Department of Alternative Energy Development and Efficiency, *Energy Situation of Thailand*. Ministry of Energy, 2020.
3. *International Energy Outlook 2017*. September 14, 2017; Available from: www.eia.gov/ieo.
4. Hanif A. Choudhury, Sankar Chakma and Vijayanand S. Moholkar, *Chapter 14 - Biomass Gasification Integrated Fischer-Tropsch Synthesis: Perspectives, Opportunities and Challenges*, in *Recent Advances in Thermo-Chemical Conversion of Biomass*, A. Pandey, et al., Editors. 2015, Elsevier: Boston. p. 383-435.
5. Congming Li, Xingdong Yuan and Kaoru Fujimoto, *Direct synthesis of LPG from carbon dioxide over hybrid catalysts comprising modified methanol synthesis catalyst and β -type zeolite*. *Applied Catalysis A: General*, 2014. **475**: p. 155-160.
6. Jianyang Wang, Anfeng Zhang, Xiao Jiang, Chunshan Song and Xinwen Guo, *Highly selective conversion of CO₂ to lower hydrocarbons (C₂-C₄) over bifunctional catalysts composed of In₂O₃-ZrO₂ and zeolite*. *Journal of CO₂ Utilization*, 2018. **27**: p. 81-88.
7. Congming Li, Xingdong Yuan and Kaoru Fujimoto, *Direct synthesis of LPG from carbon dioxide over hybrid catalysts comprising modified methanol synthesis catalyst and β -type zeolite* ☆. *Applied Catalysis A: General*, 2014. **475**: p. 155-160.
8. Jian Sun, Guohui Yang, Qingxiang Ma, Issei Ooki, Akira Taguchi, Takayuki Abe, et al., *Fabrication of active Cu-Zn nanoalloys on H-ZSM5 zeolite for enhanced dimethyl ether synthesis via syngas*. *Journal of Materials Chemistry A*, 2014. **2**: p. 8637-8643.

9. G. Bonura, M. Cordaro, L. Spadaro, C. Cannilla, F. Arena and F. Frusteri, *Hybrid Cu-ZnO-ZrO₂/H-ZSM5 system for the direct synthesis of DME by CO₂ hydrogenation*. Applied Catalysis B: Environmental, 2013. **140-141**: p. 16-24.
10. Peng Gao, Feng Li, Fukui Xiao, Ning Zhao, Nannan Sun, Wei Wei, et al., *Preparation and activity of Cu/Zn/Al/Zr catalysts via hydrotalcite-containing precursors for methanol synthesis from CO₂ hydrogenation*. Catalysis Science & Technology, 2012. **2**: p. 1447-1454.
11. Kenji Asami, Qianwen Zhang, Xiaohong Li, Sachio Asaoka and Kaoru Fujimoto, *Semi-indirect synthesis of LPG from syngas: Conversion of DME into LPG*. Catalysis Today, 2005. **106**: p. 247-251.
12. Chengguang Yang, Minghuang Qiu, Shengwei Hu, Xinqing Chen, Gaofeng Zeng, Ziyu Liu, et al., *Stable and efficient aromatic yield from methanol over alkali treated hierarchical Zn-containing HZSM-5 zeolites*. Microporous and Mesoporous Materials, 2016. **231**: p. 110-116.
13. Samia Ilias and Aditya Bhan, *Mechanism of the Catalytic Conversion of Methanol to Hydrocarbons*. ACS Catalysis, 2013. **3**: p. 18-31.
14. Yohan Richardson, Martin Drobek, Anne Julbe, Joël Blin and François Pinta, *Chapter 8 - Biomass Gasification to Produce Syngas*, in *Recent Advances in Thermo-Chemical Conversion of Biomass*, A. Pandey, et al., Editors. 2015, Elsevier: Boston. p. 213-250.
15. Jun Ma, Nannan Sun, Xuelan Zhang, Ning Zhao, Fukui Xiao, Wei Wei, et al., *A short review of catalysis for CO₂ conversion*. Catalysis Today, 2009. **148**: p. 221-231.
16. Congming Li, Xingdong Yuan and Kaoru Fujimoto, *Development of highly stable catalyst for methanol synthesis from carbon dioxide*. Applied Catalysis A: General, 2014. **469**: p. 306-311.
17. Wen Ding, Yingwei Liu, Fang Wang, Shuailing Zhou, Aiping Chen, Yiquan Yang, et al., *Promoting effect of a Cu-Zn binary precursor on a ternary Cu-Zn-Al catalyst for methanol synthesis from synthesis gas*. RSC Advances, 2014. **4**: p. 30677-30682.

18. N. J. Brown, J. Weiner, K. Hellgardt, M. S. P. Shaffer and C. K. Williams, *Phosphinate stabilised ZnO and Cu colloidal nanocatalysts for CO₂ hydrogenation to methanol*. *Chemical Communications*, 2013. **49**: p. 11074-11076.
19. Céline Tisseraud, Clément Comminges, Stéphane Pronier, Yannick Pouilloux and Anthony Le Valant, *The Cu–ZnO synergy in methanol synthesis Part 3: Impact of the composition of a selective Cu@ZnOx core–shell catalyst on methanol rate explained by experimental studies and a concentric spheres model*. *Journal of Catalysis*, 2016. **343**: p. 106-114.
20. Francesco Arena, Giuseppe Italiano, Katia Barbera, Silvia Bordiga, Giuseppe Bonura, Lorenzo Spadaro, et al., *Solid-state interactions, adsorption sites and functionality of Cu-ZnO/ZrO₂ catalysts in the CO₂ hydrogenation to CH₃OH*. *Applied Catalysis A: General*, 2008. **350**: p. 16-23.
21. Ian A. Fisher and Alexis T. Bell, *In-Situ Infrared Study of Methanol Synthesis from H₂/CO₂ over Cu/SiO₂ and Cu/ZrO₂/SiO₂*. *Journal of Catalysis*, 1997. **172**: p. 222-237.
22. Lishan Jia, Jing Gao, Weiping Fang and Qingbiao Li, *Carbon dioxide hydrogenation to methanol over the pre-reduced LaCr_{0.5}Cu_{0.5}O₃ catalyst*. *Catalysis Communications*, 2009. **10**: p. 2000-2003.
23. Kwang-Deog Jung and Alexis T. Bell, *Role of Hydrogen Spillover in Methanol Synthesis over Cu/ZrO₂*. *Journal of Catalysis*, 2000. **193**: p. 207-223.
24. R. A. Koepfel, A. Baiker and A. Wokaun, *Copper/zirconia catalysts for the synthesis of methanol from carbon dioxide: Influence of preparation variables on structural and catalytic properties of catalysts*. *Applied Catalysis A: General*, 1992. **84**: p. 77-102.
25. W. P. A. Jansen, J. Beckers, J. C. v. d. Heuvel, A. W. Denier v. d. Gon, A. Bliet and H. H. Brongersma, *Dynamic Behavior of the Surface Structure of Cu/ZnO/SiO₂ Catalysts*. *Journal of Catalysis*, 2002. **210**: p. 229-236.
26. M. Saito, T. Fujitani, M. Takeuchi and T. Watanabe, *Development of copper/zinc oxide-based multicomponent catalysts for methanol synthesis from carbon dioxide and hydrogen*. *Applied Catalysis A: General*, 1996. **138**: p. 311-318.

27. S. H. Liu, H. Paul Wang, H. C. Wang and Y. W. Yang, *In situ EXAFS studies of copper on ZrO₂ during catalytic hydrogenation of CO₂*. Journal of Electron Spectroscopy and Related Phenomena, 2005. **144-147**: p. 373-376.
28. Qian-Lin Tang, Qi-Jun Hong and Zhi-Pan Liu, *CO₂ fixation into methanol at Cu/ZrO₂ interface from first principles kinetic Monte Carlo*. Journal of Catalysis, 2009. **263**: p. 114-122.
29. Tobin C. Schilke, Ian A. Fisher and Alexis T. Bell, *In Situ Infrared Study of Methanol Synthesis from CO₂/H₂ on Titania and Zirconia Promoted Cu/SiO₂*. Journal of Catalysis, 1999. **184**: p. 144-156.
30. Dante L. Chiavassa, Sebastián E. Collins, Adrian L. Bonivardi and Miguel A. Baltanás, *Methanol synthesis from CO₂/H₂ using Ga₂O₃-Pd/silica catalysts: Kinetic modeling*. Chemical Engineering Journal, 2009. **150**: p. 204-212.
31. Hye-Won Lim, Myung-June Park, Suk-Hwan Kang, Ho-Jeong Chae, Jong Wook Bae and Ki-Won Jun, *Modeling of the Kinetics for Methanol Synthesis using Cu/ZnO/Al₂O₃/ZrO₂ Catalyst: Influence of Carbon Dioxide during Hydrogenation*. Industrial & Engineering Chemistry Research, 2009. **48**: p. 10448-10455.
32. M. Bowker, R. A. Hadden, H. Houghton, J. N. K. Hyland and K. C. Waugh, *The mechanism of methanol synthesis on copper/zinc oxide/alumina catalysts*. Journal of Catalysis, 1988. **109**: p. 263-273.
33. Yixiong Yang, Jaime Evans, Jose A. Rodriguez, Michael G. White and Ping Liu, *Fundamental studies of methanol synthesis from CO₂ hydrogenation on Cu(111), Cu clusters, and Cu/ZnO(000)*. Physical Chemistry Chemical Physics, 2010. **12**: p. 9909-9917.
34. A. Goguet, F. Meunier, J. P. Breen, R. Burch, M. I. Petch and A. Faur Ghenciu, *Study of the origin of the deactivation of a Pt/CeO₂ catalyst during reverse water gas shift (RWGS) reaction*. Journal of Catalysis, 2004. **226**: p. 382-392.
35. V. Arunajatesan, B. Subramaniam, K. W. Hutchenson and F. E. Herkes, *In situ FTIR investigations of reverse water gas shift reaction activity at supercritical conditions*. Chemical Engineering Science, 2007. **62**: p. 5062-5069.

36. Davide Ferri, Thomas Bürgi and Alfons Baiker, *Probing boundary sites on a Pt/Al₂O₃ model catalyst by CO₂ hydrogenation and in situ ATR-IR spectroscopy of catalytic solid-liquid interfaces*. *Physical Chemistry Chemical Physics*, 2002. **4**: p. 2667-2672.
37. Masahiro Fujiwara, Roger Kieffer, Hisanori Ando and Yoshie Souma, *Development of composite catalysts made of Cu-Zn-Cr oxide/zeolite for the hydrogenation of carbon dioxide*. *Applied Catalysis A: General*, 1995. **121**: p. 113-124.
38. Robert W. Dörner, Dennis R. Hardy, Frederick W. Williams, Burtron H. Davis and Heather D. Willauer, *Influence of Gas Feed Composition and Pressure on the Catalytic Conversion of CO₂ to Hydrocarbons Using a Traditional Cobalt-Based Fischer-Tropsch Catalyst*. *Energy & Fuels*, 2009. **23**: p. 4190-4195.
39. Yongqing Zhang, Gary Jacobs, Dennis E. Sparks, Mark E. Dry and Burtron H. Davis, *CO and CO₂ hydrogenation study on supported cobalt Fischer-Tropsch synthesis catalysts*. *Catalysis Today*, 2002. **71**: p. 411-418.
40. George W. Huber, Sara Iborra and Avelino Corma, *Synthesis of Transportation Fuels from Biomass: Chemistry, Catalysts, and Engineering*. *Chemical Reviews*, 2006. **106**: p. 4044-4098.
41. A. Gómez-Barea and B. Leckner, *Modeling of biomass gasification in fluidized bed*. *Progress in Energy and Combustion Science*, 2010. **36**: p. 444-509.
42. Hugo de Lasa, Enrique Saldaña, Jahirul Mazumder and Rahima Lucky, *Catalytic Steam Gasification of Biomass: Catalysts, Thermodynamics and Kinetics*. *Chemical Reviews*, 2011. **111**: p. 5404-5433.
43. Wennan Zhang, *Automotive fuels from biomass via gasification*. *Fuel Processing Technology*, 2010. **91**: p. 866-876.
44. Kristina Göransson, Ulf Söderlind, Jie He and Wennan Zhang, *Review of syngas production via biomass DFBGs*. *Renewable and Sustainable Energy Reviews*, 2011. **15**: p. 482-492.
45. José Corella, José M. Toledo and Gregorio Molina, *A Review on Dual Fluidized-Bed Biomass Gasifiers*. *Industrial & Engineering Chemistry Research*, 2007. **46**: p. 6831-6839.

46. Li Dong, Guangwen Xu, Toshiyuki Suda and Takahiro Murakami, *Potential approaches to improve gasification of high water content biomass rich in cellulose in dual fluidized bed*. Fuel Processing Technology, 2010. **91**: p. 882-888.
47. Stefan Koppatz, Christoph Pfeifer, Reinhard Rauch, Hermann Hofbauer, Tonja Marquard-Moellenstedt and Michael Specht, *H₂ rich product gas by steam gasification of biomass with in situ CO₂ absorption in a dual fluidized bed system of 8 MW fuel input*. Fuel Processing Technology, 2009. **90**: p. 914-921.
48. Walter Torres, Sourabh S. Pansare and James G. Goodwin, *Hot Gas Removal of Tars, Ammonia, and Hydrogen Sulfide from Biomass Gasification Gas*. Catalysis Reviews, 2007. **49**: p. 407-456.
49. Jun Han and Heejoon Kim, *The reduction and control technology of tar during biomass gasification/pyrolysis: An overview*. Renewable and Sustainable Energy Reviews, 2008. **12**: p. 397-416.
50. Chunshan Li and Kenzi Suzuki, *Tar property, analysis, reforming mechanism and model for biomass gasification—An overview*. Renewable and Sustainable Energy Reviews, 2009. **13**: p. 594-604.
51. Samsudin Anis and Z. A. Zainal, *Tar reduction in biomass producer gas via mechanical, catalytic and thermal methods: A review*. Renewable and Sustainable Energy Reviews, 2011. **15**: p. 2355-2377.
52. P. Hasler and Th Nussbaumer, *Gas cleaning for IC engine applications from fixed bed biomass gasification*. Biomass and Bioenergy, 1999. **16**: p. 385-395.
53. Carlo N. Hamelinck, André P. C. Faaij, Herman den Uil and Harold Boerrigter, *Production of FT transportation fuels from biomass; technical options, process analysis and optimisation, and development potential*. Energy, 2004. **29**: p. 1743-1771.
54. G. Iaquaniello and A. Mangiapane, *Integration of biomass gasification with MCFC*. International Journal of Hydrogen Energy, 2006. **31**: p. 399-404.
55. P. V. Aravind and Wiebren de Jong, *Evaluation of high temperature gas cleaning options for biomass gasification product gas for Solid Oxide Fuel Cells*. Progress in Energy and Combustion Science, 2012. **38**: p. 737-764.

56. Patrick J. Woolcock and Robert C. Brown, *A review of cleaning technologies for biomass-derived syngas*. Biomass and Bioenergy, 2013. **52**: p. 54-84.
57. H. Schulz, E. Erich, H. Gorre and E. van Steen, *Regularities of selectivity as a key for discriminating FT-surface reactions and formation of the dynamic system*. Catalysis Letters, 1990. **7**: p. 157-167.
58. J. C. Hoogendoorn and J. M. Salomon, Br. Chem. Eng., 1957: p. 368-373.
59. H. A. Choudhury and V. S. Moholkar, *Synthesis and characterization of Fe-catalyst for Fischer-Tropsch synthesis using biosyngas*. Int. J. Sci. Eng. Technol., 2013. **2**: p. 817-821.
60. H. A. Choudhury and V. S. Moholkar, *Synthesis of liquid hydrocarbons by Fischer-Tropsch process using industrial iron catalyst*. Int. J. Innov. Res. Sci. Eng. Technol., 2013. **2**: p. 3493-3499.
61. K. R. P. M. Rao, F. E. Huggins, G. P. Huffman, R. J. Gormley, R. J. O'Brien and B. H. Davis, *Mössbauer study of iron Fischer-Tropsch catalysts during activation and synthesis*. Energy and Fuels, 1996. **10**: p. 546-551.
62. H. A. Choudhury and V. S. Moholkar, *An optimization study of Fischer-Tropsch synthesis using commercial cobalt catalyst*. Int J Sci Eng Technol, 2013. **2**: p. 31-39.
63. Hania Ahouari, Ahcène Soualah, Anthony Le Valant, Ludovic Pinard and Yannick Pouilloux, *Hydrogenation of CO₂ into hydrocarbons over bifunctional system Cu-ZnO/Al₂O₃+HZSM-5: Effect of proximity between the acidic and methanol synthesis sites*. Comptes Rendus Chimie, 2015. **18**: p. 1264-1269.
64. Peng Gao, Shanshan Dang, Shenggang Li, Xianni Bu, Ziyu Liu, Minghuang Qiu, et al., *Direct Production of Lower Olefins from CO₂ Conversion via Bifunctional Catalysis*. ACS Catalysis, 2017. **8**: p. 571-578.
65. Young-Kwon Park, Kwang-Cheon Park and Son-Ki Ihm, *Hydrocarbon synthesis through CO₂ hydrogenation over CuZnOZrO₂/zeolite hybrid catalysts*. Catalysis Today, 1998. **44**: p. 165-173.
66. X. Wang, G. Yang, J. Zhang, S. Chen, Y. Wu, Q. Zhang, et al., *Synthesis of isoalkanes over a core (Fe-Zn-Zr)-shell (zeolite) catalyst by CO₂ hydrogenation*. Chem Commun (Camb), 2016. **52**: p. 7352-5.

67. K. Kim, Y. Kim, C. Yang, J. Moon, B. Kim, J. Lee, et al., *Long-term operation of biomass-to-liquid systems coupled to gasification and Fischer-Tropsch processes for biofuel production*. *Bioresource Technology*, 2013. **127**: p. 391-399.
68. Kim Young-Doo, Yang Chang-Won, Kim Beom-Jong, Moon Ji-Hong, Jeong Jae-Yong, Jeong Soo-Hwa, et al., *Fischer-tropsch diesel production and evaluation as alternative automotive fuel in pilot-scale integrated biomass-to-liquid process*. *Applied Energy*, 2016. **180**: p. 301-312.
69. Darshana Nakrani, Mihir Belani, Hari C. Bajaj, Rajesh S. Somani and Puyam S. Singh, *Concentrated colloidal solution system for preparation of uniform Zeolite-Y nanocrystals and their gas adsorption properties*. *Microporous and Mesoporous Materials*, 2017. **241**: p. 274-284.
70. G. Bonura, M. Migliori, L. Frusteri, C. Cannilla, E. Catizzone, G. Giordano, et al., *Acidity control of zeolite functionality on activity and stability of hybrid catalysts during DME production via CO₂ hydrogenation*. *Journal of CO₂ Utilization*, 2018. **24**: p. 398-406.
71. Congming Li, Hongyan Ban, Weijie Cai, Yu Zhang, Zhong Li and Kaoru Fujimoto, *Direct synthesis of iso-butane from synthesis gas or CO₂ over CuZnZrAl/Pd- β hybrid catalyst*. *Journal of Saudi Chemical Society*, 2017. **21**: p. 974-982.
72. Thiago F. Chaves, Heloise O. Pastore and Dilson Cardoso, *A simple synthesis procedure to prepare nanosized faujasite crystals*. *Microporous and Mesoporous Materials*, 2012. **161**: p. 67-75.
73. Ming Bo Yue, Teng Xue, Wen Qian Jiao, Yi Meng Wang and Ming-Yuan He, *Dealumination, silicon insertion and H-proton exchange of NaY in one step with acid ethanol solution*. *Microporous and Mesoporous Materials*, 2012. **159**: p. 50-56.
74. Ting Tang, Lei Zhang, Hai Dong, Zhongxue Fang, Wenqian Fu, Quanyong Yu, et al., *Organic template-free synthesis of zeolite Y nanoparticle assemblies and their application in the catalysis of the Ritter reaction*. *RSC Advances*, 2017. **7**: p. 7711-7717.

75. Masahiro Fujiwara and Yoshie Souma, *Hydrocarbon synthesis from carbon dioxide and hydrogen over Cu–Zn–Cr oxide/zeolite hybrid catalysts*. *Journal of the Chemical Society, Chemical Communications*, 1992: p. 767-768.
76. Lisheng Guo, Yu Cui, Peipei Zhang, Xiaobo Peng, Yoshiharu Yoneyama, Guohui Yang, et al., *Enhanced Liquid Fuel Production from CO₂ Hydrogenation: Catalytic Performance of Bimetallic Catalysts over a Two-Stage Reactor System*. *ChemistrySelect*, 2018. **3**: p. 13705-13711.
77. Haifeng Tian, Jiankang Liao, Fei Zha, Xiaojun Guo, Xiaohua Tang, Yue Chang, et al., *Catalytic Performance of In/HZSM-5 for Coupling Propane with CO₂ to Propylene*. *ChemistrySelect*, 2020. **5**: p. 3626-3637.
78. Haiyan Yang, Chen Zhang, Peng Gao, Hui Wang, Xiaopeng Li, Liangshu Zhong, et al., *A review of the catalytic hydrogenation of carbon dioxide into value-added hydrocarbons*. *Catalysis Science & Technology*, 2017. **7**: p. 4580-4598.
79. Kaoru Fujimoto, Hitoshi Saima and Hiroo Tominaga, *Hydrogenation of carbon monoxide on carbon monoxide reducing catalyst and solid acid. 6. Selective production of C₃ and C₄ hydrocarbons from synthesis gas*. *Industrial & Engineering Chemistry Research*, 1988. **27**: p. 920-926.
80. I. M. Dahl and S. Kolboe, *On the Reaction Mechanism for Hydrocarbon Formation from Methanol over SAPO-34: I. Isotopic Labeling Studies of the Co-Reaction of Ethene and Methanol*. *Journal of Catalysis*, 1994. **149**: p. 458-464.
81. Sreetama Ghosh, Joby Sebastian, Louise Olsson and Derek Creaser, *Experimental and kinetic modeling studies of methanol synthesis from CO₂ hydrogenation using In₂O₃ catalyst*. *Chemical Engineering Journal*, 2021. **416**: p. 129120-129135.
82. Meng Cui, Qingli Qian, Jingjing Zhang, Ying Wang, Bernard Baffour Asare Bediako, Huizhen Liu, et al., *Liquid fuel synthesis via CO₂ hydrogenation by coupling homogeneous and heterogeneous catalysis*. *Chem*, 2021. **7**: p. 726-737.
83. Jin Gong, Mingyu Chu, Wenhao Guan, Yu Liu, Qixuan Zhong, Muhan Cao, et al., *Regulating the Interfacial Synergy of Ni/Ga₂O₃ for CO₂ Hydrogenation toward*

- the Reverse Water–Gas Shift Reaction*. Industrial & Engineering Chemistry Research, 2021. **60**: p. 9448-9455.
84. Jong Hwa Park, Hyeon Su Heo, Young-Kwon Park, Kwang-Eun Jeong, Ho-Jeong Chae, Jung Min Sohn, et al., *Catalytic degradation of high-density polyethylene over SAPO-34 synthesized with various templates*. Korean Journal of Chemical Engineering, 2010. **27**: p. 1768-1772.
85. J. K. Jeon, K. E. Jeong, Y. K. Park and S. K. Ihm, *Selective Synthesis of C-3-C-4 Hydrocarbons Through Carbon-Dioxide Hydrogenation on Hybrid Catalysts Composed of a Methanol Synthesis Catalyst and SAPO*. Applied Catalysis A: General, 1995. **124**: p. 91-106.
86. Jatuporn Wittayakun, Pongtanawat Khemthong and Sanchai Prayoonpokarach, *Synthesis and characterization of zeolite NaY from rice husk silica*. Korean Journal of Chemical Engineering, 2008. **25**: p. 861-864.
87. Mingliang Tong, Linet Gapu Chizema, Xiaoning Chang, Emmerson Hondo, Lin Dai, Yan Zeng, et al., *Tandem catalysis over tailored ZnO-ZrO₂/MnSAPO-34 composite catalyst for enhanced light olefins selectivity in CO₂ hydrogenation*. Microporous and Mesoporous Materials, 2021. **320**: p. 111105-111117.
88. Guiling Xu, Menghui Li and Ping Lu, *Experimental investigation on flow properties of different biomass and torrefied biomass powders*. Biomass and Bioenergy, 2019. **122**: p. 63-75.
89. Roberto Melotti, Ezio Santagata, Marco Bassani, Milena Salvo and Stefano Rizzo, *A preliminary investigation into the physical and chemical properties of biomass ashes used as aggregate fillers for bituminous mixtures*. Waste Management, 2013. **33**: p. 1906-1917.
90. Yingji Wu, Shengbo Ge, Changlei Xia, Changtong Mei, Ki-Hyun Kim, Liping Cai, et al., *Application of intermittent ball milling to enzymatic hydrolysis for efficient conversion of lignocellulosic biomass into glucose*. Renewable and Sustainable Energy Reviews, 2021. **136**: p. 110442.
91. L. Wang, C. L. Weller, D. D. Jones and M. A. Hanna, *Contemporary issues in thermal gasification of biomass and its application to electricity and fuel production*. Biomass and Bioenergy, 2008. **32**: p. 573-581.

92. S. Rapagná, H. Provendier, C. Petit, A. Kiennemann and P. U. Foscolo, *Development of catalysts suitable for hydrogen or syn-gas production from biomass gasification*. Biomass and Bioenergy, 2002. **22**: p. 377-388.
93. D. J. Harris, D. G. Roberts and D. G. Henderson, *Gasification behaviour of Australian coals at high temperature and pressure*. Fuel, 2006. **85**: p. 134-142.
94. C. Franco, F. Pinto, I. Gulyurtlu and I. Cabrita, *The study of reactions influencing the biomass steam gasification process*. Fuel, 2003. **82**: p. 835-842.
95. F. Pinto, C. Franco, R. N. André, M. Miranda, I. Gulyurtlu and I. Cabrita, *Co-gasification study of biomass mixed with plastic wastes*. Fuel, 2002. **81**: p. 291-297.
96. A. Tanksale, J. N. Beltramini and G. M. Lu, *A review of catalytic hydrogen production processes from biomass*. Renewable and Sustainable Energy Reviews, 2010. **14**: p. 166-182.
97. M. Balat, M. Balat, E. Kirtay and H. Balat, *Main routes for the thermo-conversion of biomass into fuels and chemicals. Part 2: Gasification systems*. Energy Conversion and Management, 2009. **50**: p. 3158-3168.



จุฬาลงกรณ์มหาวิทยาลัย
CHULALONGKORN UNIVERSITY

VITA

NAME Jaru Natakaranakul

DATE OF BIRTH 27 March 1990

PLACE OF BIRTH Phuket

INSTITUTIONS ATTENDED Department of Chemical Technology, Faculty of Science,
Chulalongkorn University

HOME ADDRESS 90/343 Wong Sawang Rd, Bang Sue, Bangkok 10800

PUBLICATION Jaru Natakaranakul, Montree Thongkam, Hangjie Li,
Phorndranrat Suchamalawong, Noritatsu Tsubaki and
Tharapong Vitidsant, Direct Synthesis of Liquefied
Petroleum Gas from Carbon Dioxide Using a Copper/Zinc
Oxide/Zirconia/Alumina and HY Zeolite Hybrid Catalyst.
ChemistrySelect, 2021. 6: p. 7103-7110.